Appendix C

CFD Analysis

Appendix C: CFD Analysis

Unlike previous work, which strictly concentrated on the two-phase flow within the crack, the current methodology includes two-phase (water to steam) multi-component (steam/air mixture) flow within the crevice and wastage space. The overall thermal fluids analysis was broken down into a two-step calculation. Aamir et al.[1] have applied a similar two-step approach when studying a comparable problem. The first step computes two-phase information (steam quality, temperature, velocity and density) through the crack based on its size and known conditions. The second step applies this two-phase information as input into a Computational Fluid Dynamics (CFD) model to compute two-phase multi-component flow downstream of the crack within the crevice and wastage space.

A total of five CFD cases that varied crack size and wastage volume are contained in Table C.1. The first four cases employ a Lagrangian/Eulerian methodology[2], while case five employs a Volume of Fluid (VOF) free surface methodology[3].

Table C.1. CFD Cases varying crack size, flow rate, and wastage features.

Case Number	Crack Length (Inches)	Flow Rate (gpm)	Wastage Features	Number of Cells	CFD Methodology
1	0.50	0.001	Long Thin Gap with Cavity	740,000	Lagrangian/Eulerian
2	0.80	0.010	Long Thin Gap with Cavity	740,000	Lagrangian/Eulerian
3	1.00	0.020	Short Thin Gap with Cavity	750,000	Lagrangian/Eulerian
4	1.83	0.170	Final Wastage	1,500,000	Lagrangian/Eulerian
5	1.83	0.170	Final Wastage	1,500,000	VOF – Free Surface Flow

The first case is based on the wastage cavity found near CRDM nozzle 2 at RF013 with a crack length of 0.5 inches. The second case is also based on the wastage geometry from the cavity found near CRDM nozzle 2 at RF013 with a crack length of 0.8 inches. The third case increases the cavity volume by dropping the bottom of the wastage surface below the tip of a 1.0-inch crack. The fourth case models the final wastage state of CRDM nozzle 3 with a 1.13-inch crack above the J-groove and a 0.7-inch crack below the J-groove weld. The results from the first four cases show that large velocities are present even for modest flow rates (0.01 gpm) when accounting for the rapid expansion and acceleration of the fluid due to phase change downstream of the crack.

The fifth CFD case was analyzed with a transient isothermal multi-phase VOF free surface flow calculation. This analysis was used to determine the likelihood of the final wastage state remaining full of liquid boric acid, or if the steam emanating from the crack would eject the boric acid out of the cavity.

C.1 - Two-phase Flow Rate Versus Crack Height

The first step in modeling two-phase flow within the crevice and wastage space is to determine the flow rate as a function of crack size. The empirical relation derived by John et al.[4] allows the definition of a friction factor as a function of crack size and surface roughness. Figure C.1 depicts the flow rate as function of crack height for an ideal nozzle, a relation used in previous work[5] and the John et al. relation. In the present calculation an effective roughness factor, for use in the John et al. relation, was calculated by fitting the flow rate through the 1.83” long crack (nozzle #3, crack 1 at the later stage) to the 0.17 gpm expected leakage. This resulted in an estimated surface roughness factor of 5 μm. This 5 μm effective roughness was therefore employed to predict discharge factors at other crack sizes.

As a jet of liquid exits the crack and enters the cavity in the reactor head, it will partially flash and expand as the pressure decreases to the pressure in the cavity. Flash boiling sprays have various mass and heat transfer mechanisms (heterogeneous and homogeneous bubble nucleation, bubble growth, bubble vaporization, bubble disruption, et cetera) that are dependent on upstream crack tortuosity and local conditions. Since the exact crack tortuosity

is unknown, an isentropic expansion after the crack was taken to bring the two-phase flow to nominal fluid pressure between the RPV head and insulation (1 atm). The velocity, cross sectional area, and steam quality of the jet, when expanded to 1 atm, was then used as an inlet condition for the CFD model. The expanded jet consists of a high-speed (2,244 ft/s) stream of wet steam (35% steam quality) at 1 atm and 212 ˚F.

C.2 - Two-phase Flow within Crevice and Wastage Space

Computing the flow within the crevice and wastage space is a two-step process. The first step computes two-phase information (steam quality, temperature, velocity and density) through the crack based on its size and known conditions. The second step applies this two-phase information to a CFD model to compute the two-phase multi-component fluid behavior downstream of the crack within the crevice and wastage space. A crack in CRDM nozzle 3 leaked subcooled water into the “empty” space between the RPV head and insulation. Under normal operating conditions, the space between the RPV head and mirror insulation is filled with warm air at the same temperature as the subcooled water, but at a much lower pressure. When subcooled water enters this “empty” space, it changes phase from a liquid to a gas, expands volumetrically, accelerates and cools due to the pressure differential. This fluid flow, phase change and heat transfer near CRDM nozzle 3 can be modeled with STAR-CD, a commercial CFD tool.

CFD is a technique that tracks various engineering metrics (mass, energy, momentum, et cetera) that enter, pass through, and exit an open thermodynamic system. This open thermodynamic system is a selected control volume of interest that surrounds the CRDM nozzle 3, which is bounded vertically by the outer radius of RPV head and lower surface of mirror insulation. Figure C.2 displays the RPV head, insert locations for CRDM nozzles, bottom of the mirror insulation, and steel support structure for the mirror insulation. Figure C.3 highlights the control volume of interest near CRDM nozzle 3, which is surrounded by nozzles 1, 6, 11, and 7.

Figure C.4 displays a control volume of interest that maintains geometric features near CRDM nozzle 3. Figure C.5 displays orange colored surfaces that span between CRDM

nozzles 1 to 6, 6 to 11, 11 to 7, and 7 to 1. It should be noted that the control volume of interest is located above the RPV head (blue) and below the bottom surface of the insulation. The volume of interest will also include various head wastage states, as depicted in Figure C.6. The CRDM nozzle 3 crack will be included at the base of the wastage as noted in Figure C.6, starting at the outer diameter of the nozzle.

In essence, RPV head water can enter this control volume starting at the outer diameter of CRDM nozzle 3 (the crack outlet), change phase, expand volumetrically (accelerate), exchange heat with its surroundings and eventually leave the system. Fluid can leave the system at the large orange surfaces or the thin surfaces located between the nozzles and insulation bottom surface (outlined in yellow in Figured C.4 and C.5).

C.2.1 - Description of CFD Models and Results

A total of five CFD cases that varied crack size and wastage volume are contained in Table C.1. The first four cases employ a Lagrangian/Eulerian methodology while case 5 employs a VOF free surface methodology.

The CFD simulation of liquid water changing phase to steam was modeled with the Lagrangian/Eulerian methodology in STAR-CD. The Lagrangian/Eulerian methodology accounts for non-equilibrium based phase transfer between the liquid water droplets and steam/air mixture. The Lagrangian/Eulerian methodology also couples the exchange of momentum, energy, and mass transfer between the water droplets and steam/air mixture. In addition, the employed Lagrangian/Eulerian methodology includes water droplet breakup[6], while allowing water droplets to impinge, splash[7] and rebound off surfaces. In this CFD model, the steam/air mixture is considered viscous and compressible. The liquid water is volatile and can exchange heat and mass with the steam/air mixture. The liquid water changes phase to steam when exposed to temperatures at or above its boiling temperature for a given pressure. The CFD simulation accounts for turbulent, steady state behavior as well as the effects of gravity and buoyancy. Walls can exchange heat with both the liquid water and steam/air mixture.

The fifth CFD case was a transient VOF free surface flow analysis with STAR-CCM+ to determine if the final wastage state would remain full of liquid boric acid, or, if the steam emanating from the crack would eject the boric acid out of the cavity. This VOF free surface flow calculation treated the flow to be inviscid, incompressible, isothermal, and multi-phased (steam and boric acid).

Given that warm stagnant air exists between the RPV head and insulation, the boundary surfaces located in Figures C.5 and C.6 between nozzles 1 to 6, 6 to 11, 11 to 7, and 7 to 1 all allow warm air (605 ˚F) to enter the volume or exit at the upstream temperature at a mean atmospheric pressure of 1 atm. In addition, flow can enter or exit the volume between the thin gap between the insulation and CRDM nozzles. The Lagrangian/Eulerian calculations applied a one-dimensional heat transfer resistance at all walls (except the mirror insulation) based upon the thermal conductivity of the solid material and the minimum distance to RPV head or nozzle inner surface. The Lagrangian/Eulerian simulations allowed the mirror insulation surface to have a small heat sink (120 BTU/hr-ft^2). The VOF simulations assumed all of the subcooled water flashed to steam instantaneously at the crack.

C.2.1.1 – CASE 1

Figure C.7 represents the fluid wastage geometry used in case 1. The first CFD case included a crack that was 0.5-inches above the J-groove weld with a 0.001 gpm leak rate. The base of the crack was located approximately 2.4 inches below the bottom of the small wastage cavity within a 2-mil annular gap between the nozzle and the alloy steel head. The average and maximum velocities for the fluid stream exiting the 0.5-inch CRDM nozzle crack are shown in Figure C.8. These results show the average and maximum velocity magnitude as a function of distance from the J-groove weld. A representation of the relative size of the wastage cavity used in this calculation is provided by the schematic cross-section located above the plot. These results demonstrate that while the maximum velocity within the fluid is over 2,000 feet per second (fps) (1,360 mph) as the fluid exits the crack, the average velocity for the entire mass of fluid is less than 100 fps (68 mph) and decreases as the fluid enters the small wastage cavity located approximately 1.9 inches above the top of the crack.

The average wall temperature, shown in Figure C.9, indicates the cooling effect of this low flow rate on regions deep within the annulus. As the fluid exits the crack and flashes to steam, the average wall temperature within the annulus drops to less than 350°F. As the fluid travels up the annulus (to the right on the figure), the temperature remains relatively constant as the liquid portions of the fluid stream continue to change phase into steam.

The average fluid pressure, shown in Figure C.10, indicates a small pressure drop across the domain (compared to the pressure within the RPV head), mainly due to the small leak rate and a moderately large annulus. The average steam quality is depicted as a function of distance to the J-groove weld in Figure C.11.

Three-dimensional plots of surface/boundary temperature contours are depicted in Figures C.12 and C.13. Obviously, the temperature distribution is very three-dimensional. Often, the temperature ranges from 212 to 605 degrees F at a constant distance from the J-groove weld. Three-dimensional plots of velocity magnitude contour/vector profiles at gap midsection are displayed in Figure C.14. It can be seen that the velocity magnitude and vectors are extremely three-dimensional in nature. Steam quality contour plots at the gap midsection in Figure C-15 show that the fluid is quickly vaporized prior to reaching the cavity. These results suggest that the fluid was fully vaporized prior to reaching the small wastage cavity. This is due to the relatively small leak rate of 0.001 gpm (526 gallons per year).

The process used to compute the average velocity was accomplished by first collecting a group of cells within a minimum/maximum distance to the J-groove weld. For each cell in the group, the individual product of the cell volume and velocity magnitude was computed. The “average velocity” was then defined by the sum of these products for all cells in the group divided by the total volume of the cells in the group. Since the CFD mesh is not one-dimensional, there is no mean to guarantee that lower and upper surfaces to each group are flat. This same procedure was used to calculate “average” steam quality, and pressure. This averaging procedure was also employed in cases 2 and 3.

The average temperature was computed in a similar fashion, where a group of cell wall faces were defined that was within a minimum/maximum distance to the J-groove weld. For each

face in the group, the individual product of face area and wall temperature was computed. The "average temperature" was then defined by the sum of these products for all the faces in the group divided by the total area of the cell faces in the group. This averaging procedure was also employed in cases 2 and 3.

The localized undulations in temperature, velocity, and steam quality profiles in Figures C.8, C.9 and C.10 can be attributed to the averaging of truly three-dimensional down to a one-dimensional form.

C.2.1.2 – CASE 2

Figure C.16 represents the fluid wastage geometry used in case 2. Significant changes in the flow velocities and average wall temperatures were noted for the second case considered in these calculations. Using a crack length of 0.80 inches above the J-groove weld and a leak rate of 0.01 gpm (5,260 gal/yr), we found a very large increase in the average velocity of the fluid in the annulus below the small wastage cavity and an increase in the maximum fluid velocity near the top of the crack, as shown in Figure C.17.

The average velocity in the annulus exceeded 500 fps (341 mph) from the top of the crack to the bottom of the small wastage cavity. The maximum fluid velocity just slightly above the top of the 0.8-inch crack exceeded 2,200 fps (1,500 mph). The maximum fluid velocity also remained between 800 fps and 1,100 fps (545 mph and 750 mph) in the annular region below the small wastage cavity. Upon reaching the wastage cavity, both the average and maximum fluid velocity decreased considerably due to the expansion of the fluid stream into the larger cavity volume.

The results for the average wall temperature for the 0.8 inch crack with a flow rate of 0.01 gpm are somewhat similar to those provided in Case 1. As shown in Figure C.18, the average wall temperature adjacent to the crack in approximately 300°F. The temperature increases as the fluid travels up the annular region toward the small wastage cavity at which point the wall temperature increases to about 500°F. As noted in Case 1, this temperature increase in the wastage cavity is due to the increase in heat transfer area within the cavity.

The average fluid pressure, shown in Figure C.19, indicates a small pressure drop across the domain (compared to upstream conditions), mainly due to the small leak rate and a moderately large annulus. The average steam quality is depicted as a function of distance to the J-groove weld in Figure C.20.

Three-dimensional plots of surface/boundary temperature distributions are depicted in Figures C.21 and C.22. Obviously, the temperature distribution is very three-dimensional. Often, the temperature ranges from 212 to 605 degrees F at a constant distance from the J-groove weld. Three-dimensional plots of velocity magnitude contour/vector profiles at gap midsection are displayed in Figure C.23. It can be seen that the velocity magnitude and vectors are extremely three-dimensional in nature. Steam quality contour plots at the gap midsection in Figure C.24 show that the fluid is mostly vaporized prior to reaching the cavity.

The localized undulations in temperature, velocity, and steam quality profiles in Figures C.17, C.18 and C.19 can be attributed to the averaging of truly three-dimensional data down to a one-dimensional form.

C.2.1.3 – CASE 3

Figure C.25 represents the fluid wastage geometry used in case 3. The third case undertaken in our CFD calculations was completed for a 1.0-inch crack and the associated 0.02 gpm (10,520 gal/yr) leak rate from the axial nozzle crack that intersected a larger wastage cavity than used for Cases 1 and 2.

In this case, the crack extended approximately 0.2 inch into the larger wastage cavity, as shown in the schematic diagrams at the top of Figures C.26, C.27, C.28, and C.29.

Starting near the bottom of the crack on Figure C.26, the average velocity rapidly increases to 620 feet per second as the water expands and changes phase to steam. The fluid moves away from the crack toward the outer region of the thin annular gap. Once the fluid exits the top of the annular gap (0.8 inches from the J-groove weld), it decelerates to an average velocity of less then 75 feet per second due to the substantial increase in cross-sectional area.

However, very large maximum velocities of approximately 2,700 fps (about 1,800 mph) develop in the lower section of the wastage cavity where the crack extends above the bottom of the cavity.

Figure C.27 shows the variation in the average wall temperature of the wastage cavity as a function of distance from the J-groove weld for the 1.0-inch crack with a leak rate of 0.02 gpm. The average wall wastage temperature decreases near the top of the crack due to the cooling effect of the phase change from water to steam. Once the fluid expands into the wastage cavity, the average wall temperature approaches 500°F.

The average fluid pressure, shown in Figure C.28, indicates a small pressure drop across the domain (compared to upstream conditions), mainly due to the small leak rate and a moderately large annulus. The average steam quality is depicted as a function of distance to the J-groove weld in Figure C.29. Once the flashing stops, the fluid begins to increase in temperature due to heat transfer from the RPV head and nozzle. As the fluid enters the small wastage cavity, the surface area for heat transfer increases and the temperature again rises to approximately 600°F until it exits the crevice.

Three-dimensional plots of surface/boundary temperature distributions are depicted in Figures C.30 and C.31. Obviously, the temperature distribution is very three-dimensional. Often, the temperature ranges from 212 to 605 degrees F at a constant distance from the J-groove weld. Three-dimensional plots of velocity magnitude contour/vector profiles at gap midsection are displayed in Figure C.32. It can be seen that the velocity magnitude and vectors are extremely three-dimensional in nature. Steam quality contour plots at the gap midsection in Figure C.33 show that the fluid is mostly vaporized prior to reaching the cavity.

The localized undulations in temperature, velocity, and steam quality profiles in Figures C.26, C.27 and C.28 can be attributed to the averaging of truly three-dimensional data down to a one-dimensional form.

C.2.1.4 – CASE 4

CFD Case 4 employed similar calculations to model the fluid flow conditions in the final wastage cavity at the end of Cycle 13. This modeling effort began by defining the volume of the final wastage state, which included a 195 cubic inch cavity that extended from the top of the RPV head to the base of the stainless steel cladding between Nozzles 3 and 11. The crack in Nozzle 3 extended 1.17 inches above the J-groove weld and 0.70 inches through the J-groove weld. The estimated leak rate, based on the unidentified leak rates late in Cycle 13, and the calculated leak rates for a 1.8-inch total crack length as shown in Figure C.1, was 0.17 gpm (89,350 gal/yr).

Starting near the crack, the leaking, sub-cooled water changes phase to steam, expands, and rapidly accelerates. Slightly further away from the crack, the stream of water and steam expands into the open wastage space.

Figures C.34-36 display the final wastage geometry from various points of view. Figures C.37-38 show the far field CFD mesh and local refinements to resolve the crack geometry.

Figures C.40-43 show the final temperature contour near CRDM nozzle 3 from various points of view. Significant cooling develops above the wastage space as the cool water/steam mixture is redirected off the wall adjacent to the crack and finally exits the wastage cavity.

Figures C.44-54, C.55-66 and C.67-78 clearly show planar sections of the stream of fluid as it disperses and cools everything in its path. These figures also show warm air being drawn into the domain between nozzles 7-11 and 11-6 and cooler air/steam exiting between nozzles 7-1 and 1-6. The warm air enters the larger side of the wastage cavity on the nozzle 6 side. The cool steam exits the smaller side of the wastage cavity on the nozzle 11 side.

Figures C.79-90, C.91-102 and C.103-114 clearly show planar sections of fluid velocity contours/vectors. Figure C.97 shows the velocity at a cross section of the final wastage state within the wastage cavity. This figure shows that high fluid velocity (75 ft/s) still exists near the wastage wall of this large cavity. Once the fluid hits the wastage wall, it is redirected up and out of the cavity. As the stream of fluid disperses it cools all surfaces in its

path. Overall, these figures show how a high velocity cool fluid is ejected out of the cavity towards Nozzle 1 and in turn draws warm air into the cavity from above.

Figures C.115-116 display the mass fraction of air near boundary surfaces of the final wastage cavity. Figures C.117-122 display contoured section plots of mass fraction of air within the wastage cavity. Clearly, the wastage volume is highly concentrated with air.

C.2.1.5 – CASE 5

The fifth CFD case was a transient VOF analysis with STAR-CCM+ to determine if the final wastage state would remain full of liquid boric acid, or, if the steam emanating from the crack would eject the boric acid out of the cavity. Since the density of steam and boric acid are different many orders of magnitude, the VOF model treated the flow to be incompressible. It is also felt that the inclusion of viscosity effects would only have significant effects near walls, so the model was run inviscidly.

The CFD results for the Case 5 transient analysis are presented in Figures C.124-126. These figures present a top view and a perspective view of the final wastage cavity near CRDM Nozzle 3. Figure C.124 shows the initial configuration with a pool of aqueous boric acid filling the cavity during time steps 0.001 seconds, 0.005 seconds, and 0.02 seconds. The darker blue surface in each view represents a liquid vapor interface. For the three top views shown in Figure C.124, the dark blue area represents the surface of the aqueous boric acid pool. For the three perspective views, the top surface of the pool and the interface between the boric acid pool and the steam/liquid mixture exiting the crack are evident. Note that the volume of the steam/liquid mixture exiting the crack increases as the time steps increase from 0.001 seconds to 0.02 seconds.

Figure C.125 shows the progression of the transient for times from 0.05 seconds through 0.10 seconds. During this period, the steam/liquid mixture exiting the crack continues to grow in volume until it finally disrupts the surface of the aqueous boric acid pool. Figure C.125 also show the continued progression of the transient for times from 0.12 seconds through 0.20 seconds.

Significant disruption of the aqueous boric acid pool occurs, liquid boric acid is ejected from the wastage cavity, and strikes the mirror insulation and support structures above the wastage cavity. Figure C.126 shows the final time steps of the transient analysis (from 0.25 seconds to 0.40 seconds). The majority of the aqueous boric acid that originally resided in the wastage cavity has been ejected.

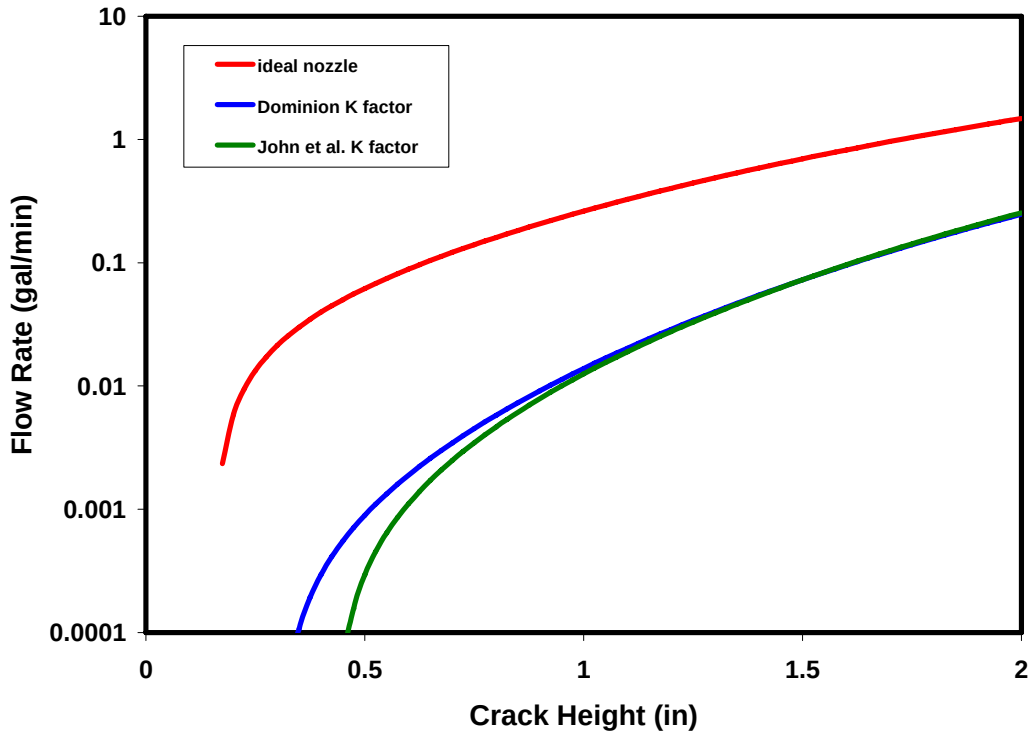

Figure C.1 Calculated flow rate versus crack height.

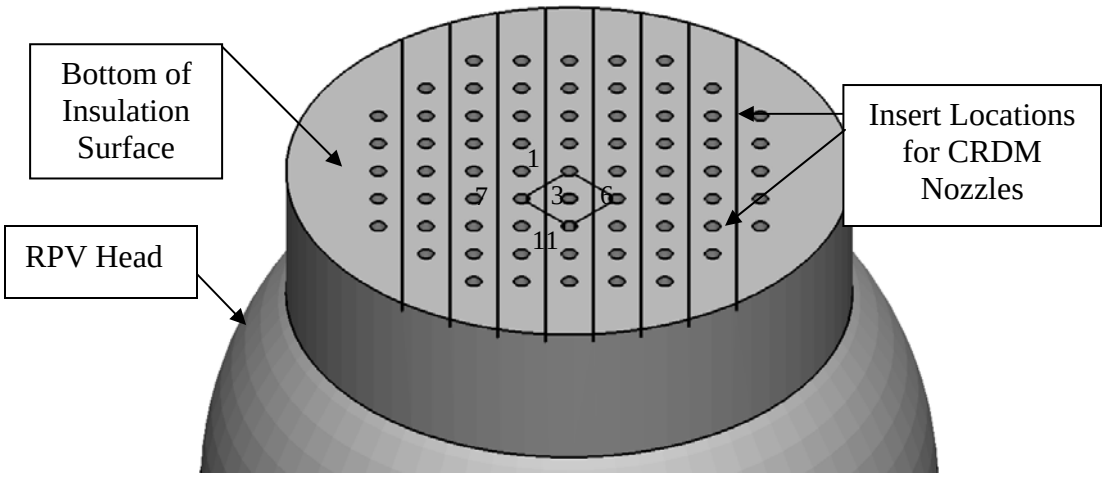

Figure C.2 Davis Besse RPV head, insert locations for CRDM nozzles, insulation and steel support structure. CRDM nozzle 3 is surrounded by nozzles 1, 6, 11, and 7.

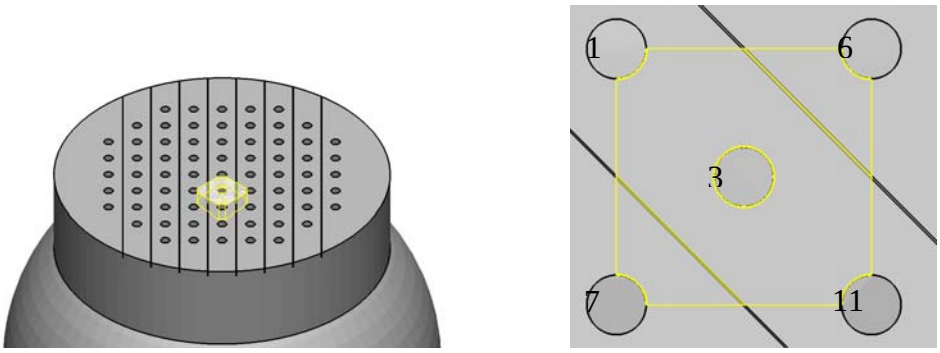

Figure C.3 Davis Besse RPV volume of interest surrounding CRDM nozzle 3. CRDM nozzle 3 is surrounded by nozzles 1, 6, 11, and 7.

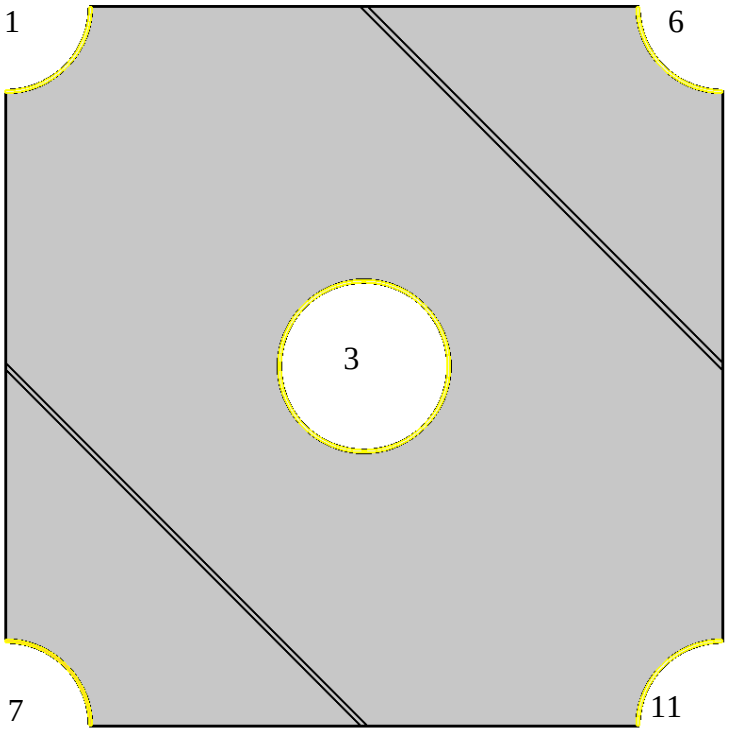

Figure C.4 Control volume of interest near CRDM nozzle 3.

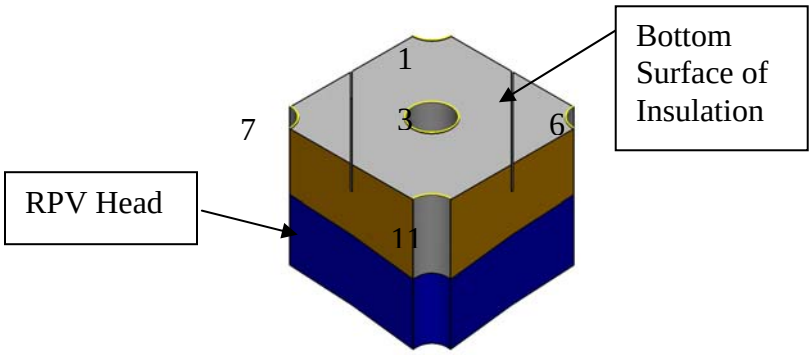

Figure C.5 Volume of interest near CRDM nozzle 3 including RPV head (blue) and bottom surface of insulation. Viewpoint is looking from above the RPV head.

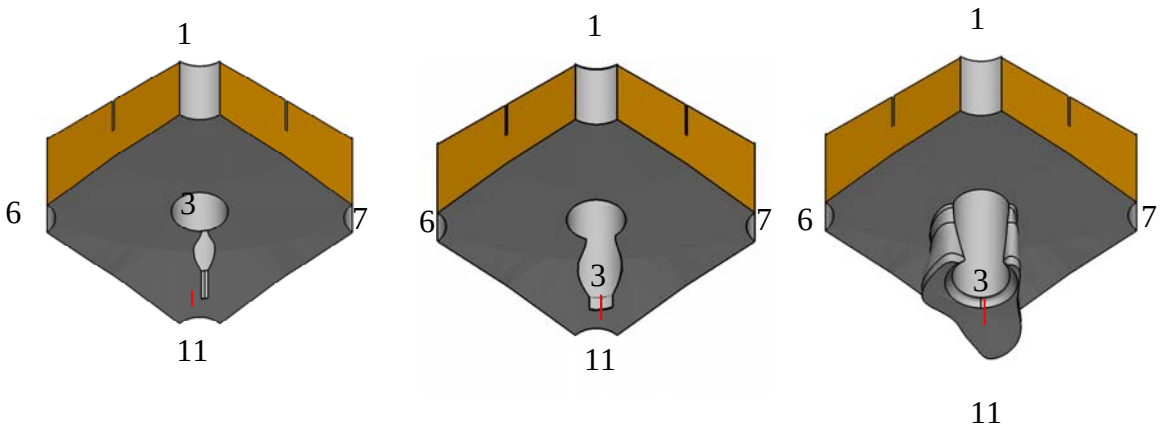

Figure C.6 Example head wastage at various states. Crack locations are marked by the red lines (10 degree rotation from nozzle 11 to 7). Viewpoint is looking from below RPV head at the crack.

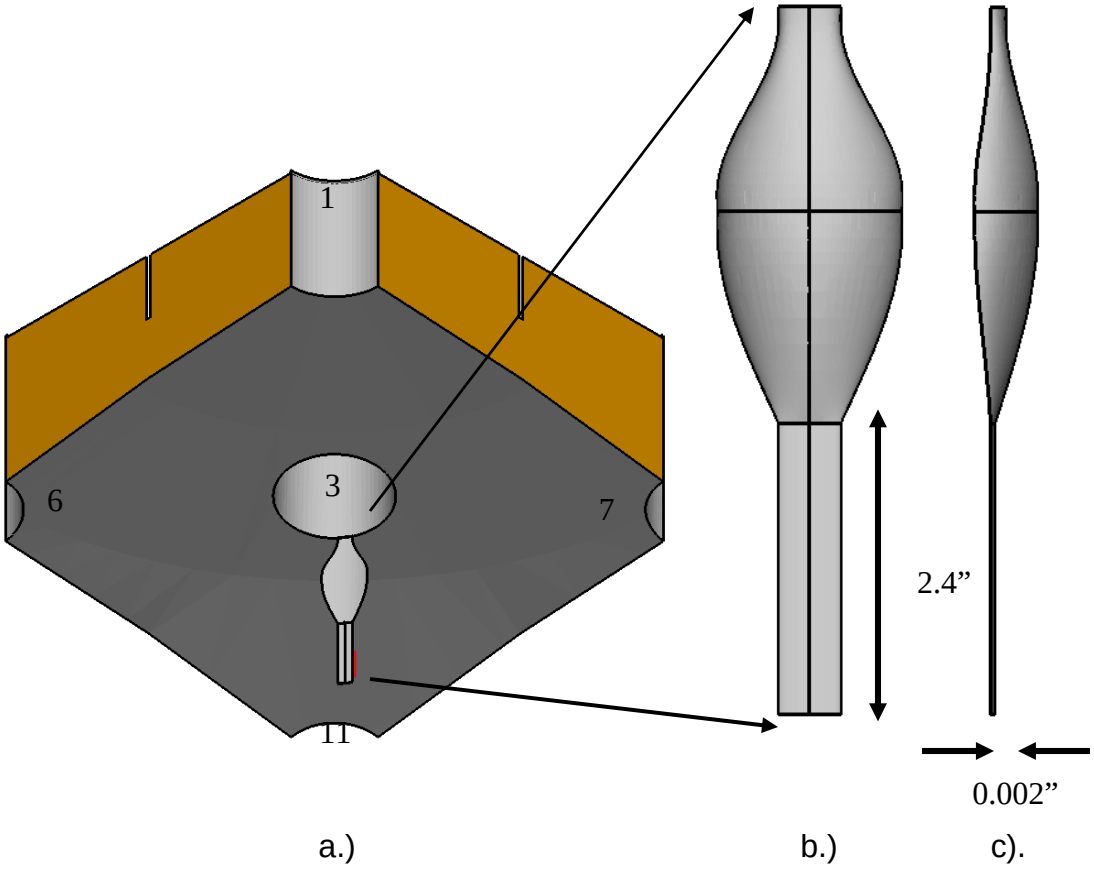

Figure C.7 Case 1: Fluid wastage geometry. Viewpoint a.) Looking from below the RPV head at the crack, b.) Looking from the side at the opposite side of crack, c.) Looking from the side of the crack.

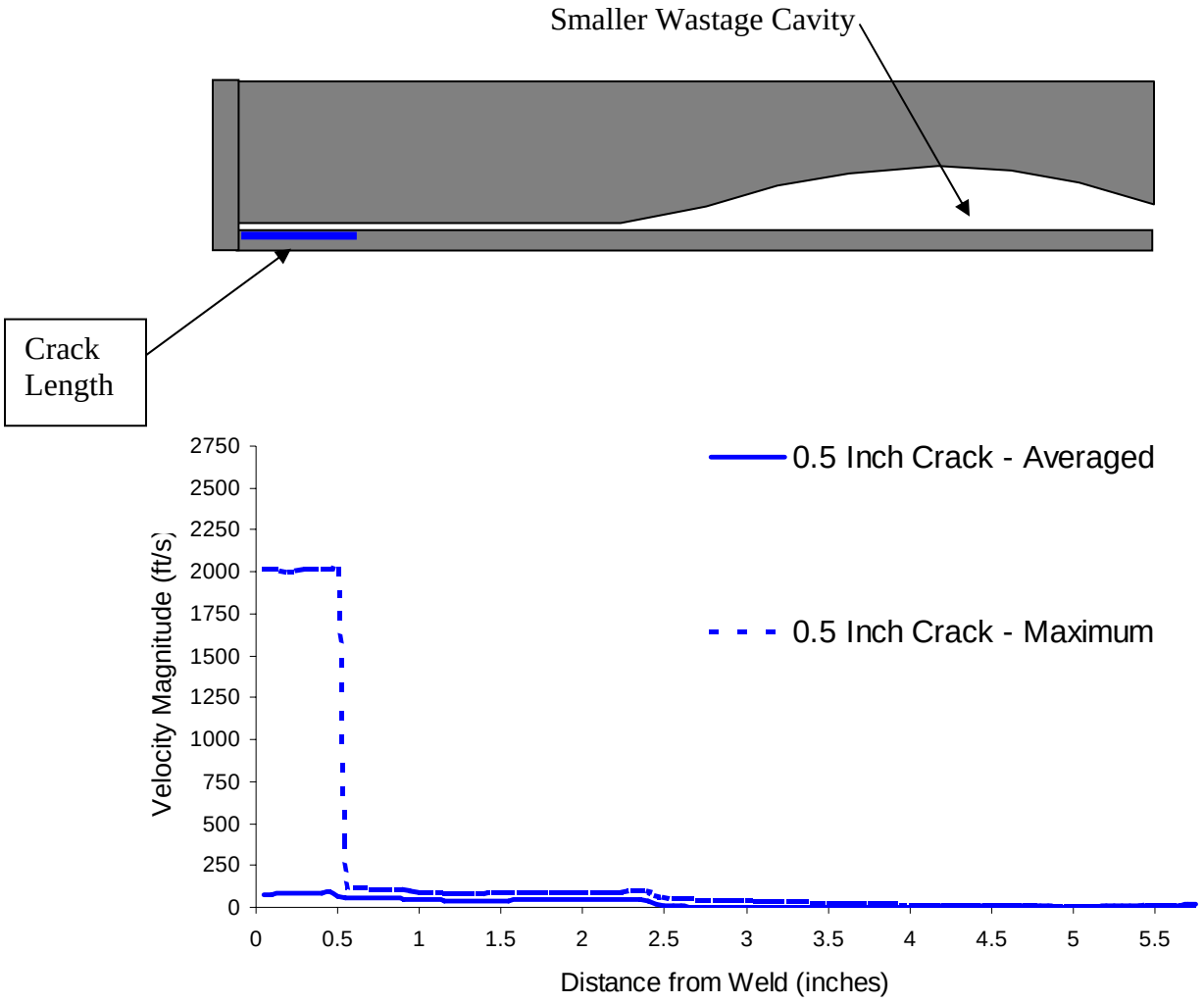

Figure C.8 Case 1: Maximum and average fluid velocity magnitude within wastage as a function of distance to the J-groove weld for a 0.5-inch crack with a leak rate of 0.001 gpm.

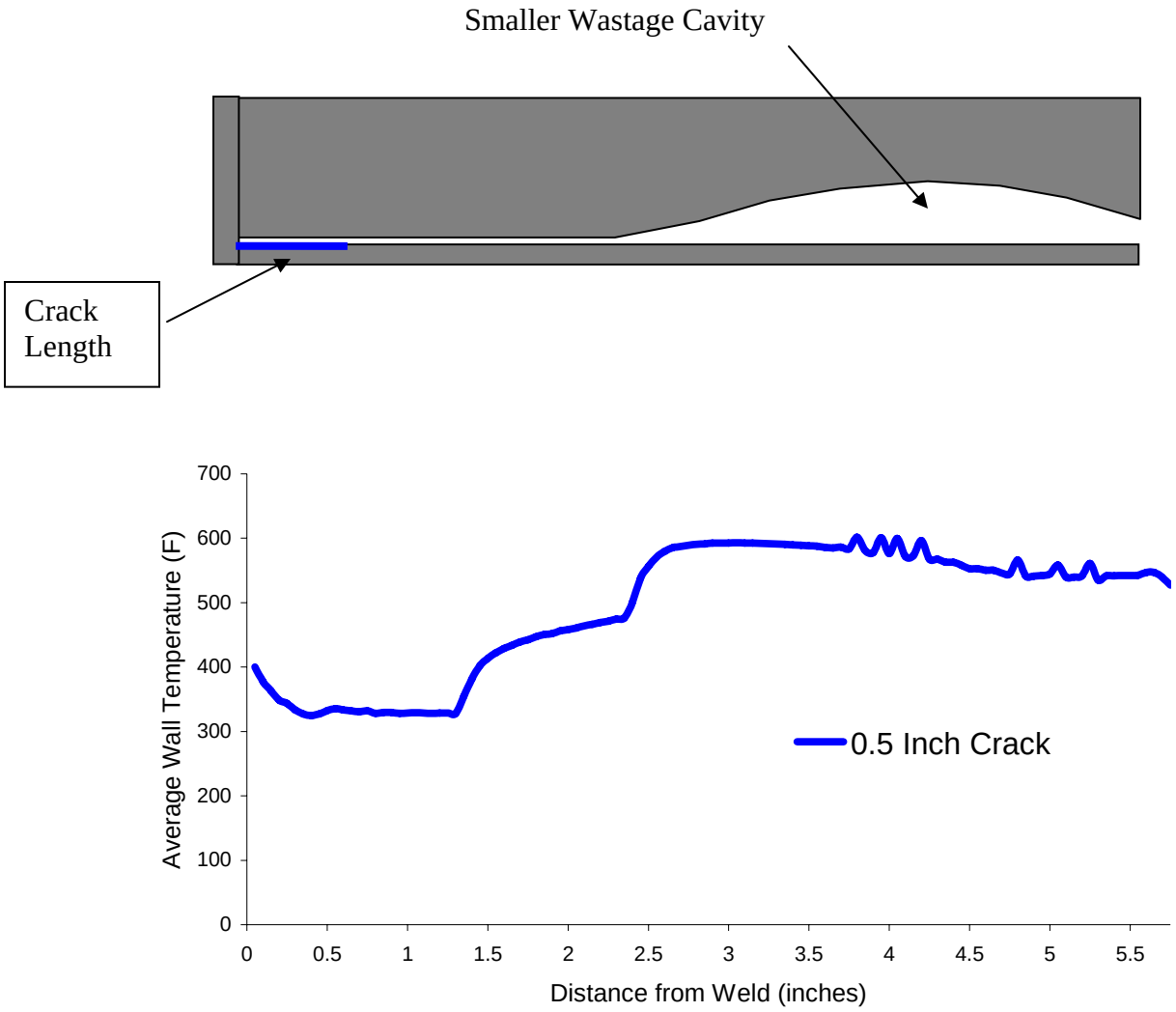

Figure C.9 Case 1: Average wall temperature within wastage as a function of distance to the J-groove weld for a 0.5-inch crack with a leak rate of 0.001 gpm.

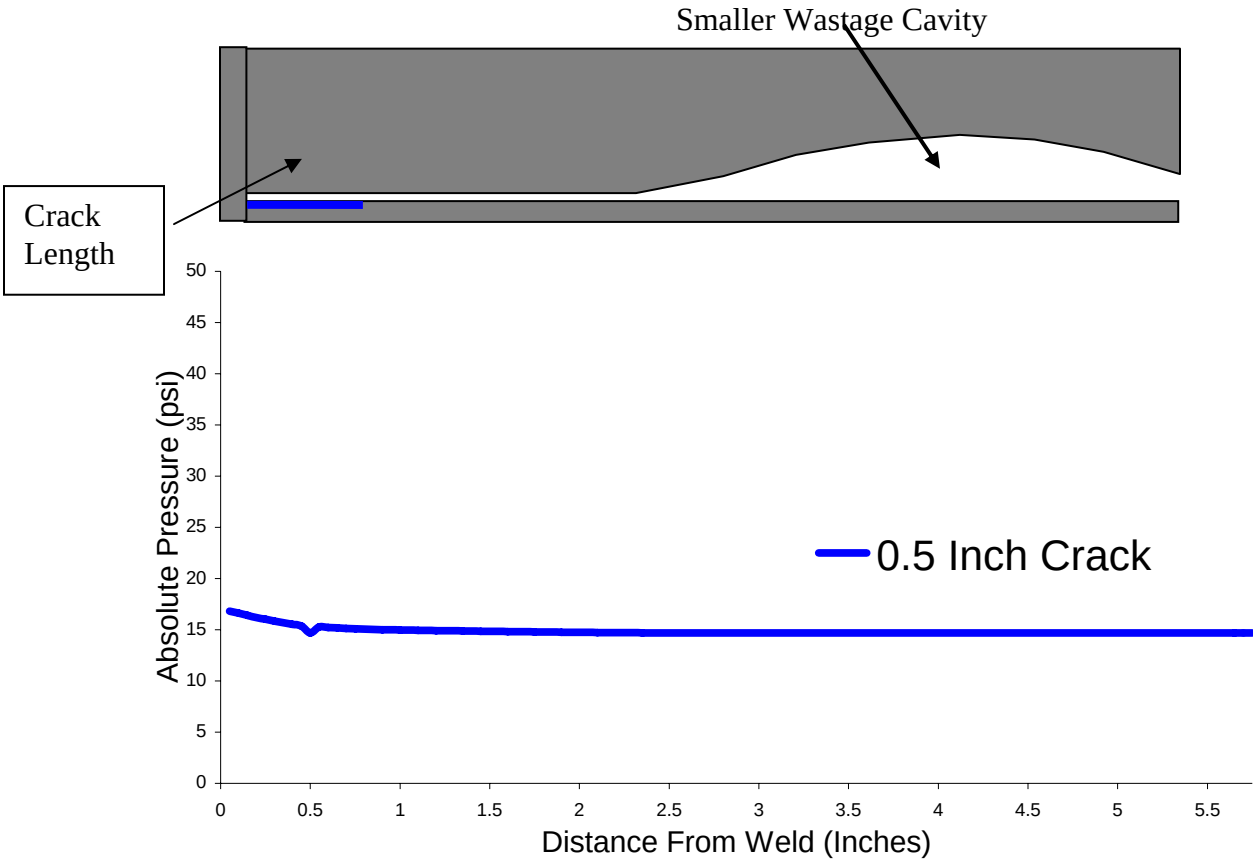

Figure C.10 Case 1: Average fluid pressure within wastage as a function of distance to the J-groove weld for a 0.5-inch crack with a leak rate of 0.001 gpm.

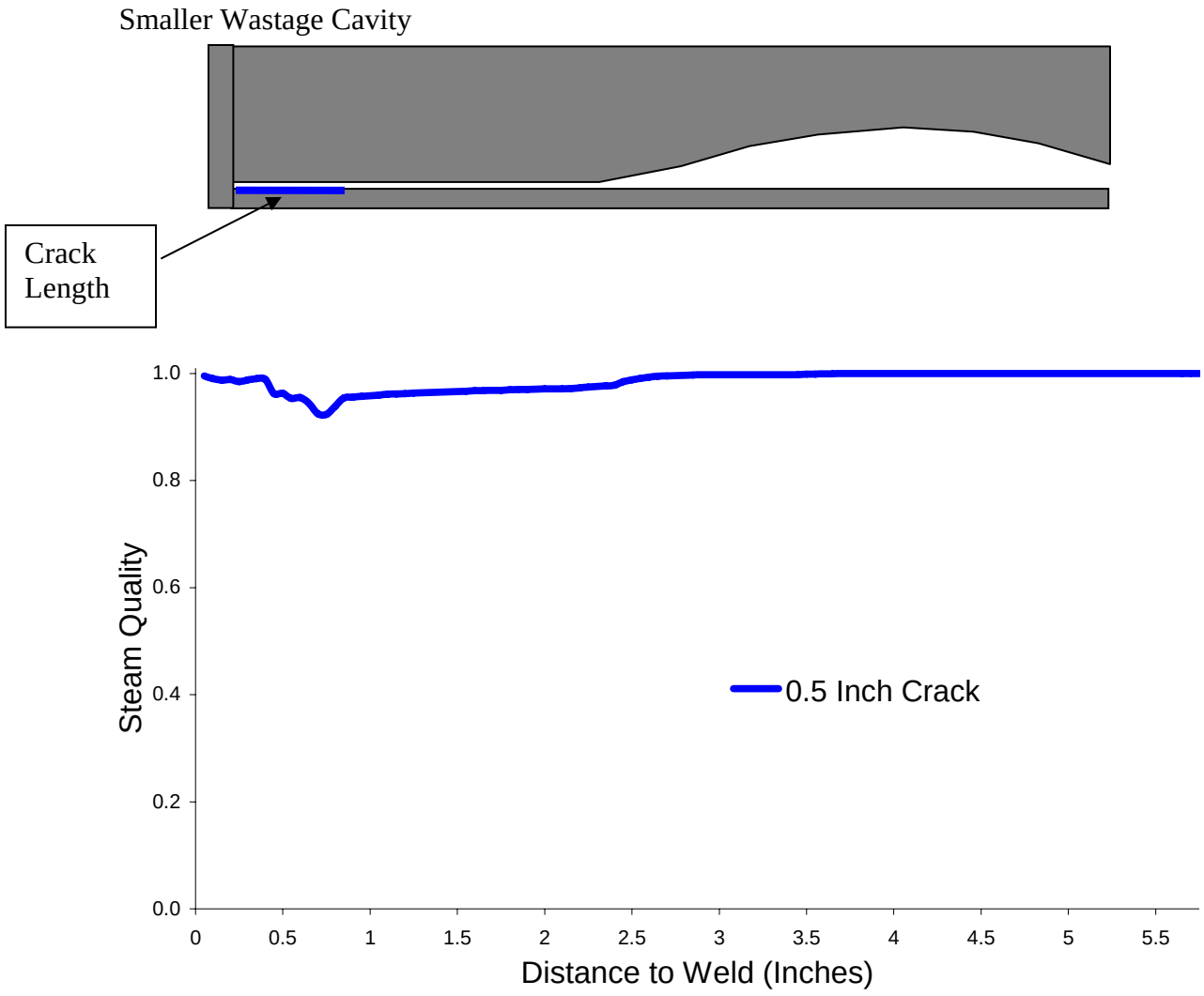

Figure C.11 Case 1: Average steam quality within wastage as a function of distance to the J-groove weld for a 0.5-inch crack with a leak rate of 0.001 gpm.

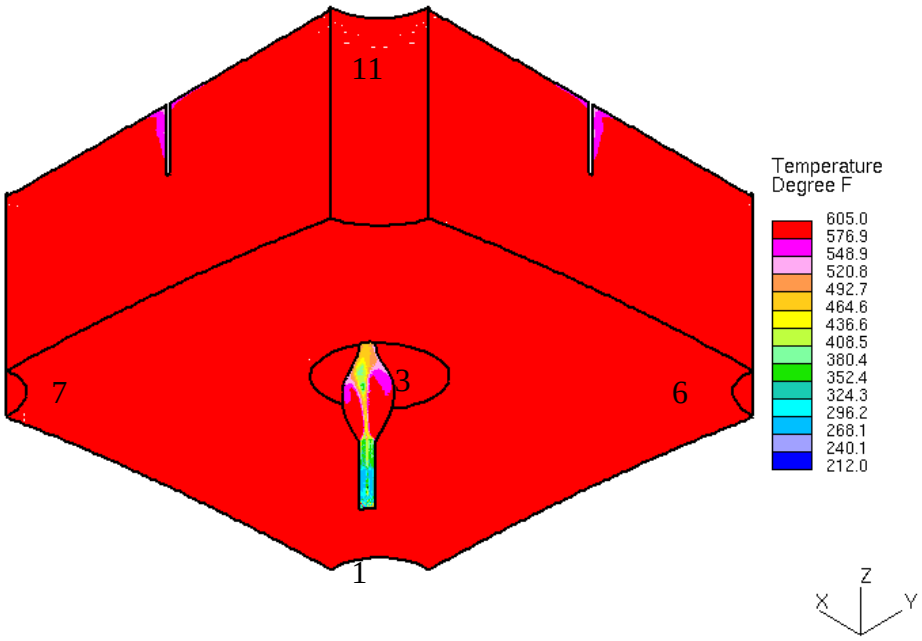

Figure C.12 Case 1: Surface/boundary temperature distribution.

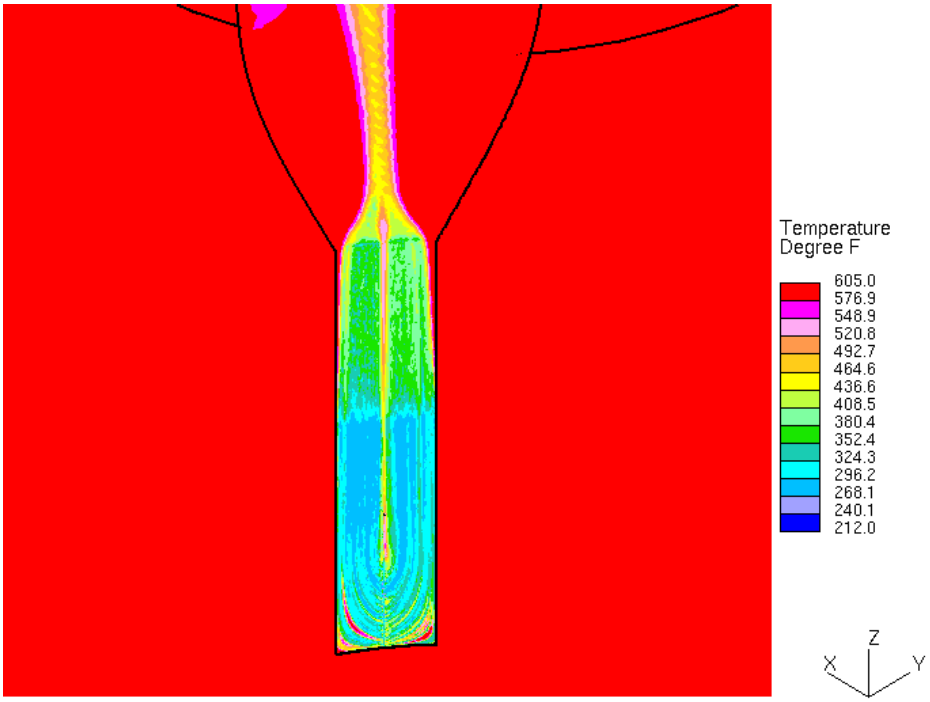

Figure C.13 Case 1: Surface/boundary temperature distribution.

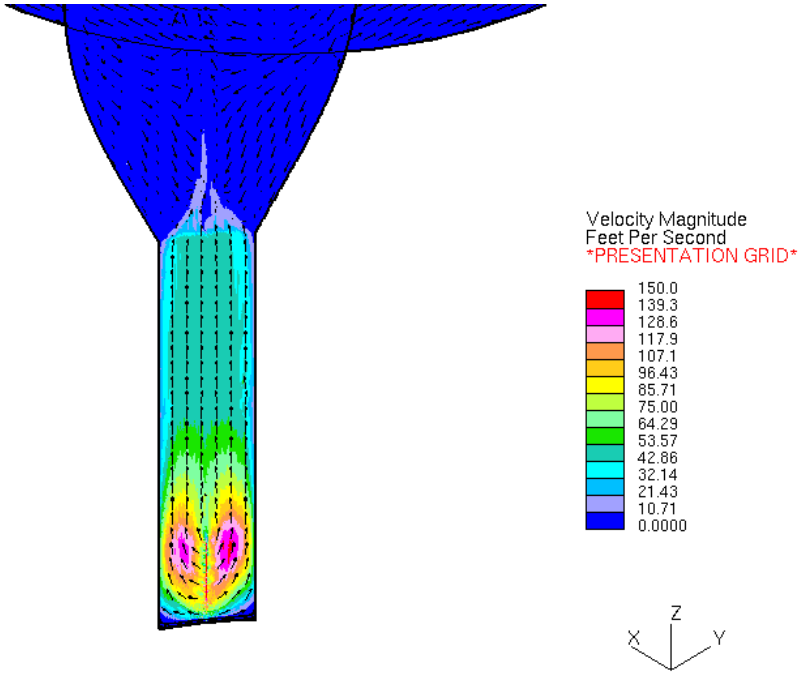

Figure C.14 Case 1: Velocity magnitude contour/ vector profile at gap midsection.

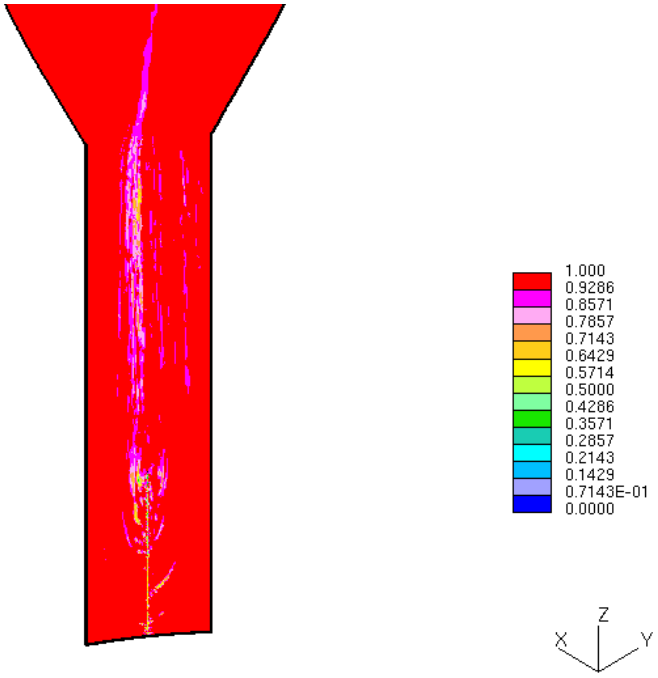

Figure C.15 Case 1: Steam quality contour profile at gap midsection.

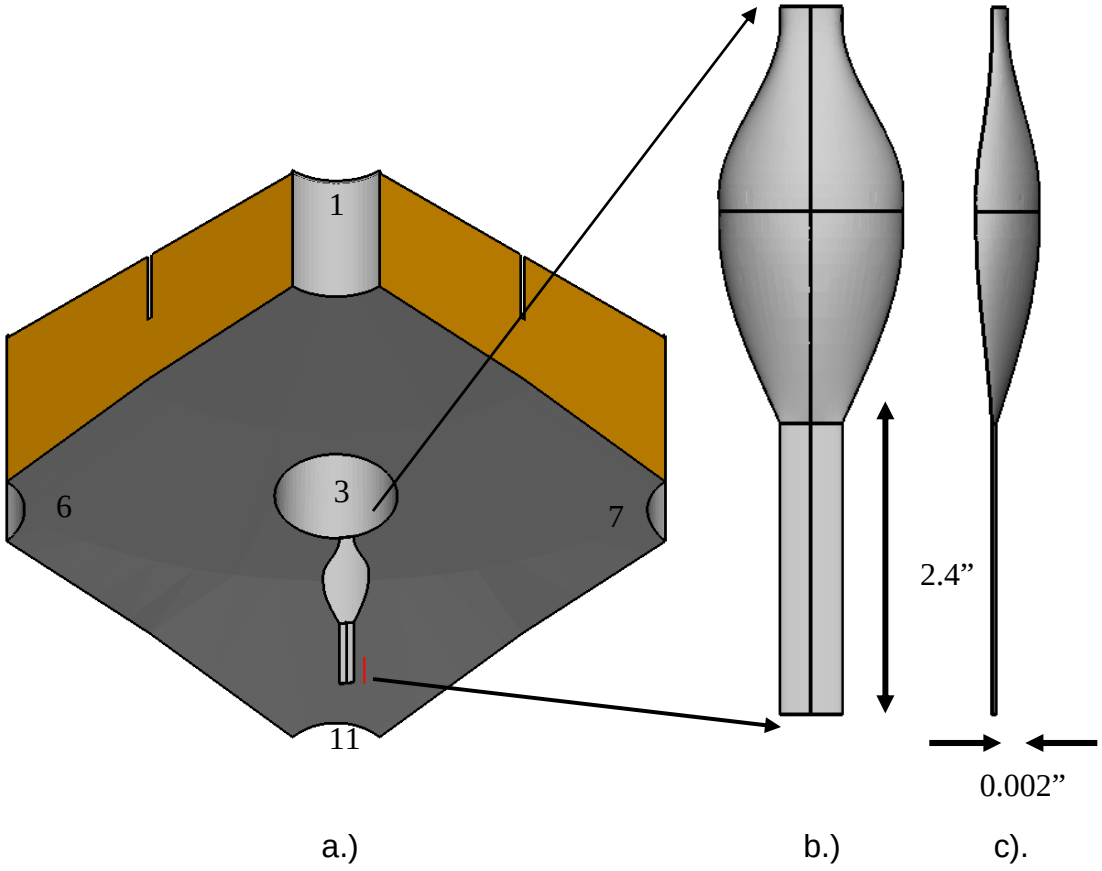

Figure C.16 Case 2: Fluid wastage geometry. Viewpoint a.) Looking from below the RPV head at the crack, b.) Looking from the side at the opposite side of crack, c.) Looking from the side of the crack.

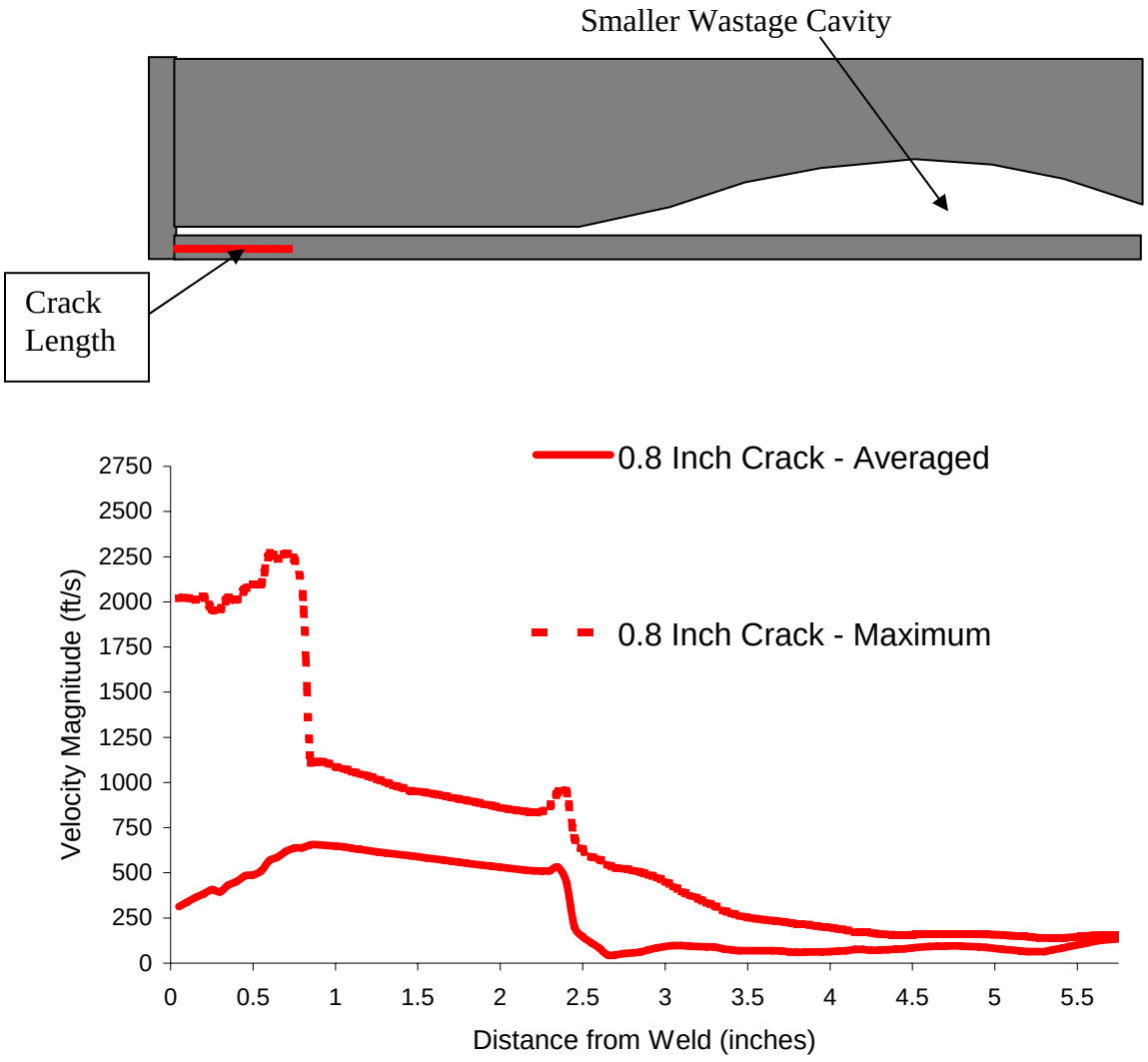

Figure C.17 Case 2: Maximum and average fluid velocity magnitude within wastage as a function of distance from the J-groove weld for a 0.8-inch crack with a leak rate of 0.01 gpm.

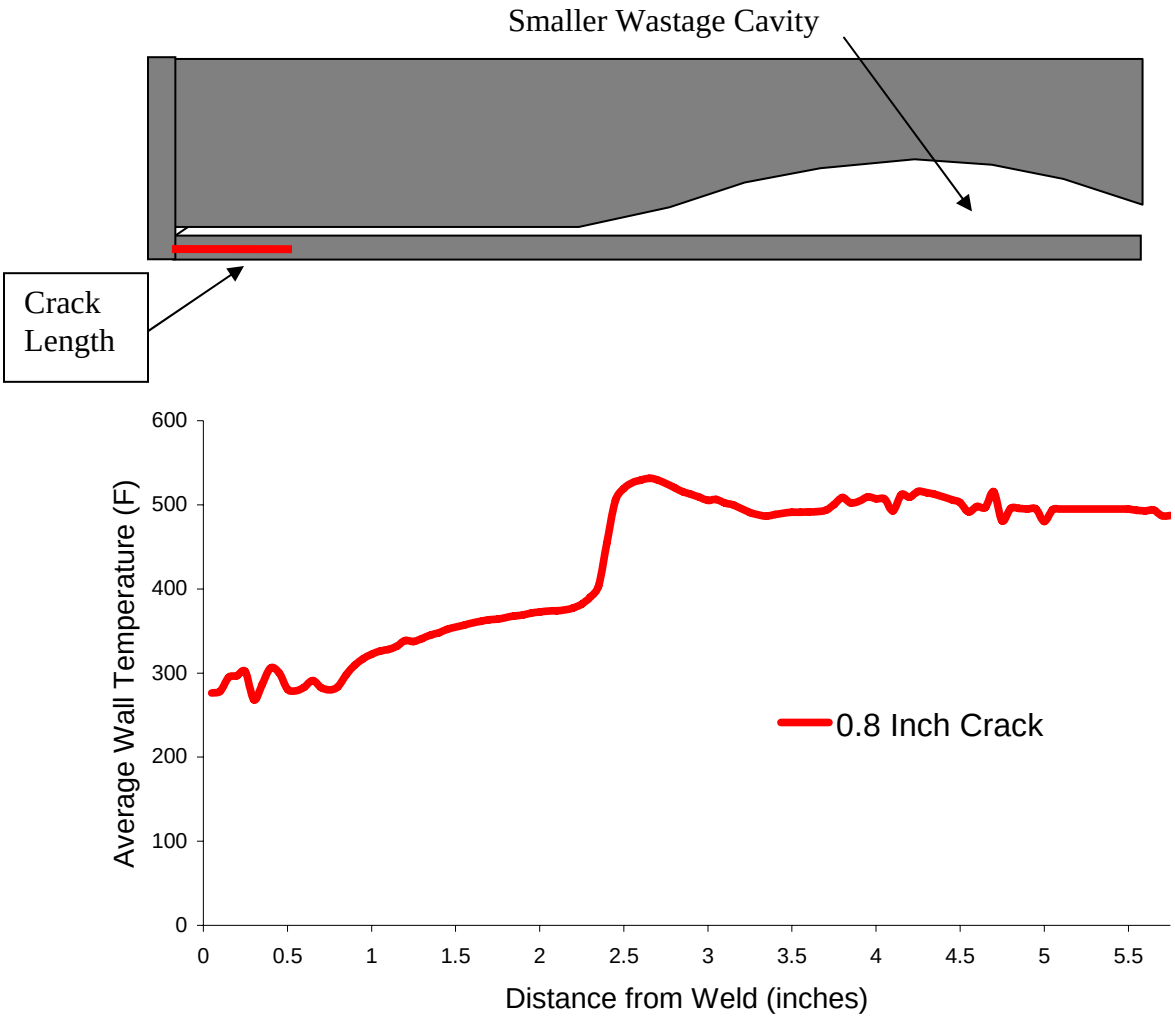

Figure C.18 Case 2: Average wall temperature within wastage as a function of distance to the J-groove weld for a 0.8-inch crack with a leak rate of 0.01 gpm.

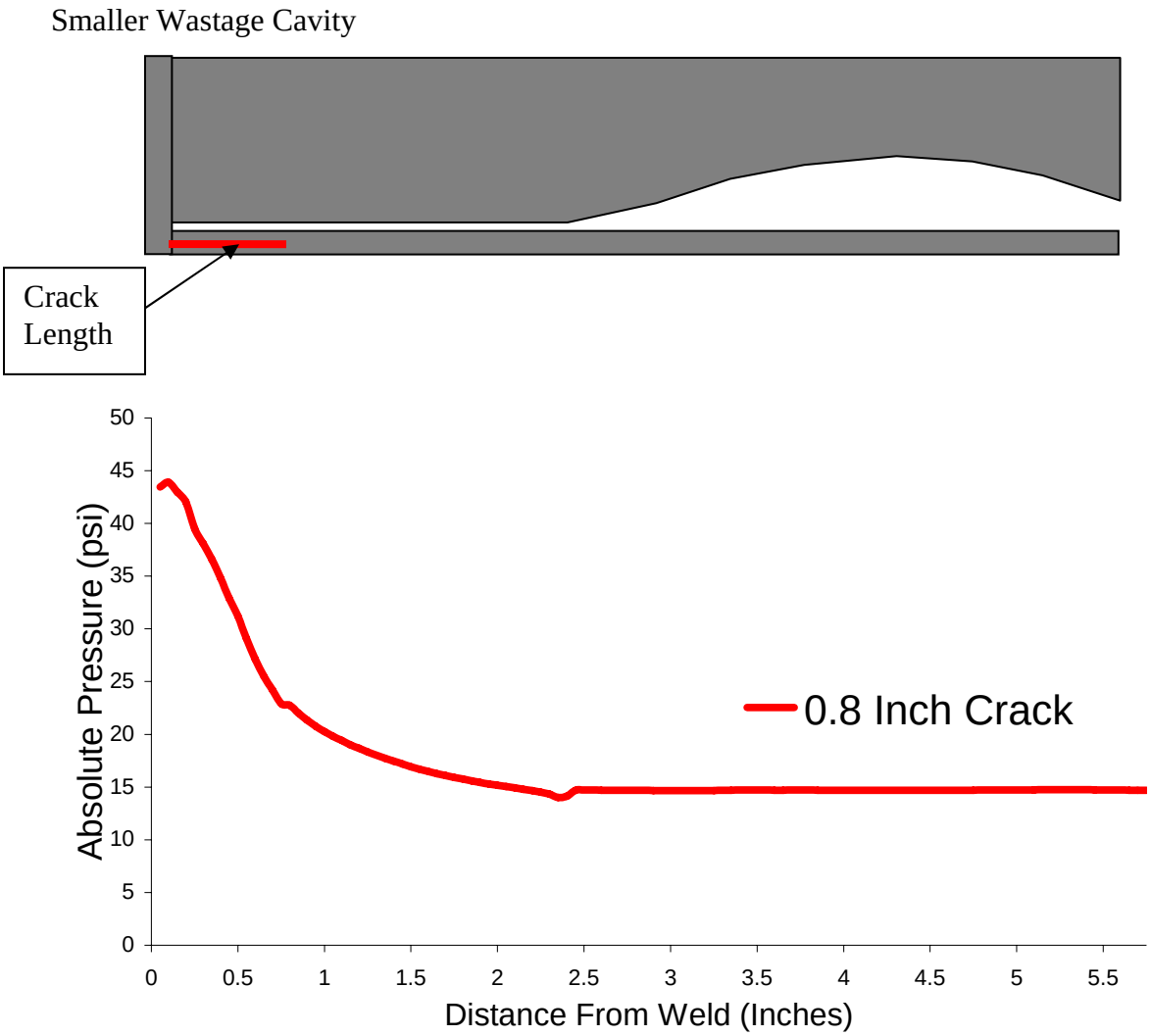

Figure C.19 Case 2: Average fluid pressure within wastage as a function of distance to the J-groove weld for a 0.8-inch crack with a leak rate of 0.01 gpm.

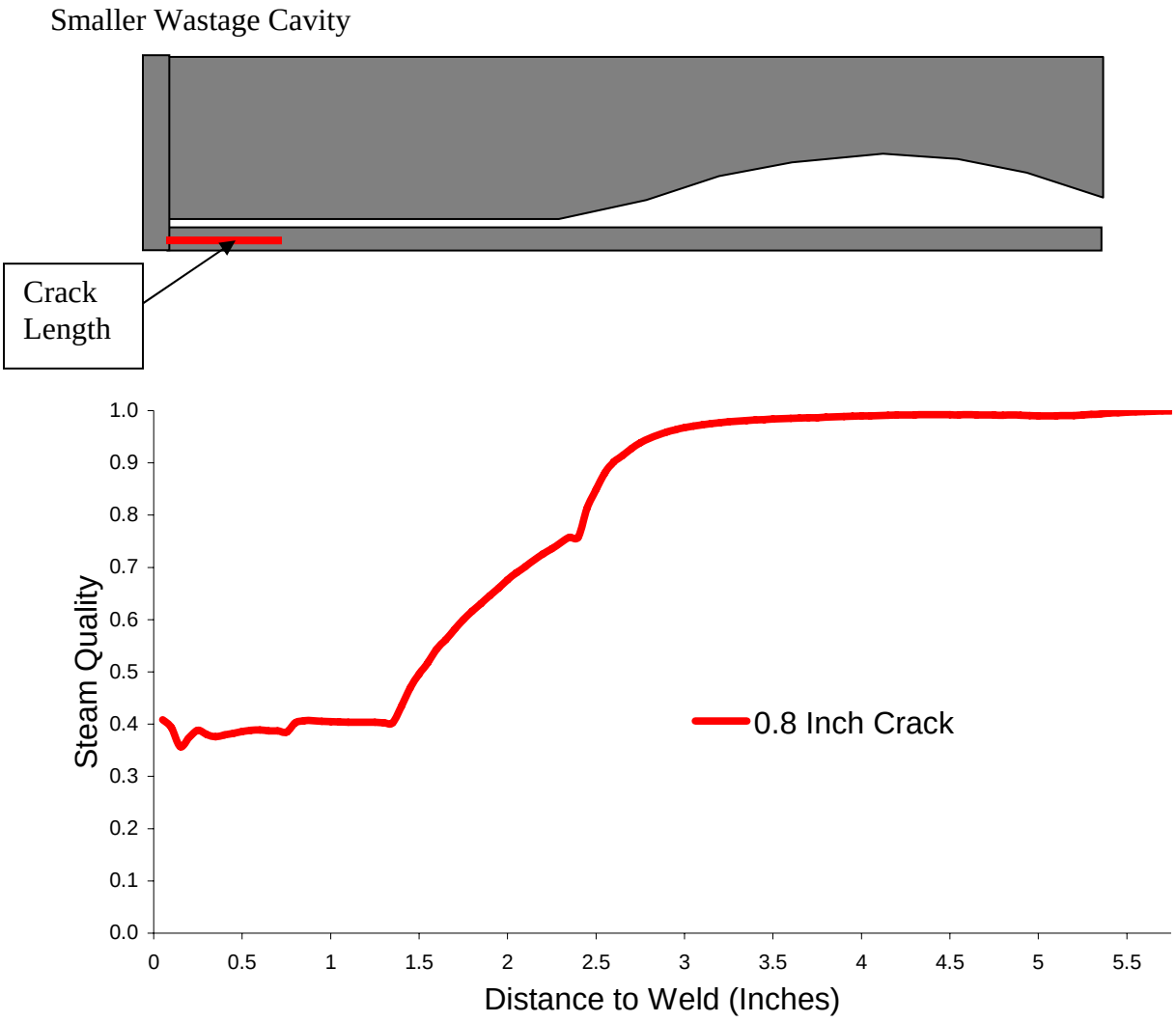

Figure C.20 Case 2: Average steam quality within wastage as a function of distance to the J-groove weld for a 0.8-inch crack with a leak rate of 0.01 gpm.

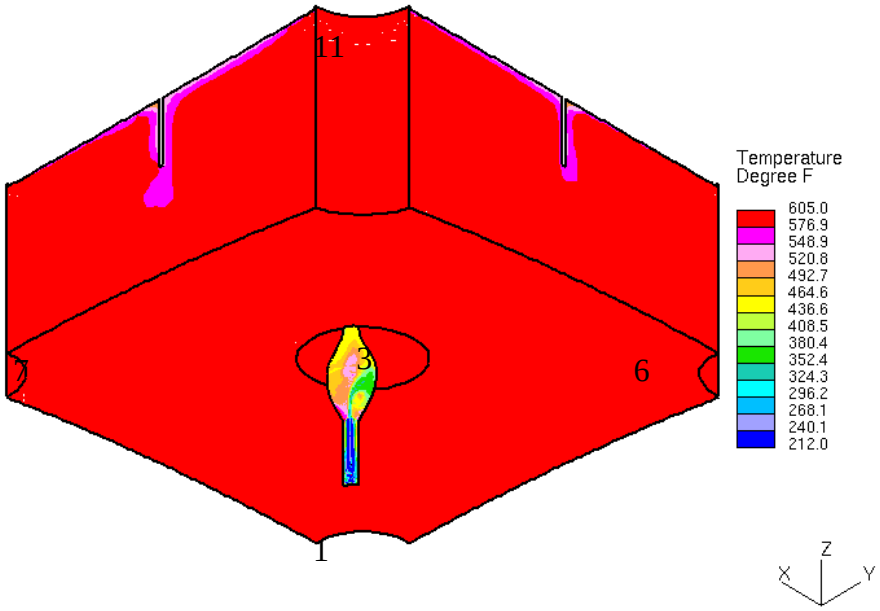

Figure C.21 Case 2: Surface/boundary temperature distribution.

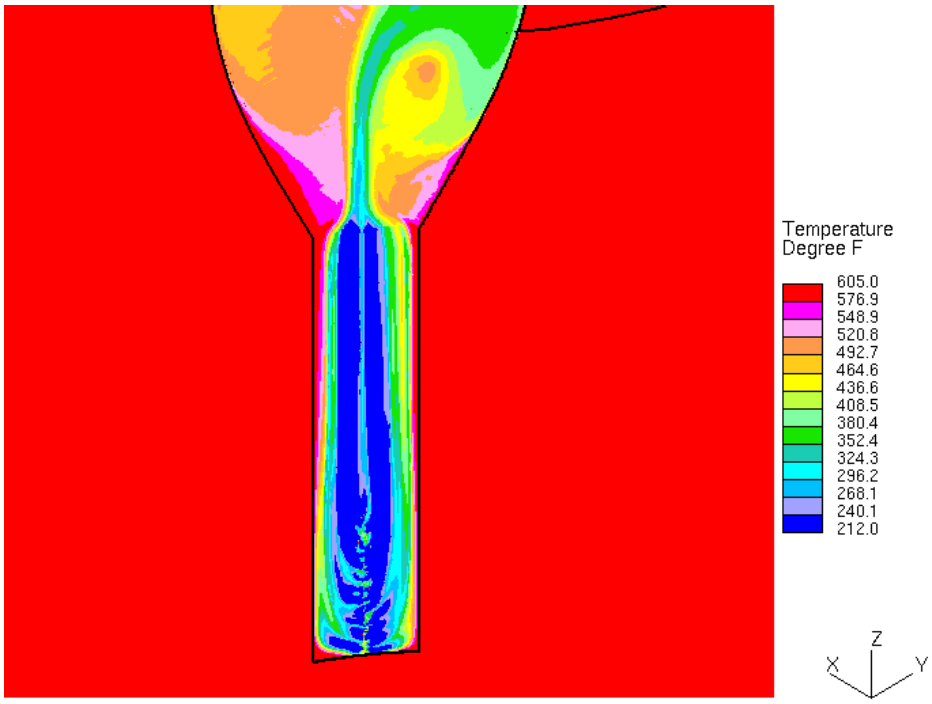

Figure C.22 Case 2: Surface/boundary temperature distribution.

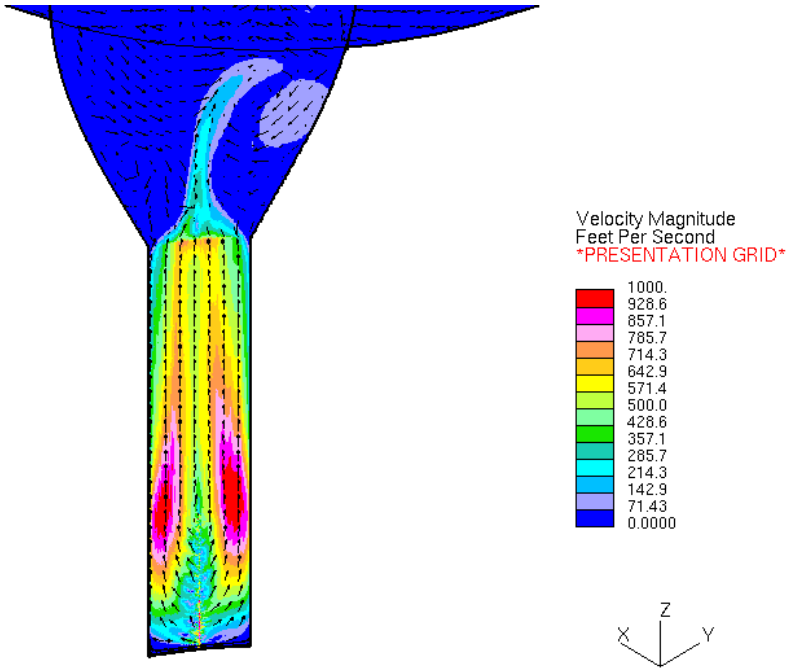

Figure C.23 Case 2: Velocity magnitude contour/ vector profile at gap midsection.

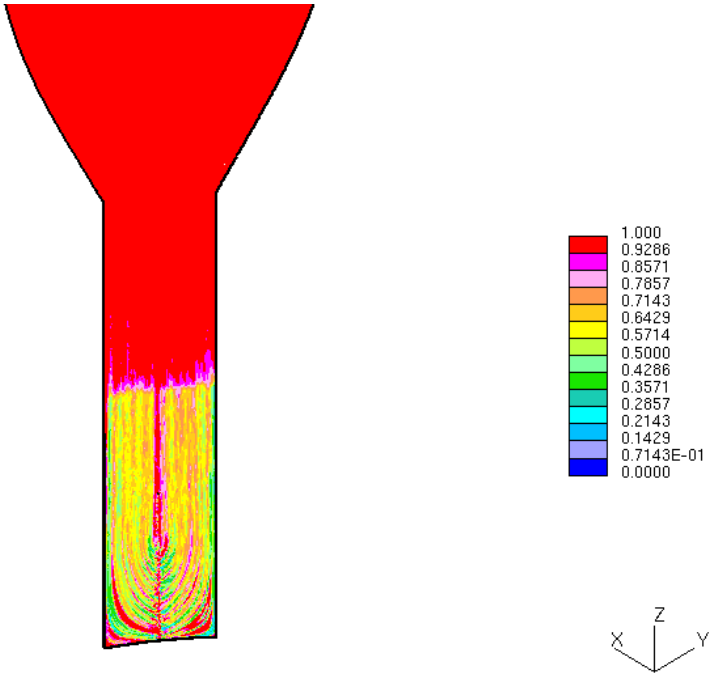

Figure C.24 Case 2: Steam quality contour profile at gap midsection.

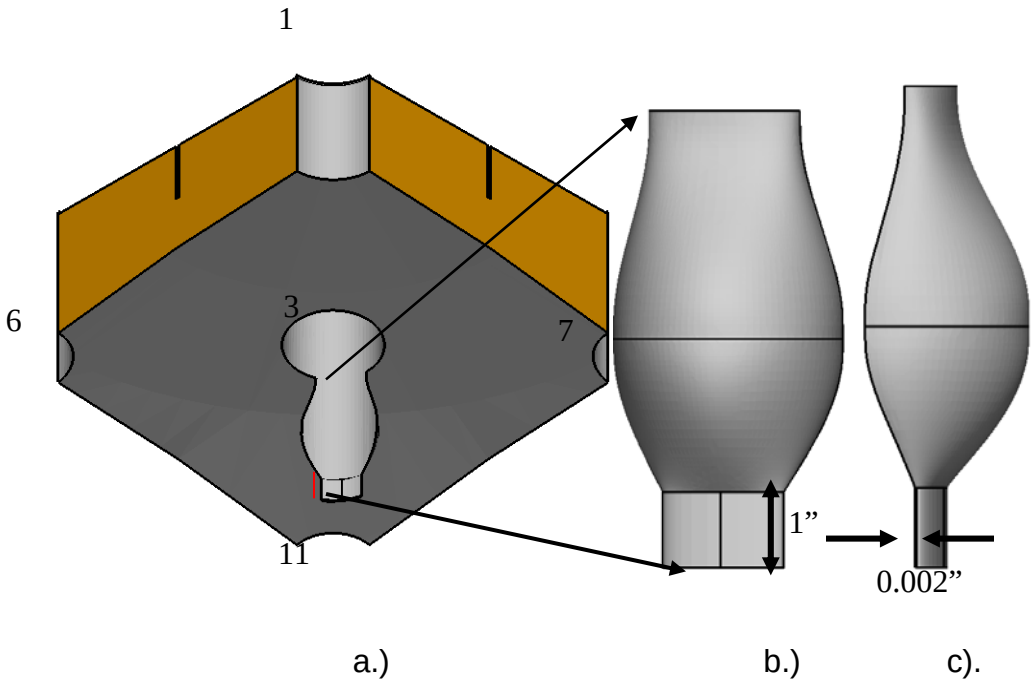

Figure C.25 Case 3: Fluid wastage geometry. Viewpoint a.) Looking from below the RPV head at the crack, b.) Looking from the side at the opposite side of crack, c.) Looking from the side of the crack.

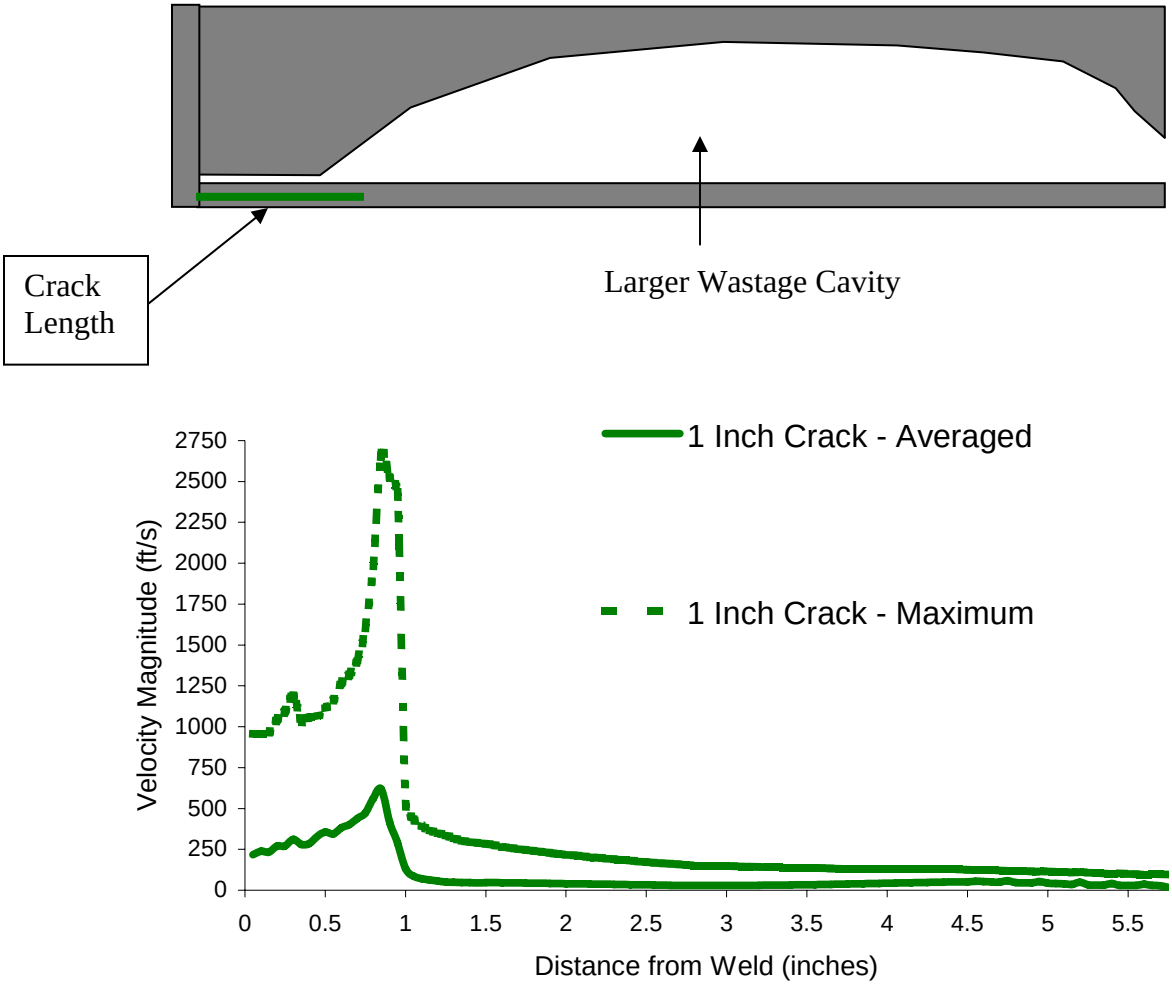

Figure C.26 Case 3: Maximum and average fluid velocity magnitude within wastage as a function of distance to the J-groove weld for a 1.0-inch crack with a leak rate of 0.02 gpm.

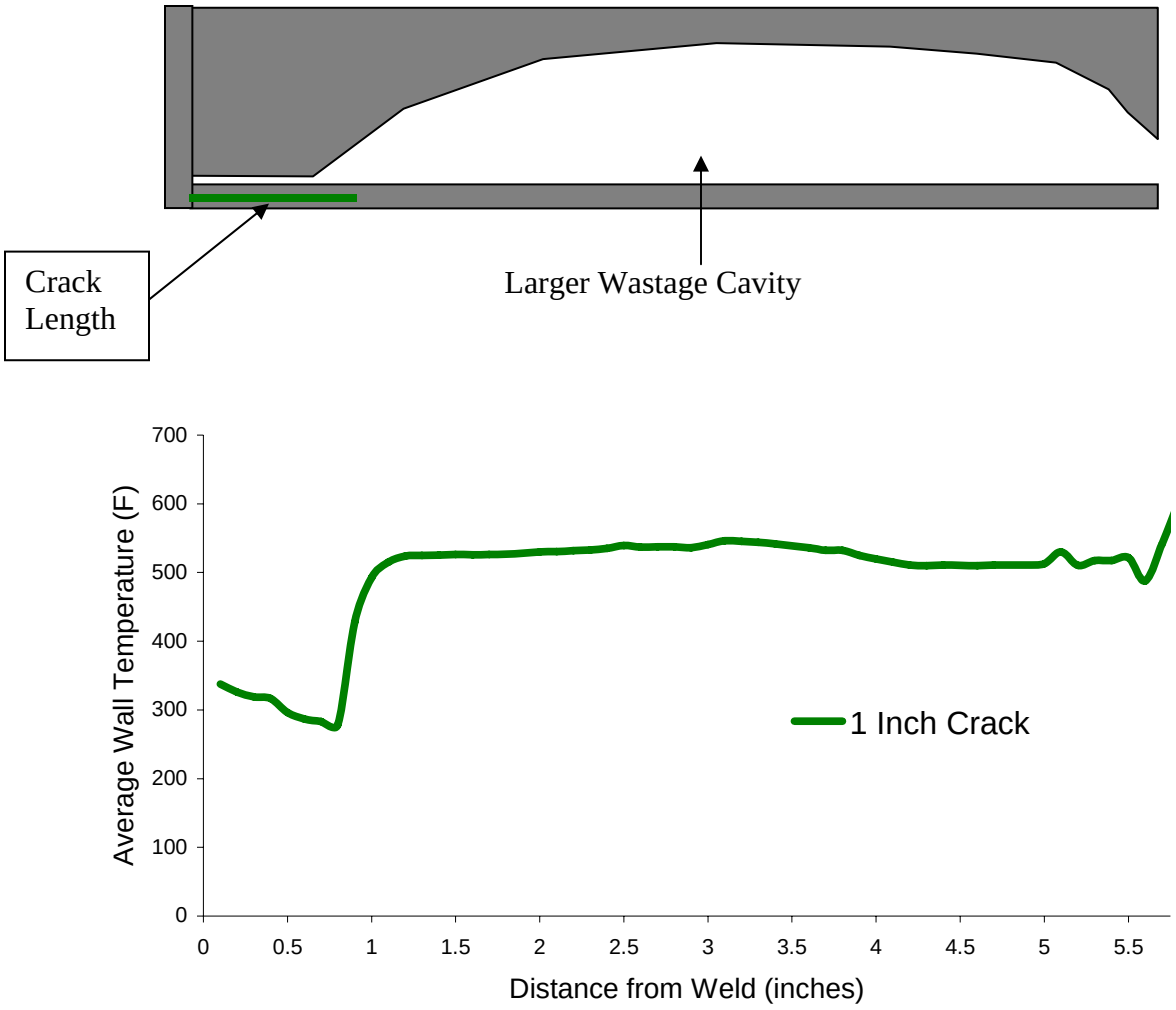

Figure C.27 Case 3: Average temperature within wastage as a function of distance to the J-groove weld for a 1.0-inch crack with a leak rate of 0.02 gpm.

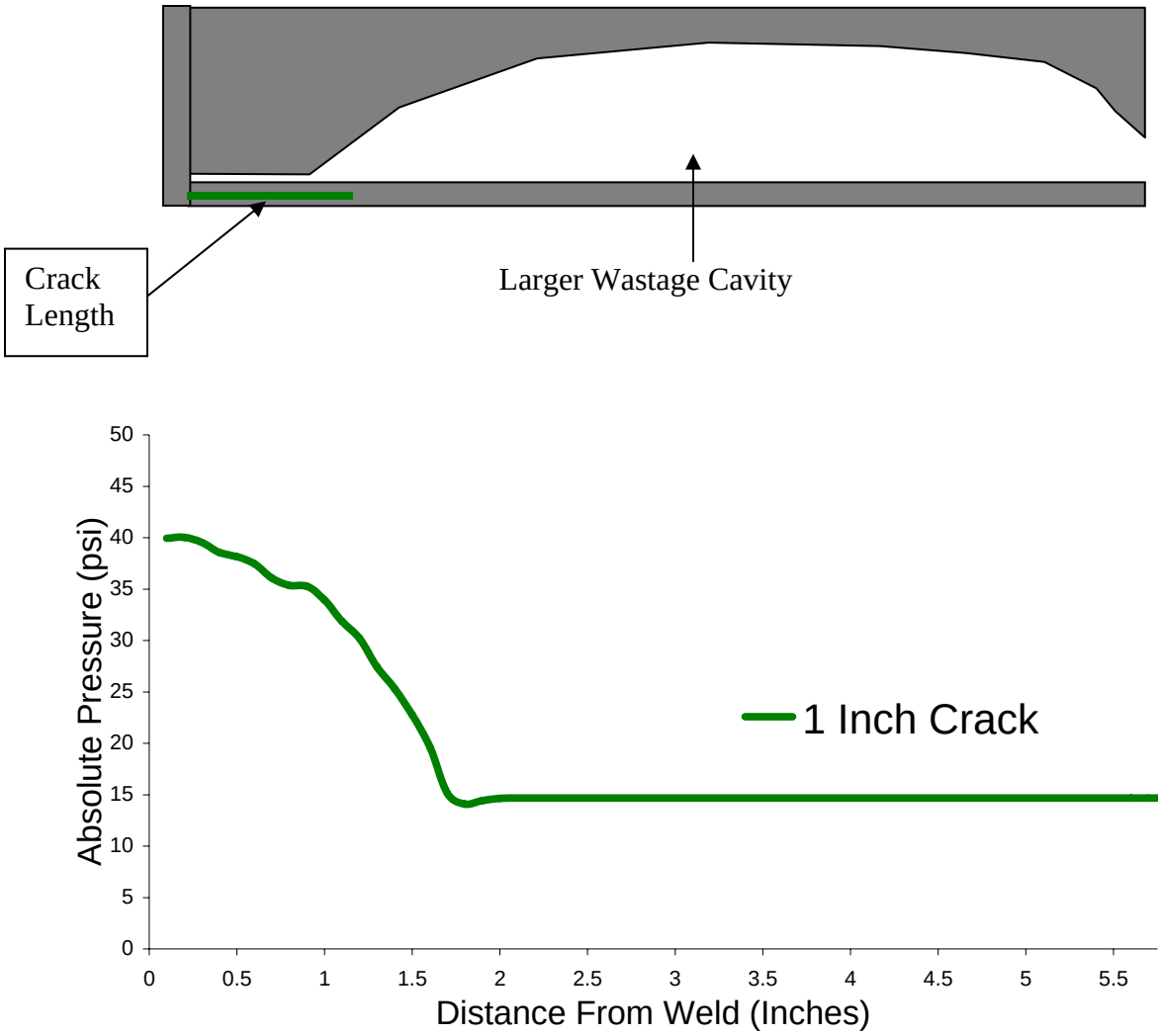

Figure C.28 Case 3: Average fluid pressure within wastage as a function of distance to the J-groove weld for a 1.0-inch crack with a leak rate of 0.02 gpm.

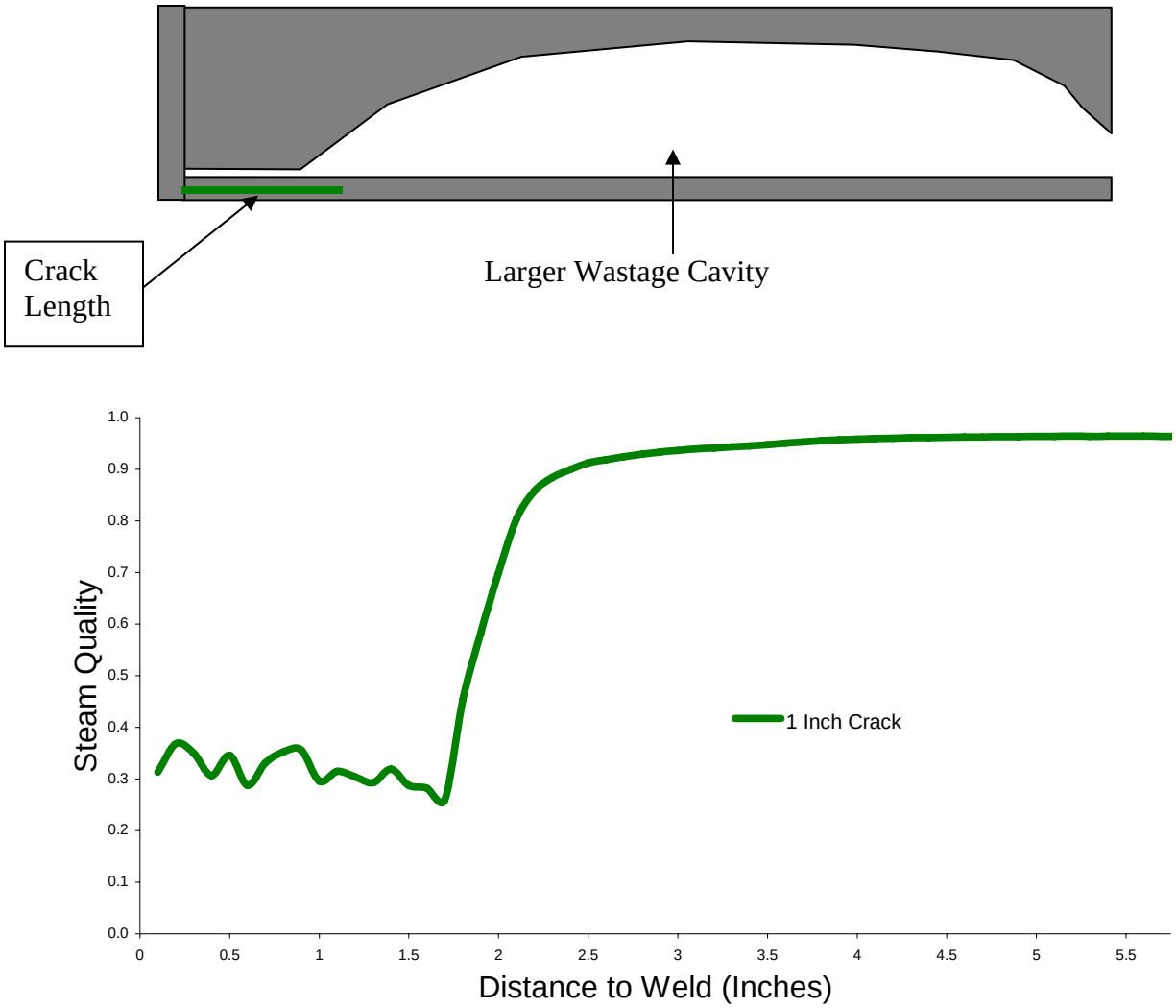

Figure C.29 Case 3: Average steam quality within wastage as a function of distance to the J-groove weld for a 1.0-inch crack with a leak rate of 0.02 gpm.

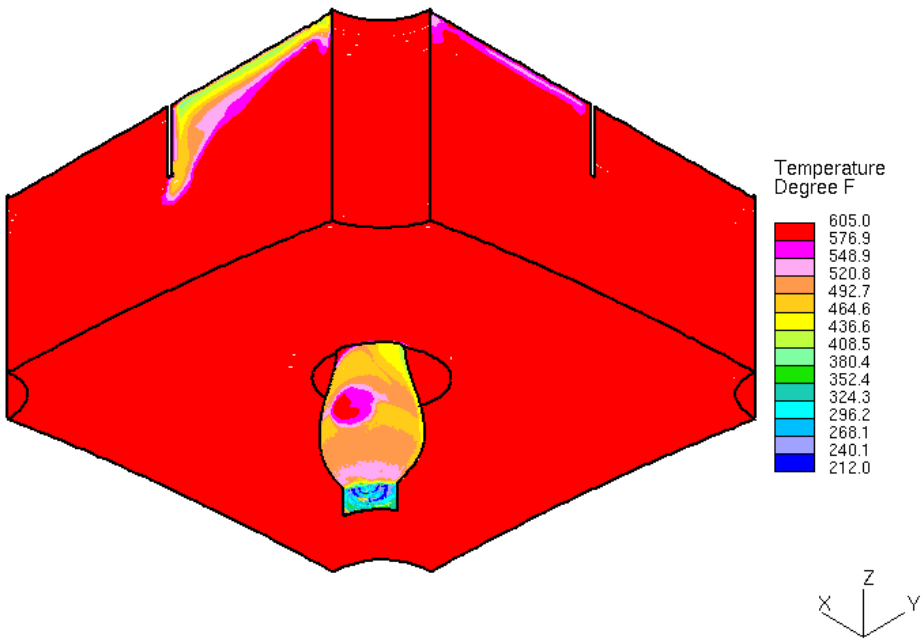

Figure C.30 Case 3: Surface/boundary temperature distribution.

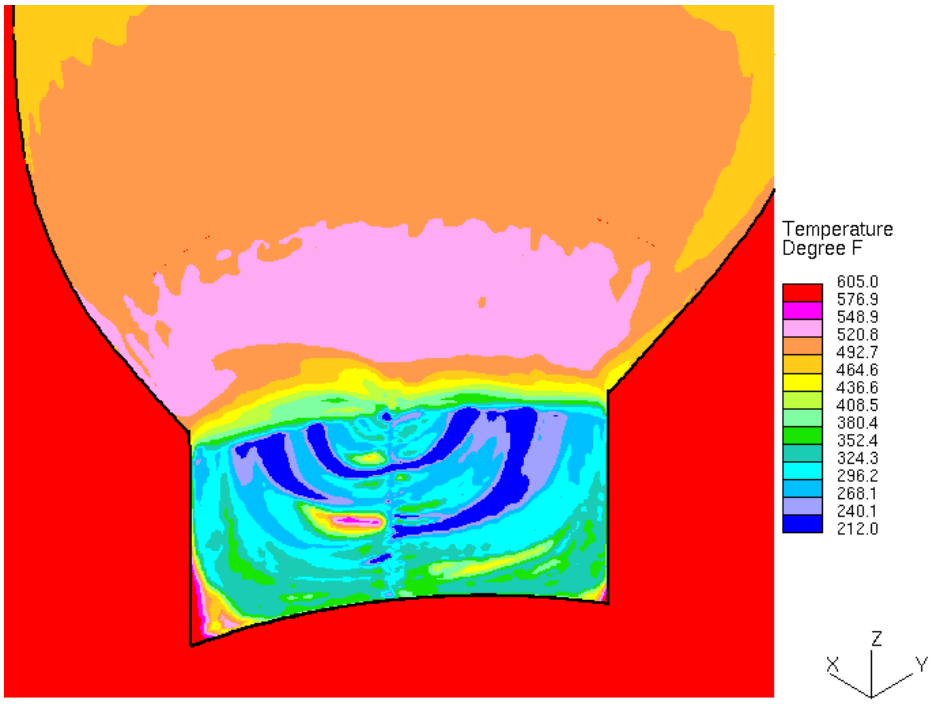

Figure C.31 Case 3: Surface/boundary temperature distribution.

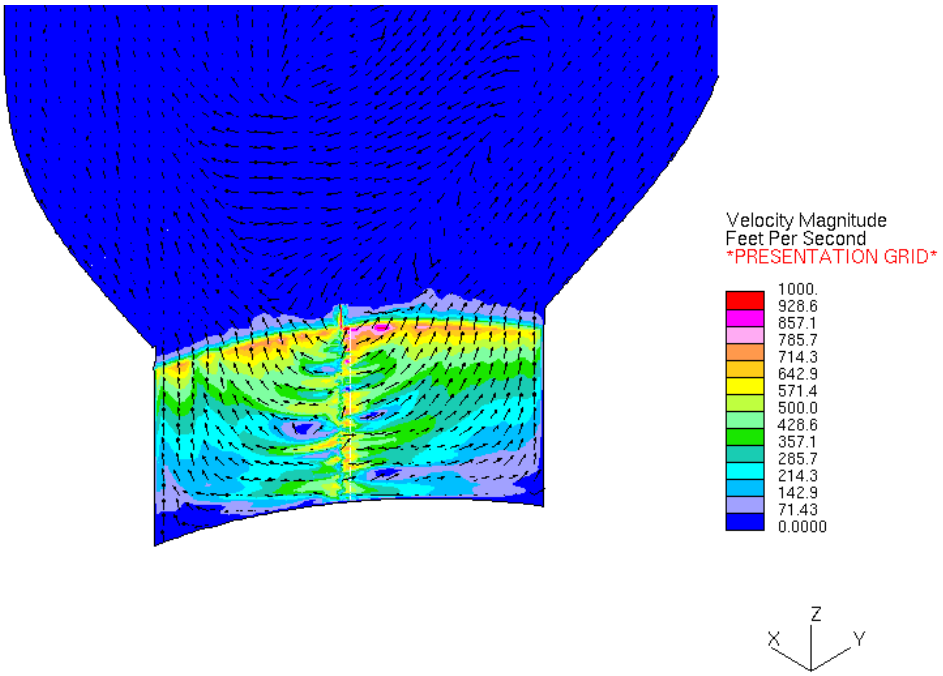

Figure C.32 Case 3: Velocity magnitude contour/vector profile at gap midsection.

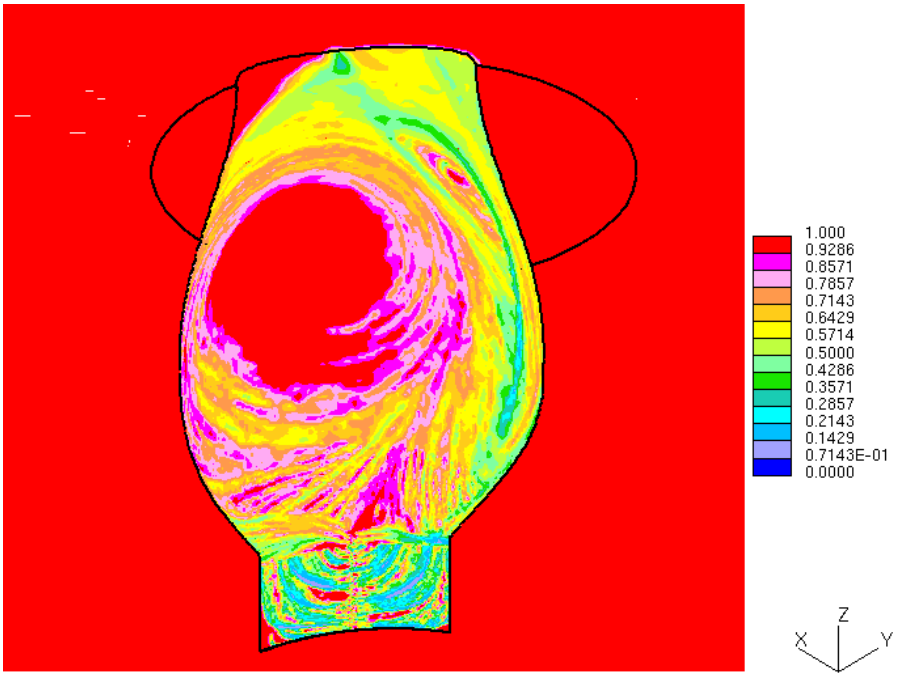

Figure C.33 Case 3: Steam quality near wastage surface.

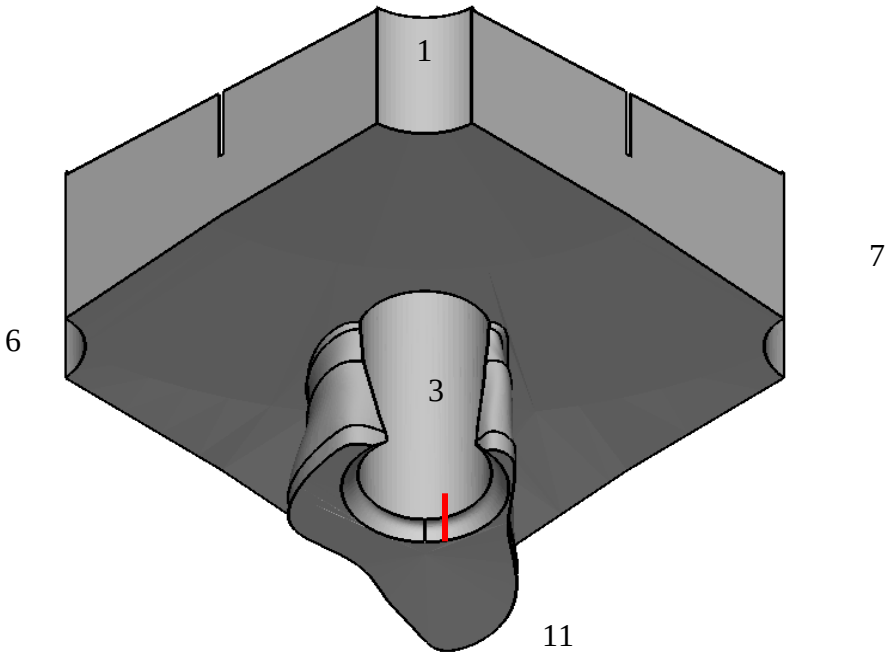

Figure C.34 Case 4: Fluid wastage geometry. Viewpoint is looking from below RPV head at the 180° location.

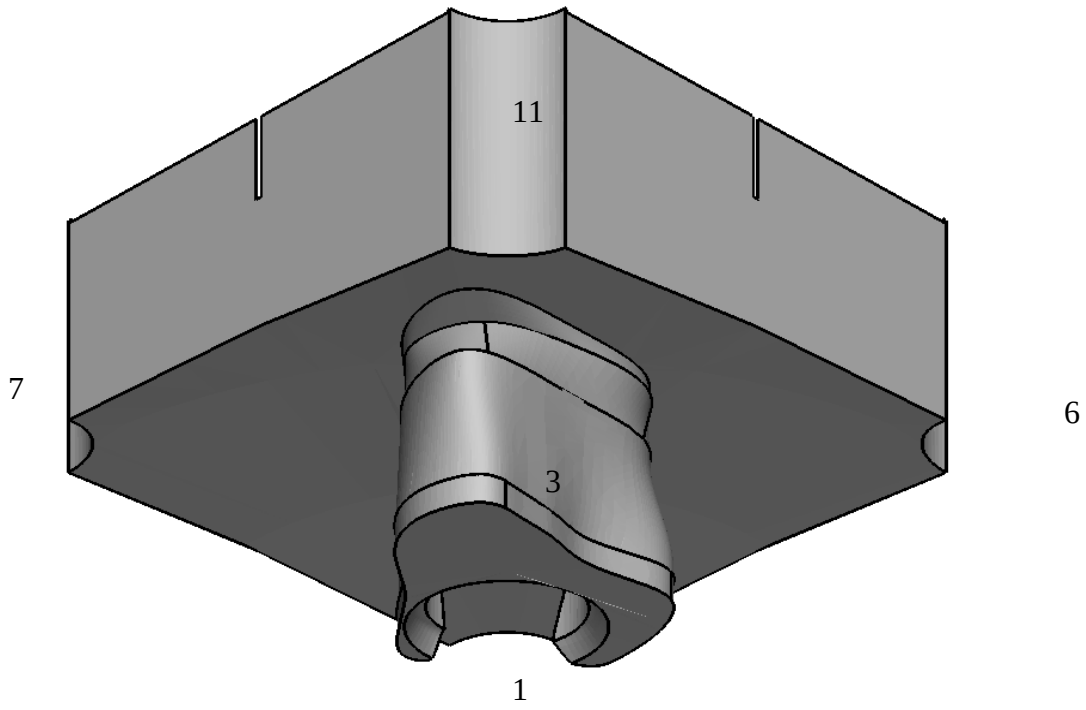

Figure C.35 Case 4: Fluid wastage geometry. Viewpoint is looking from below RPV head at the opposite side of the crack.

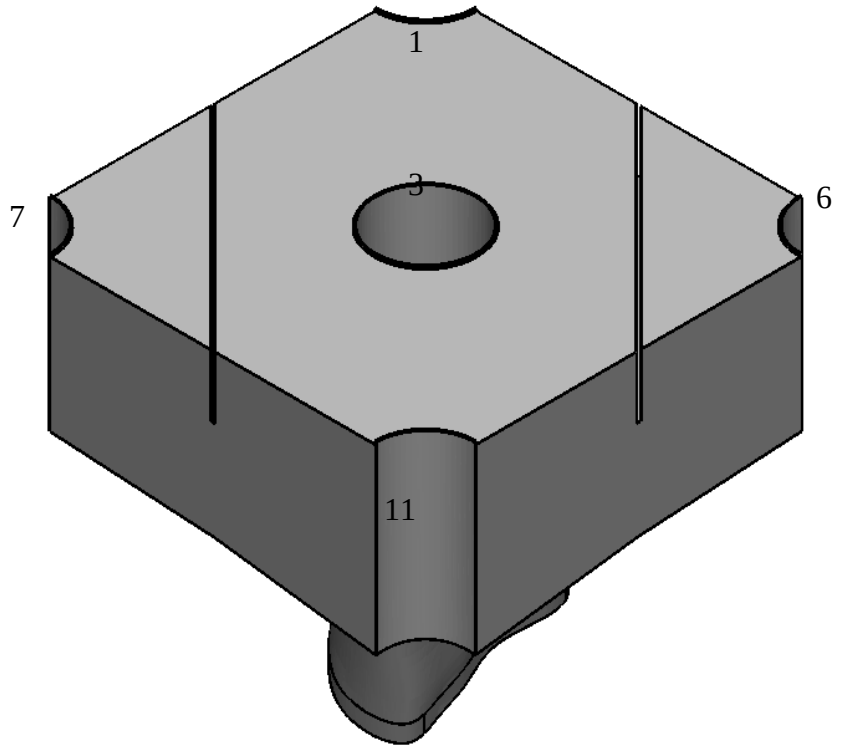

Figure C.36 Case 4: Fluid wastage geometry. Viewpoint is looking from above RPV head at the opposite side of the crack.

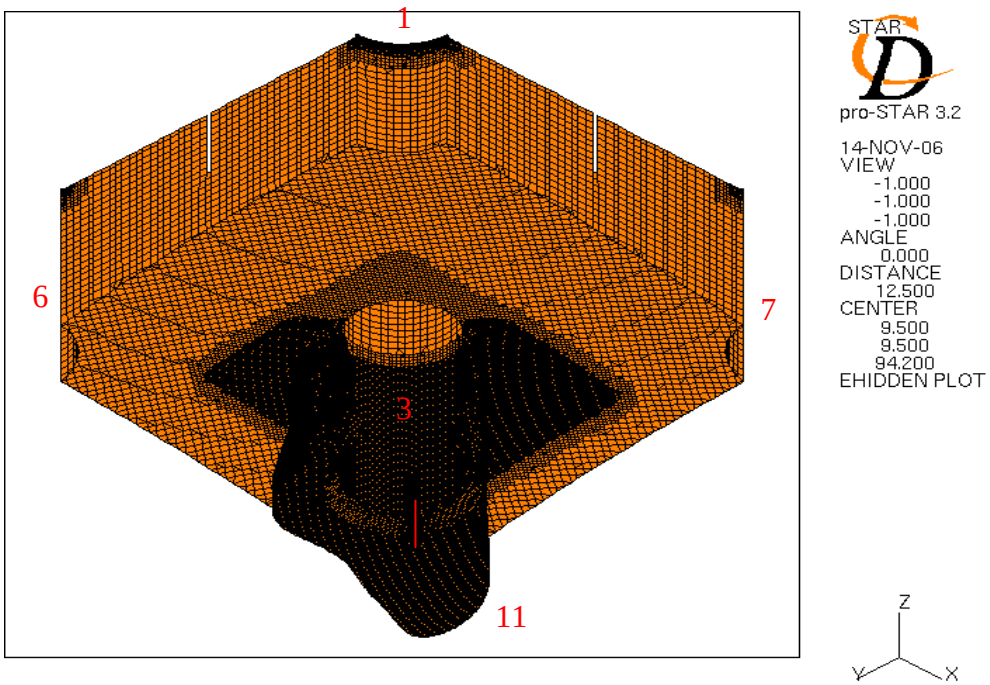

Figure C.37 Case 4: CFD mesh near CRDM nozzle 3 including final wastage. The red line denotes location of crack (10 degrees from CRDM nozzle 11 to 7). Viewpoint is looking from below the RPV head at the crack.

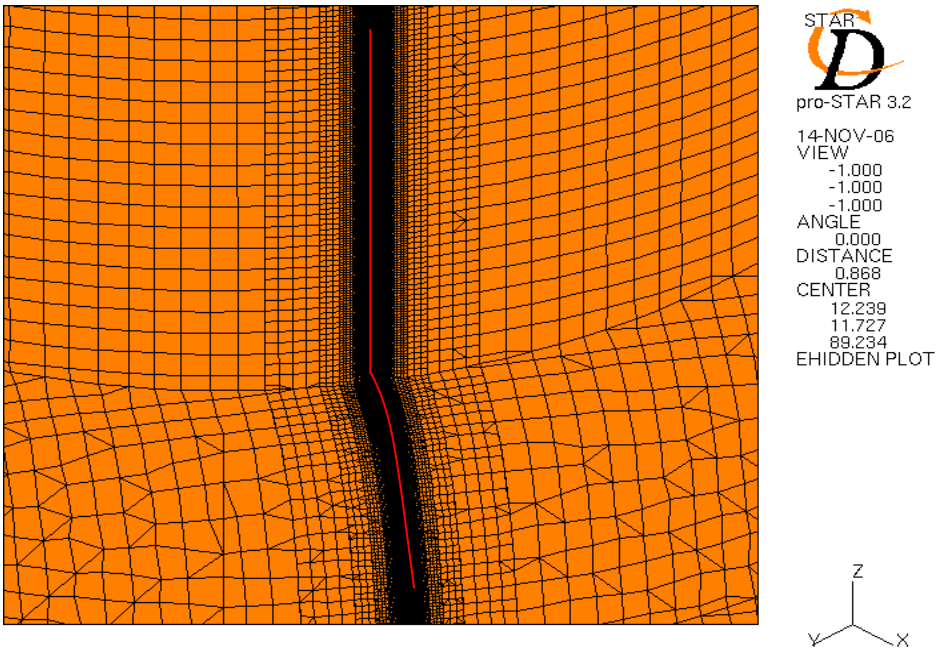

Figure C.38 Case 4: CFD mesh refinement near CRDM nozzle 3 crack. Viewpoint is looking from below the RPV head at the crack.

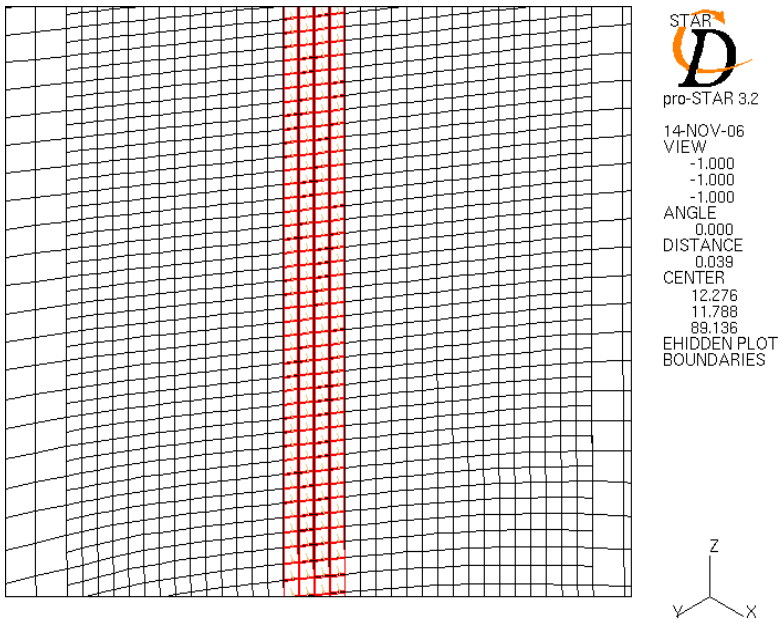

Figure C.39 Case 4: CFD mesh refinement at CRDM nozzle 3 crack. The red faces denote location of crack. Viewpoint is looking from below the RPV head at the crack.

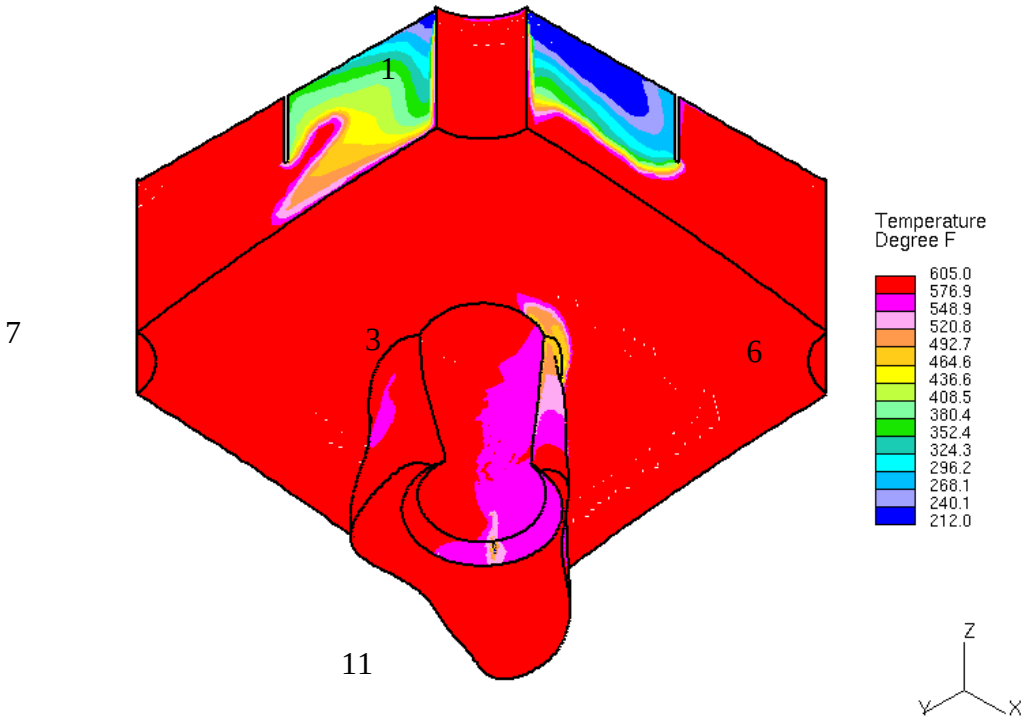

Figure C.40 Case 4: Final wastage state surface/boundary temperature distribution near CRDM nozzle 3 crack. Viewpoint is looking from below the RPV head at the crack.

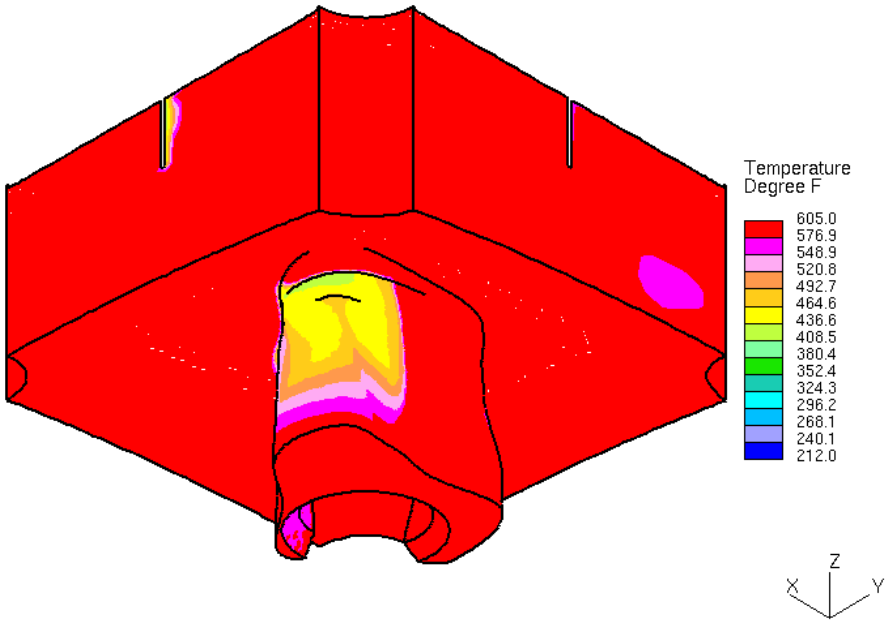

Figure C.41 Case 4: Final wastage state surface/boundary temperature distribution near CRDM nozzle 3 crack. Viewpoint is looking from below the RPV head at opposite side of crack.

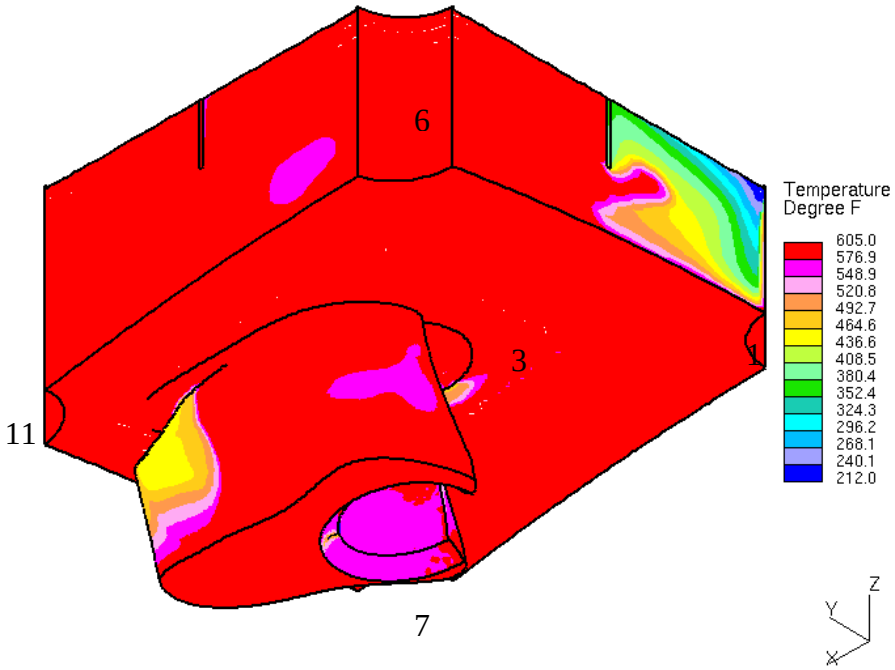

Figure C.42 Case 4: Final wastage state surface/boundary temperature distribution near CRDM nozzle 3 crack. Viewpoint is looking from below the RPV head on the side of the crack.

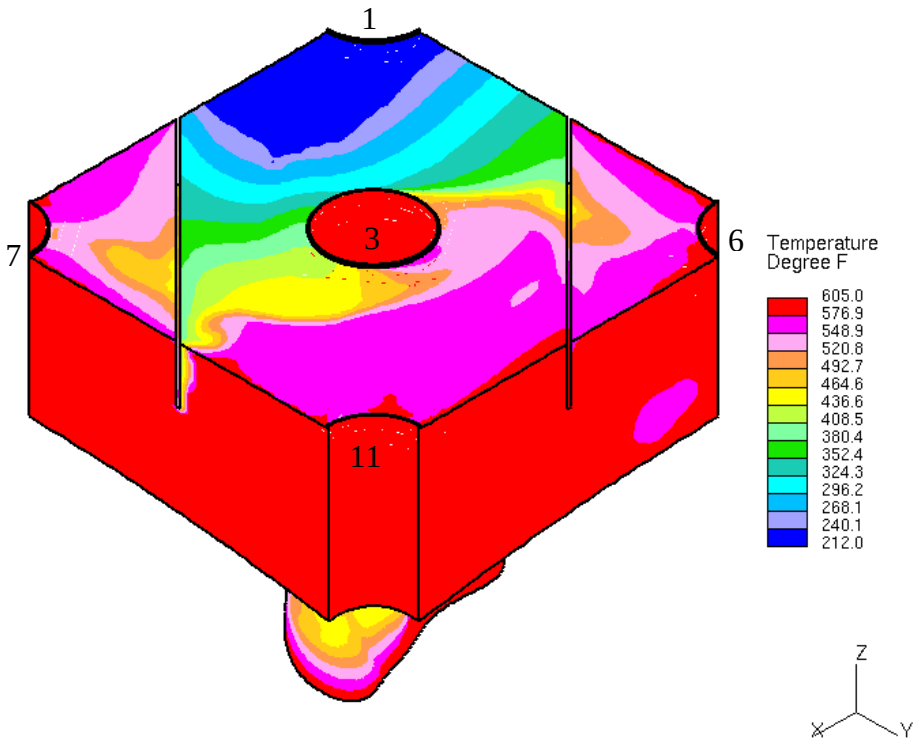

Figure C.43 Case 4: Final wastage state surface/boundary temperature distribution near CRDM nozzle 3 crack. Viewpoint is looking from above the RPV head at the opposite side of the crack.

Figure C.44 Case 4: Temperature contour plot through a section of final wastage fluid volume. Viewpoint is looking from below the RPV head on the side of the crack.

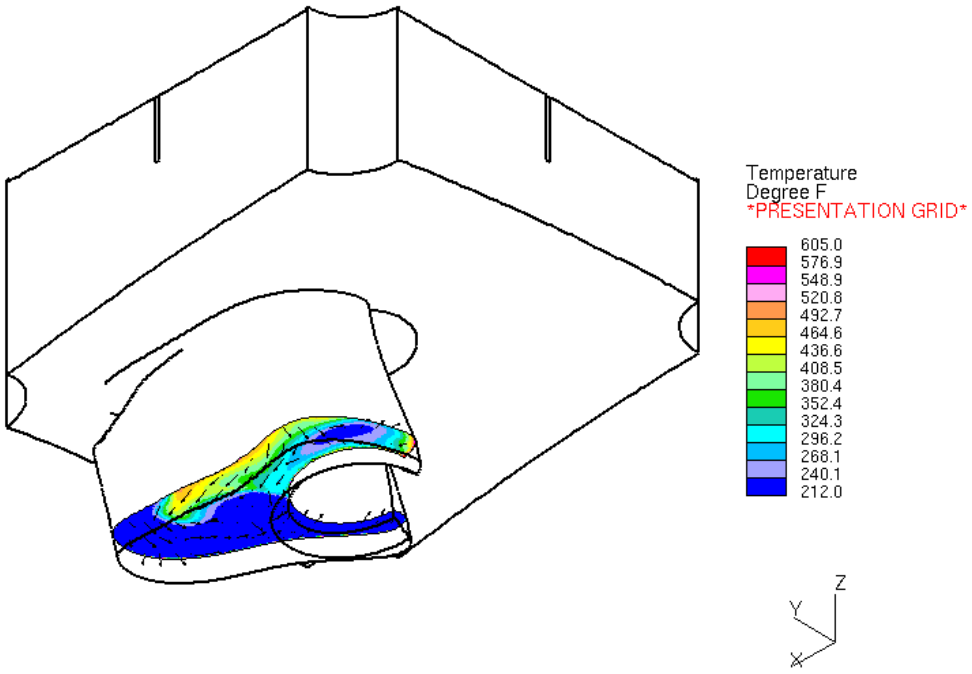

Figure C.45 Case 4: Temperature contour plot through a section of final wastage fluid volume. Viewpoint is looking from below the RPV head on the side of the crack.

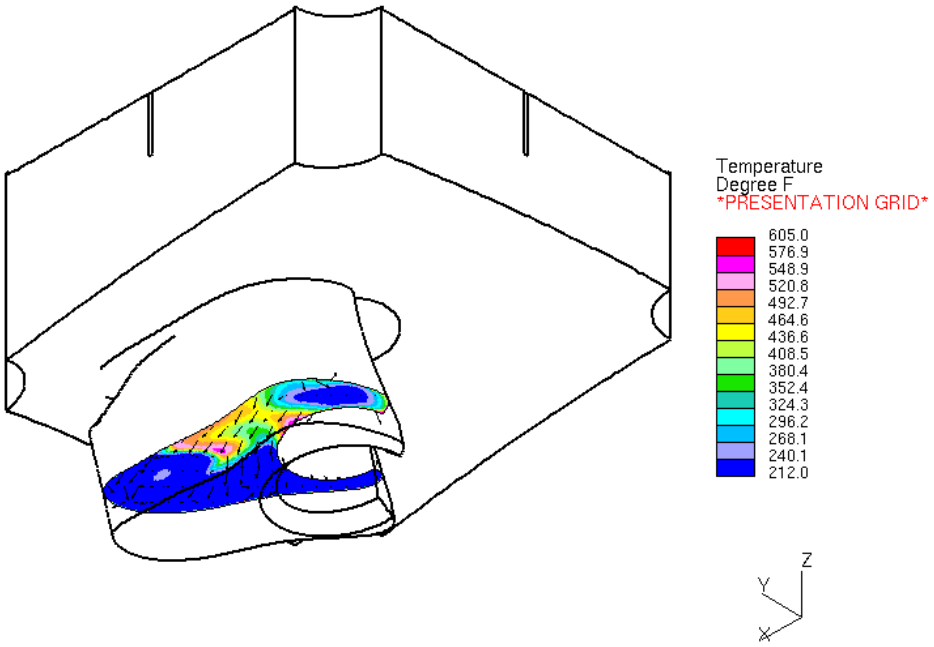

Figure C.46 Case 4: Temperature contour plot through a section of final wastage fluid volume. Viewpoint is looking from below the RPV head on the side of the crack.

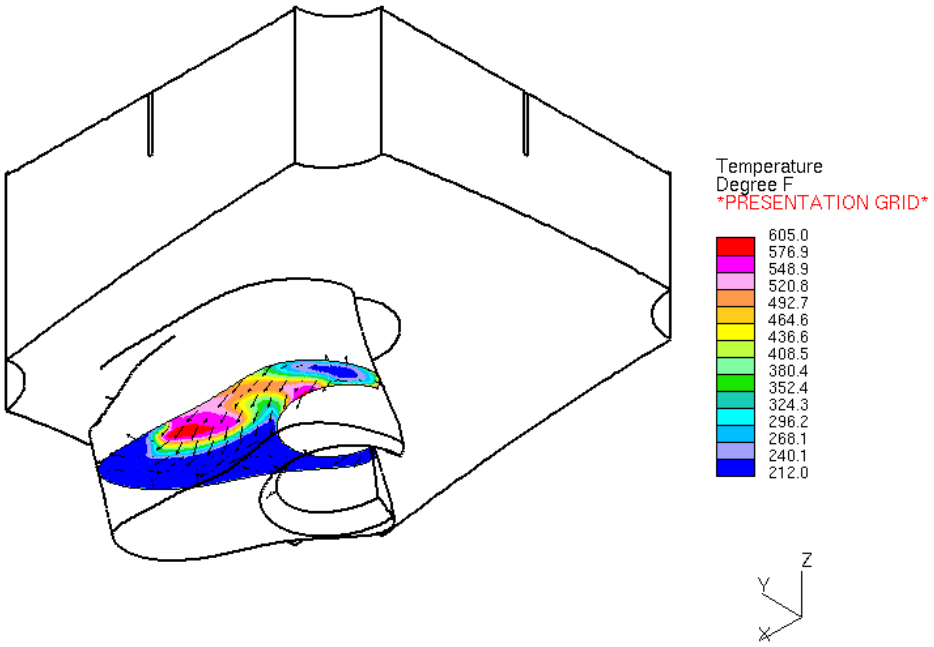

Figure C.47. Case 4: Temperature contour plot through a section of final wastage fluid volume. Viewpoint is looking from below the RPV head on the side of the crack.

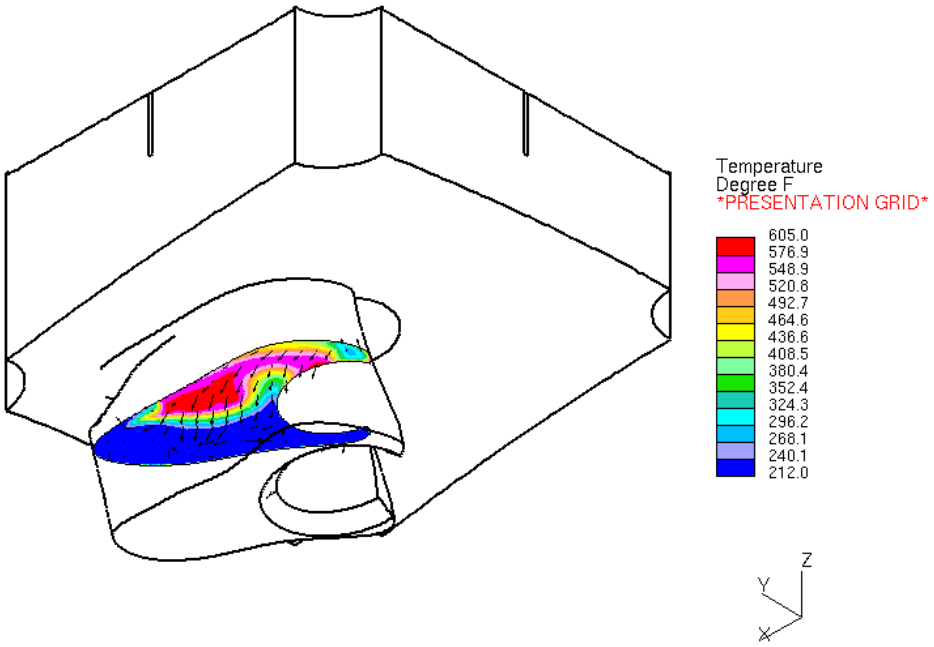

Figure C.48 Case 4: Temperature contour plot through a section of final wastage fluid volume. Viewpoint is looking from below the RPV head on the side of the crack.

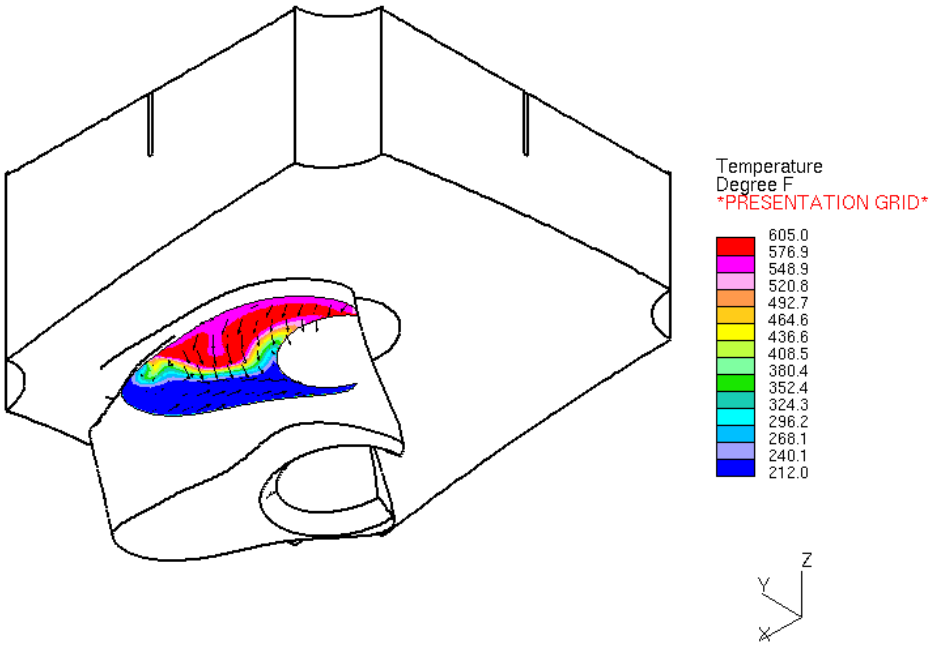

Figure C.49 Case 4: Temperature contour plot through a section of final wastage fluid volume. Viewpoint is looking from below the RPV head on the side of the crack.

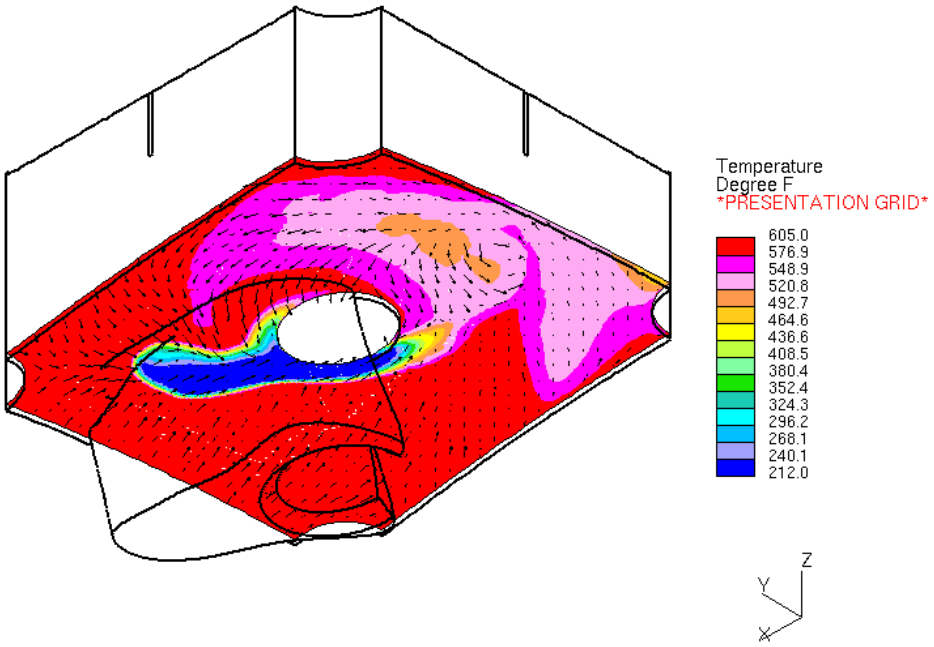

Figure C.50 Case 4: Temperature contour plot through a section above final wastage fluid volume. Viewpoint is looking from below the RPV head on the side of the crack.

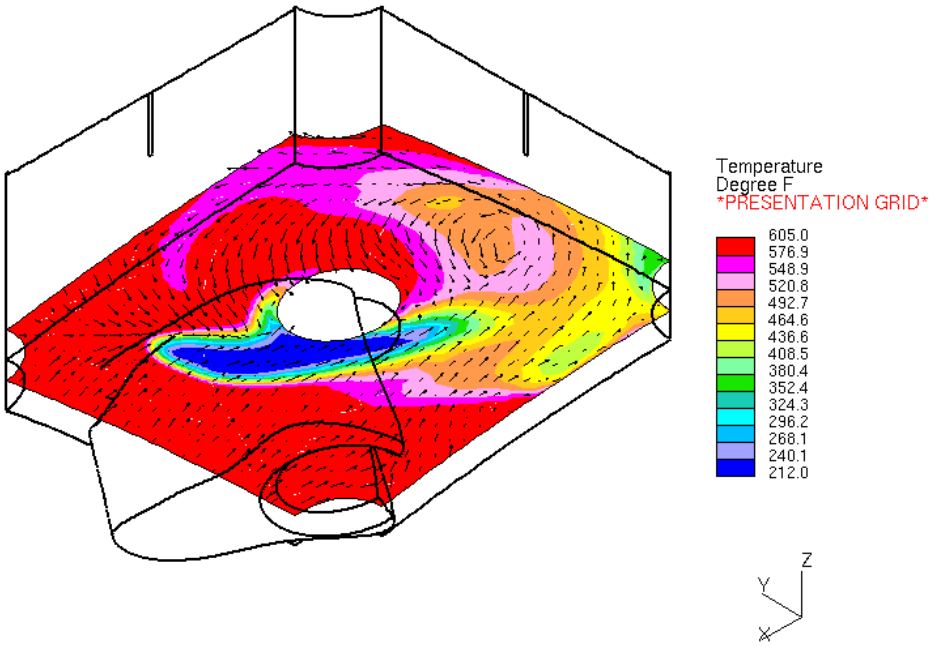

Figure C.51 Case 4: Temperature contour plot through a section above final wastage fluid volume. Viewpoint is looking from below the RPV head on the side of the crack.

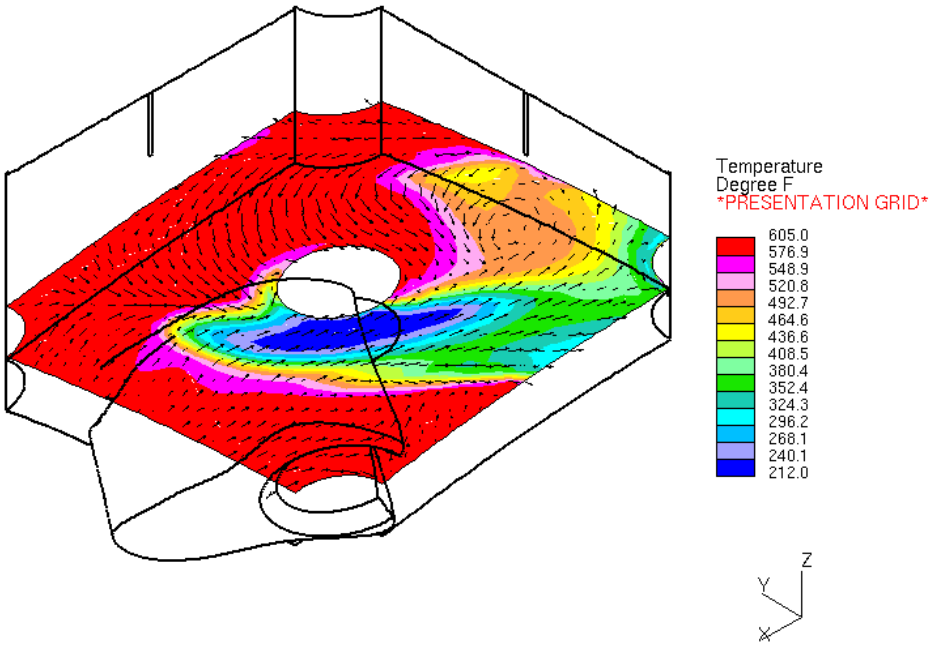

Figure C.52 Case 4: Temperature contour plot through a section above final wastage fluid volume. Viewpoint is looking from below the RPV head on the side of the crack.

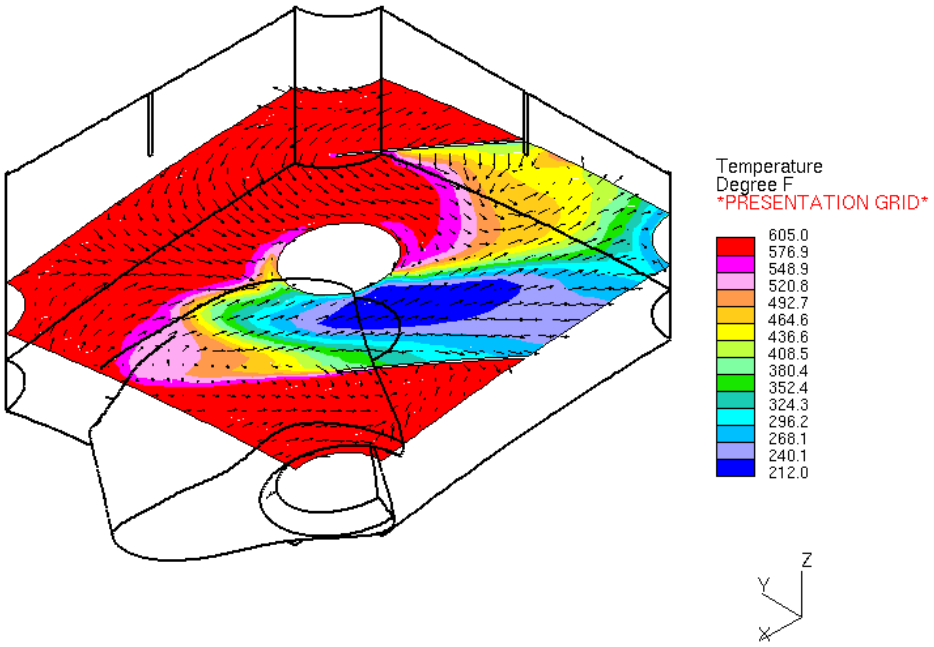

Figure C.53 Case 4: Temperature contour plot through a section above final wastage fluid volume. Viewpoint is looking from below the RPV head on the side of the crack.

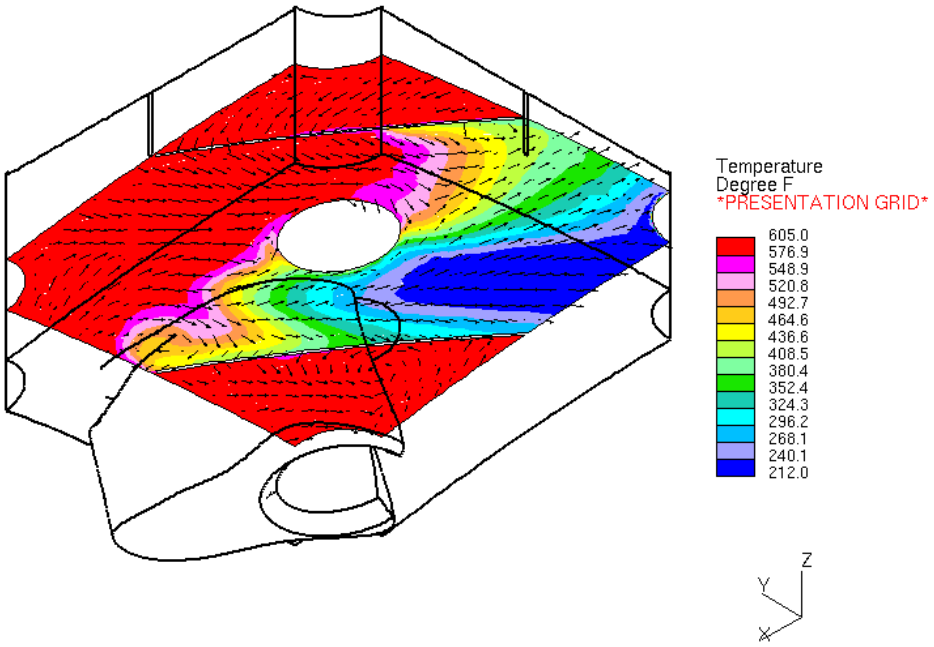

Figure C.54 Case 4: Temperature contour plot through a section above final wastage fluid volume. Viewpoint is looking from below the RPV head on the side of the crack.

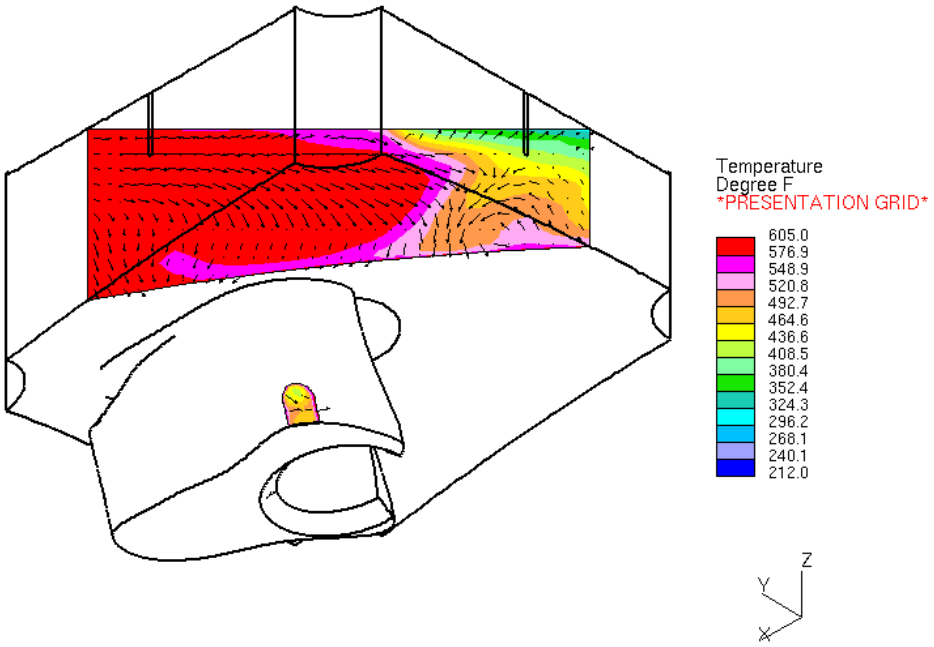

Figure C.55 Case 4: Temperature contour plot through a section of final wastage fluid volume. Viewpoint is looking from below the RPV head on the side of the crack.

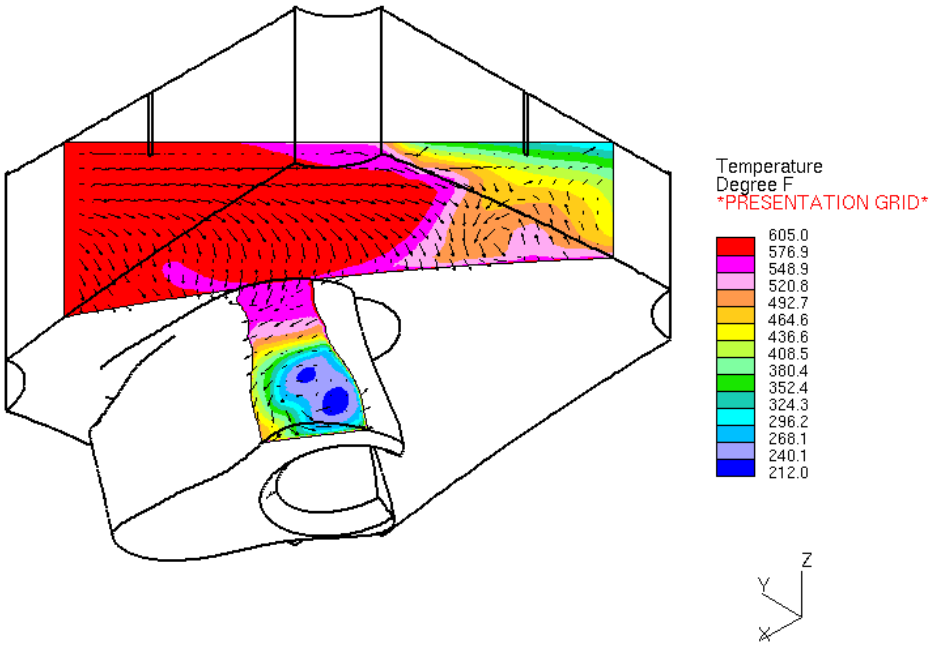

Figure C.56 Case 4: Temperature contour plot through a section of final wastage fluid volume. Viewpoint is looking from below the RPV head on the side of the crack.

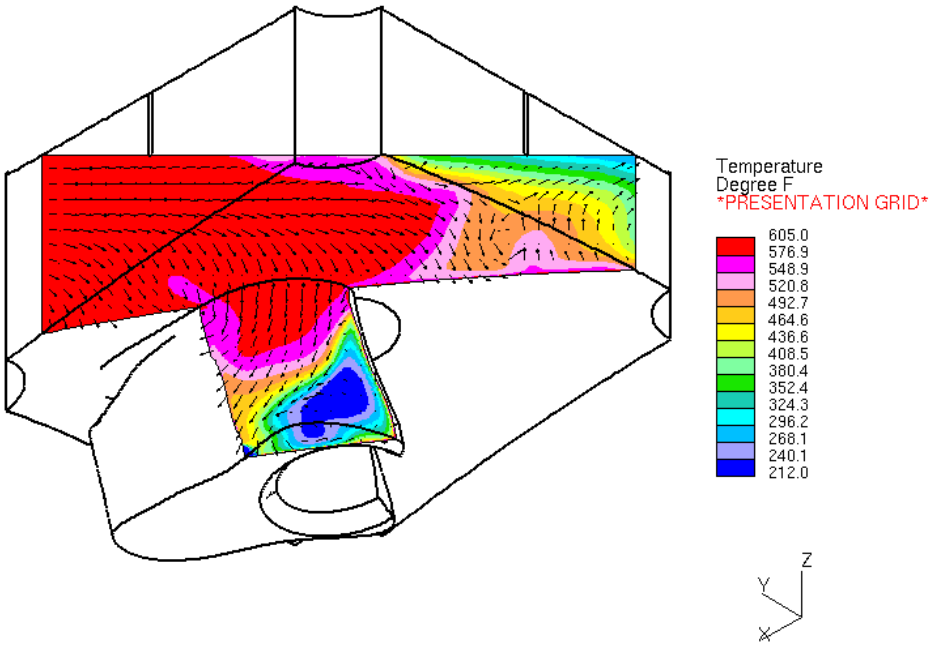

Figure C.57 Case 4: Temperature contour plot through a section of final wastage fluid volume. Viewpoint is looking from below the RPV head on the side of the crack.

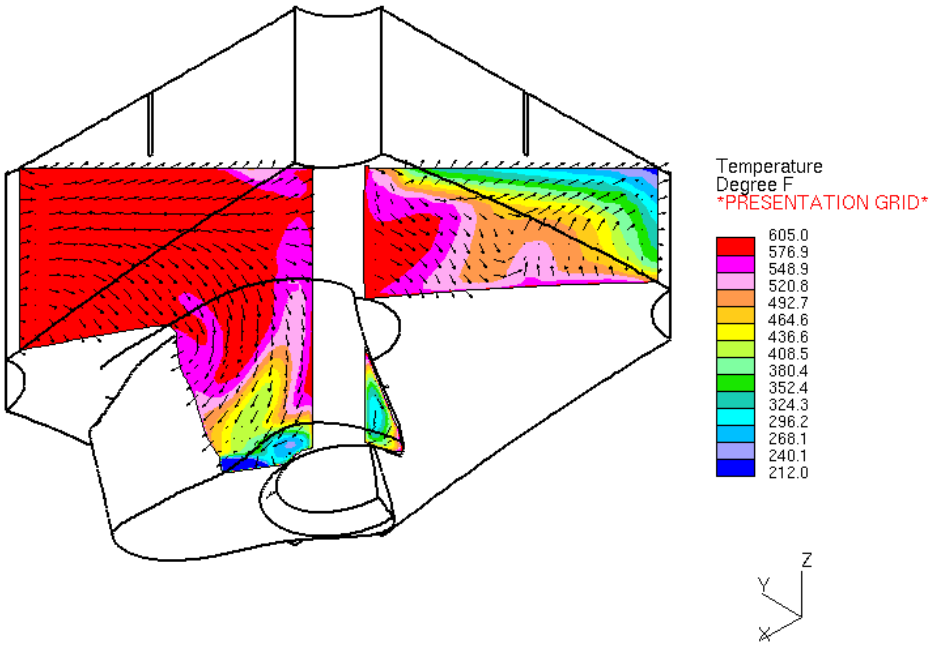

Figure C.58 Case 4: Temperature contour plot through a section of final wastage fluid volume. Viewpoint is looking from below the RPV head on the side of the crack.

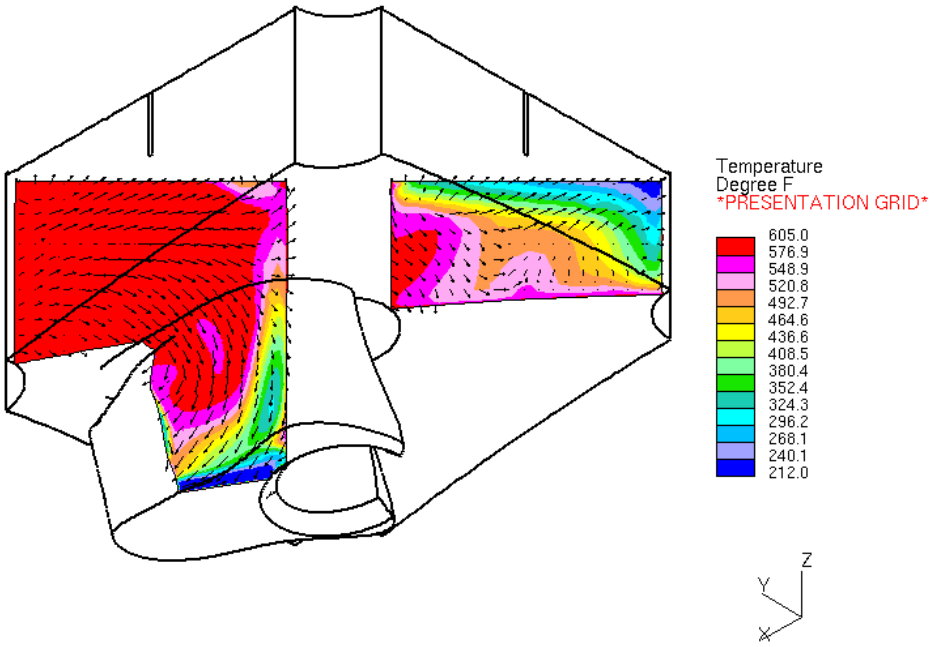

Figure C.59 Case 4: Temperature contour plot through a section of final wastage fluid volume. Viewpoint is looking from below the RPV head on the side of the crack.

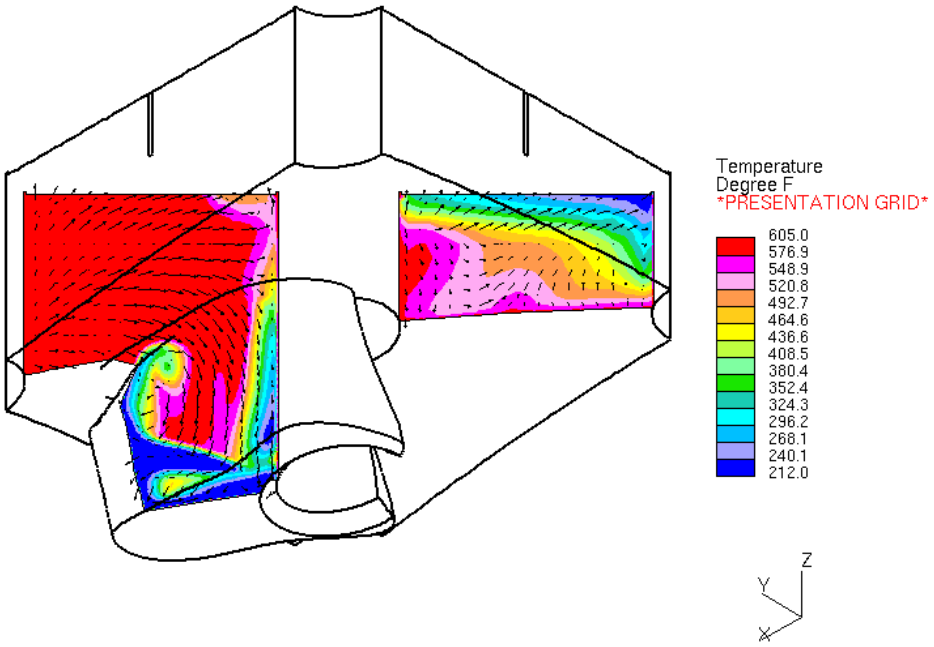

Figure C.60 Case 4: Temperature contour plot through a section of final wastage fluid volume. Viewpoint is looking from below the RPV head on the side of the crack.

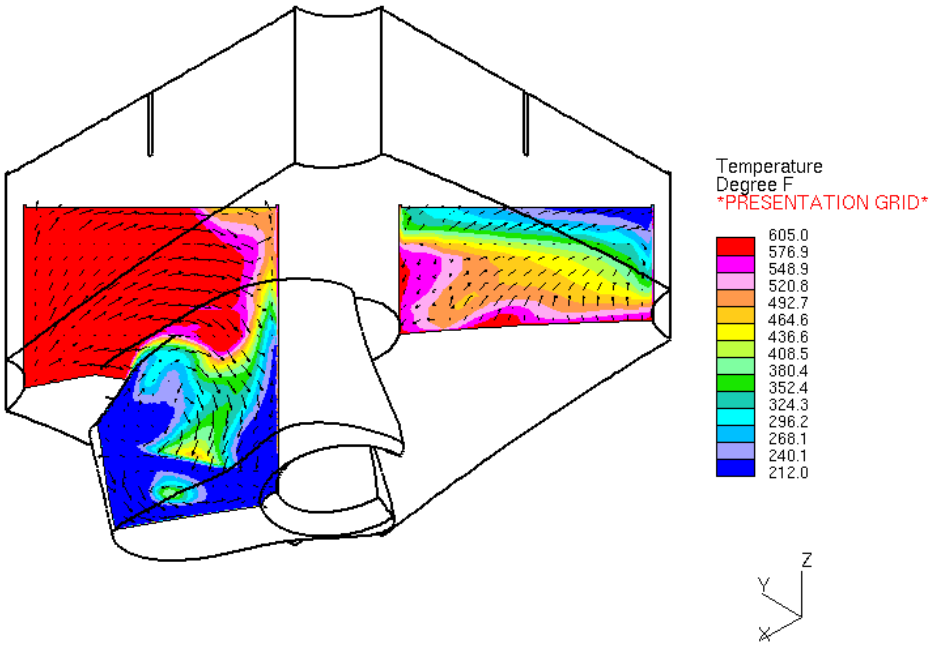

Figure C.61 Case 4: Temperature contour plot through a section of final wastage fluid volume. Viewpoint is looking from below the RPV head on the side of the crack.

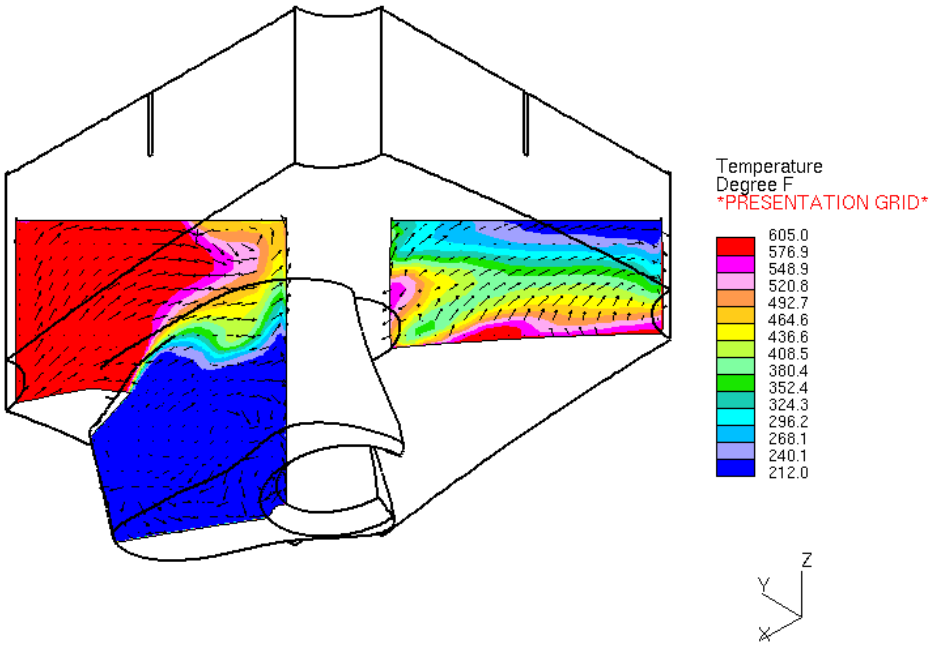

Figure C.62 Case 4: Temperature contour plot through a section of final wastage fluid volume. Viewpoint is looking from below the RPV head on the side of the crack.

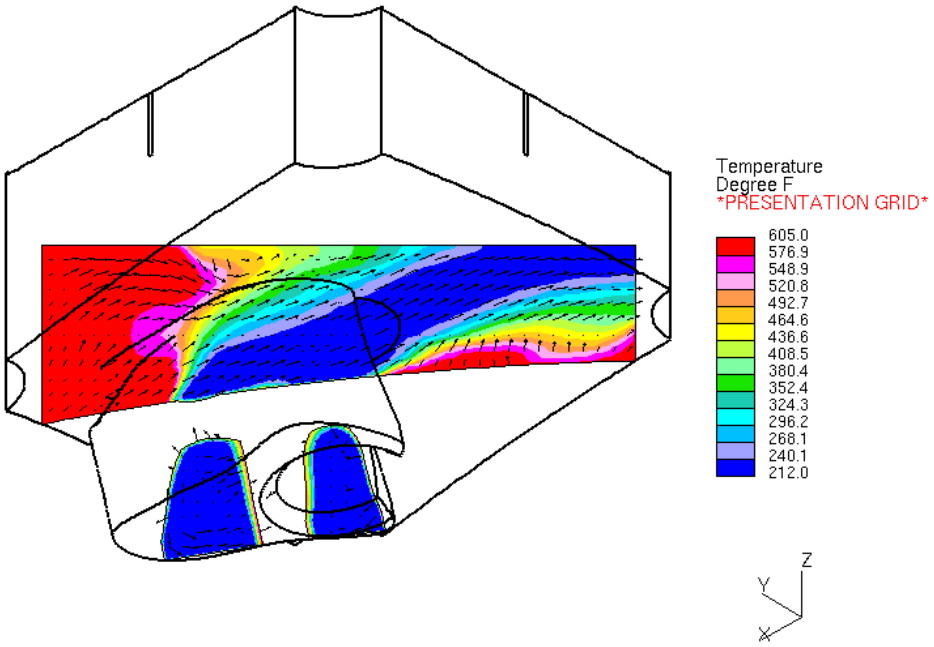

Figure C.63 Case 4: Temperature contour plot through a section of final wastage fluid volume. Viewpoint is looking from below the RPV head on the side of the crack.

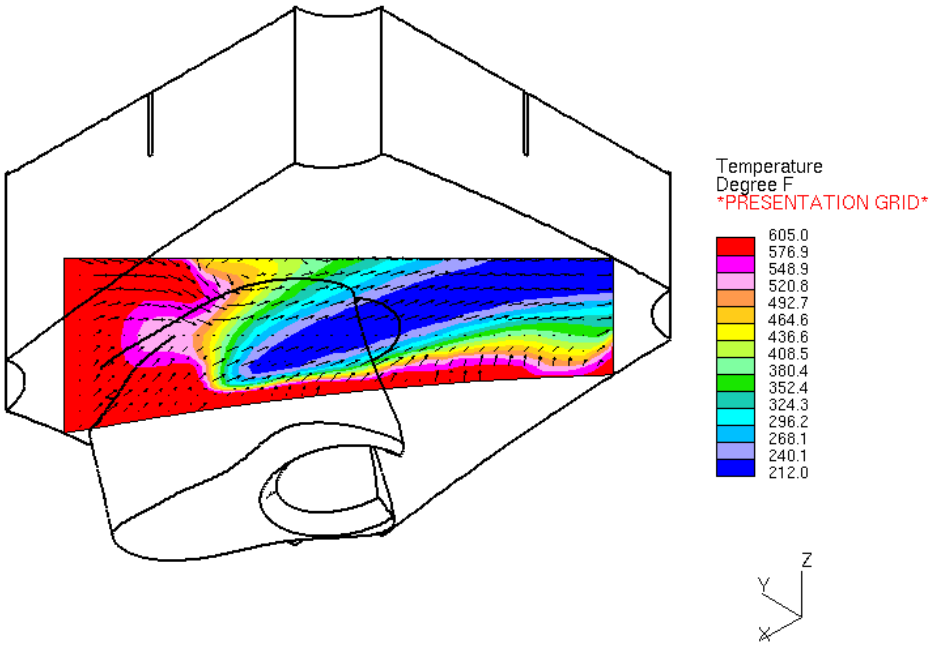

Figure C.64 Case 4: Temperature contour plot through a section of final wastage fluid volume. Viewpoint is looking from below the RPV head on the side of the crack.

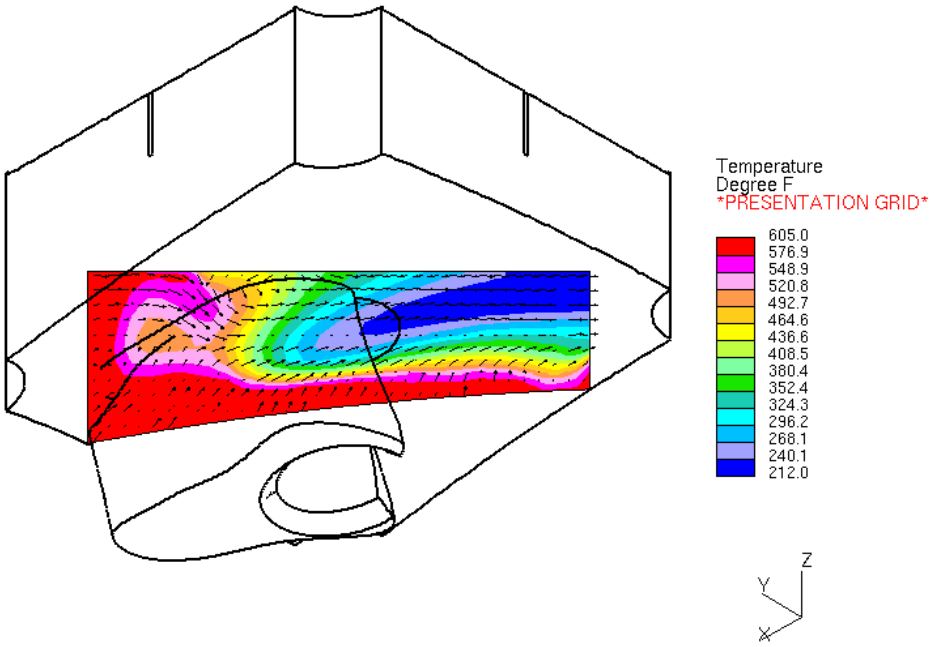

Figure C.65 Case 4: Temperature contour plot through a section of final wastage fluid volume. Viewpoint is looking from below the RPV head on the side of the crack.

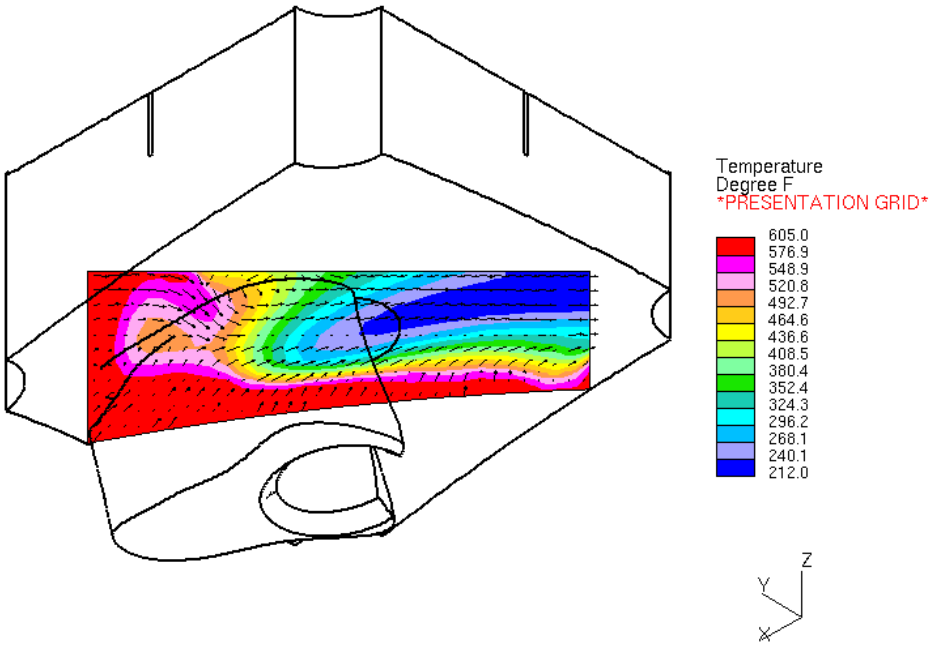

Figure C.66 Case 4: Temperature contour plot through a section of final wastage fluid volume. Viewpoint is looking from below the RPV head on the side of the crack.

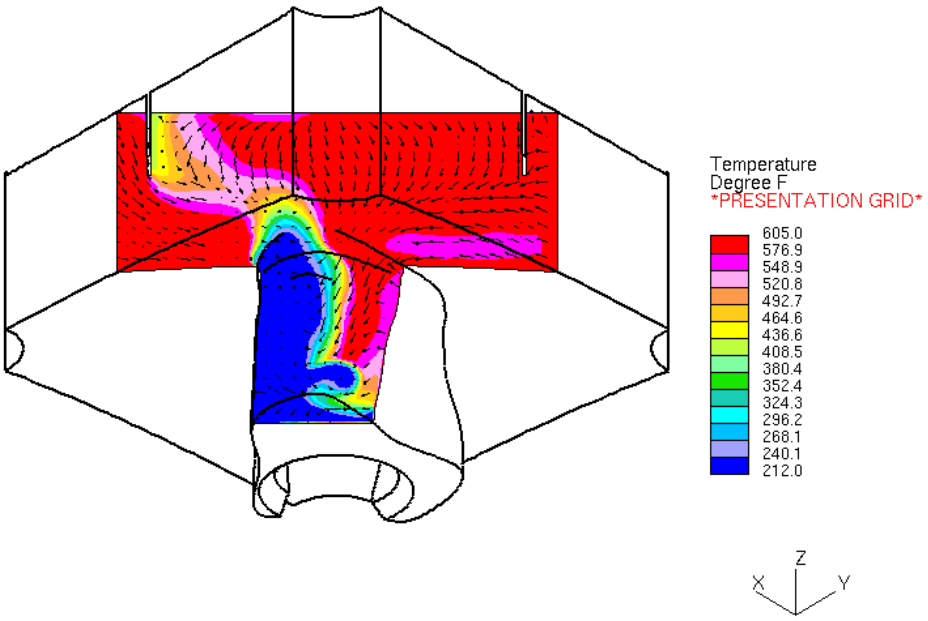

Figure C.67 Case 4: Temperature contour plot through a section of final wastage fluid volume. Viewpoint is looking from below the RPV head at the opposite side of the crack.

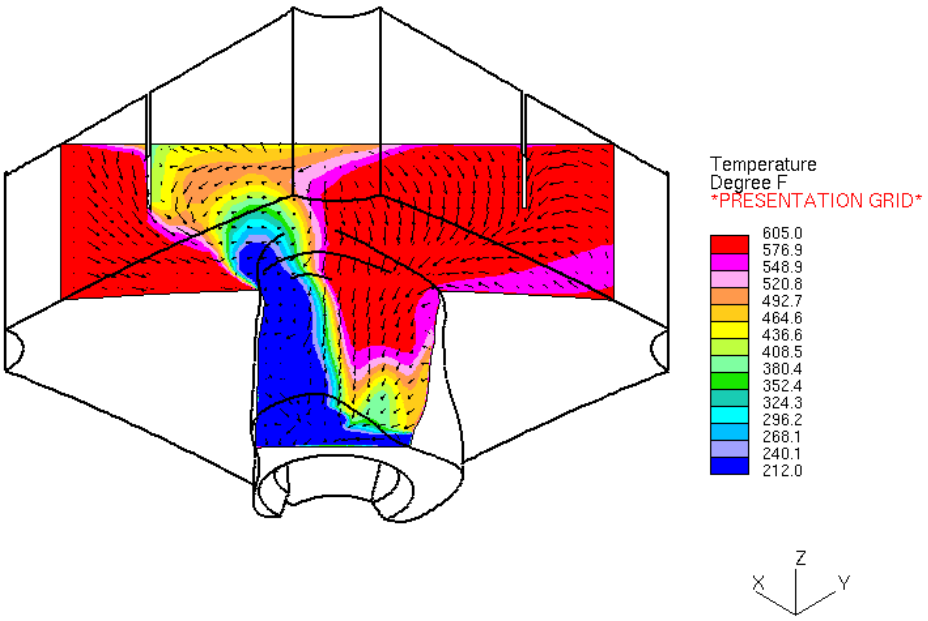

Figure C.68 Case 4: Temperature contour plot through a section of final wastage fluid volume. Viewpoint is looking from below the RPV head at the opposite side of the crack.

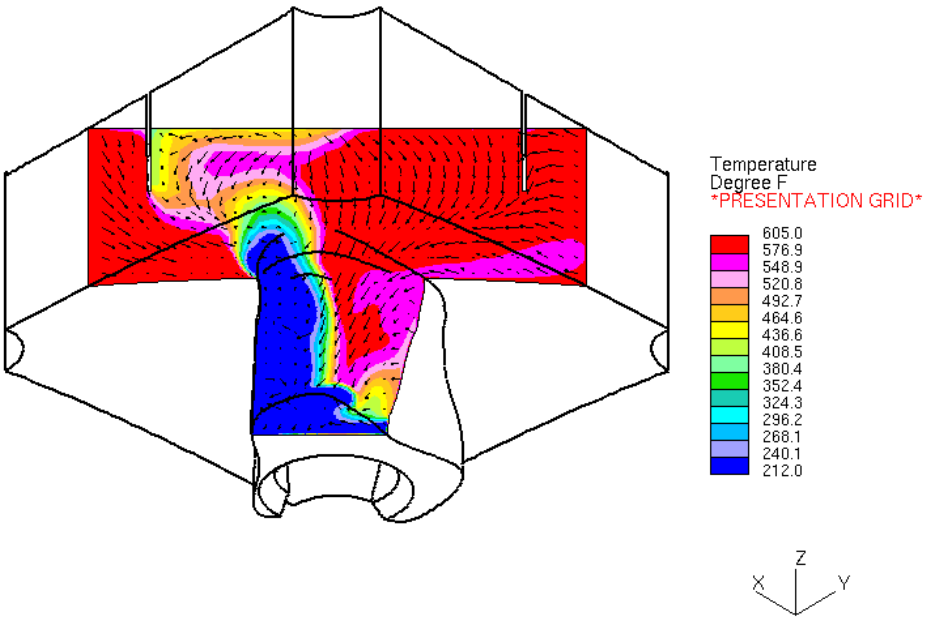

Figure C.69 Case 4: Temperature contour plot through a section of final wastage fluid volume. Viewpoint is looking from below the RPV head at the opposite side of the crack.

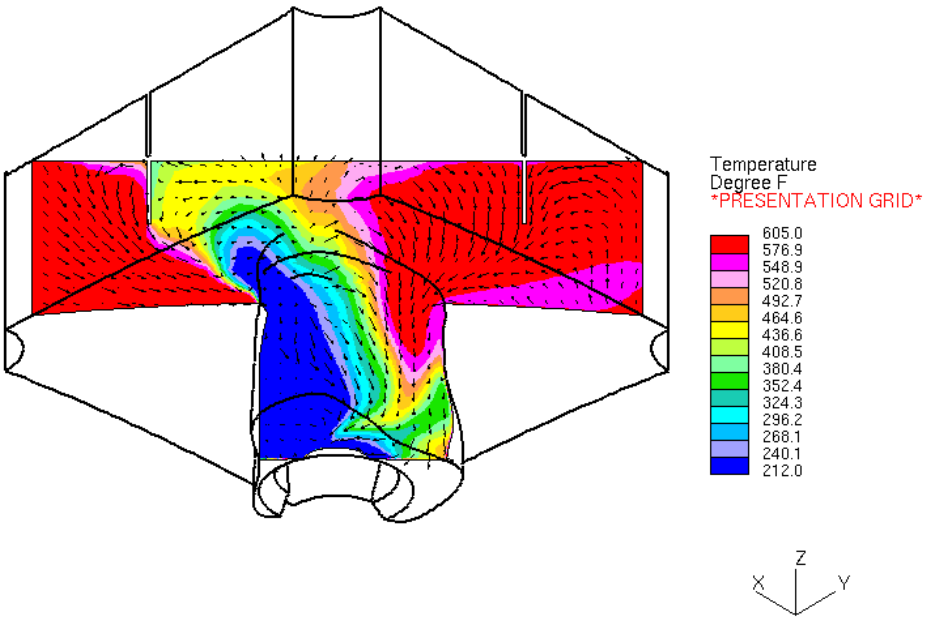

Figure C.70 Case 4: Temperature contour plot through a section of final wastage fluid volume. Viewpoint is looking from below the RPV head at the opposite side of the crack.

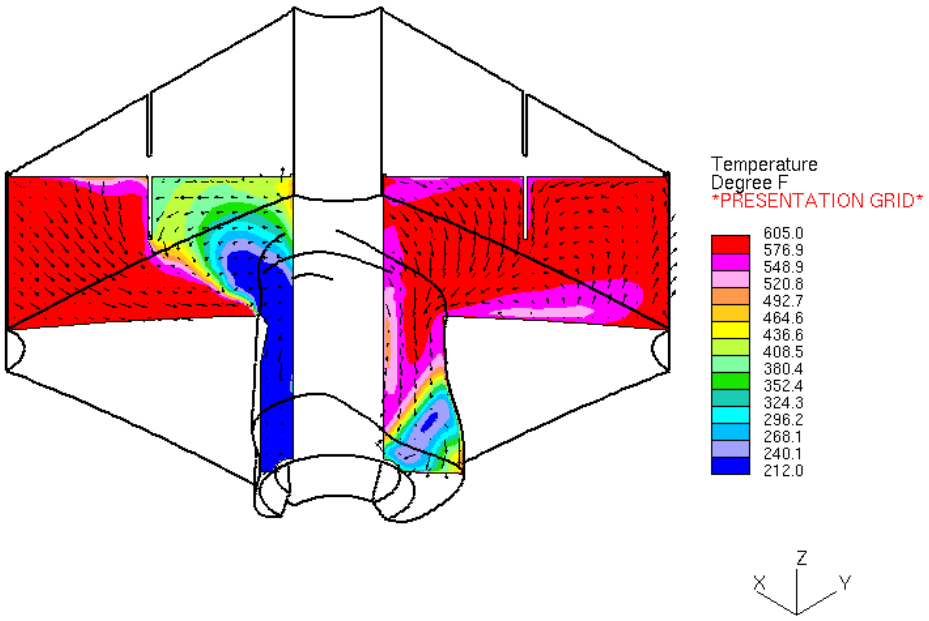

Figure C.71 Case 4: Temperature contour plot through a section of final wastage fluid volume. Viewpoint is looking from below the RPV head at the opposite side of the crack.

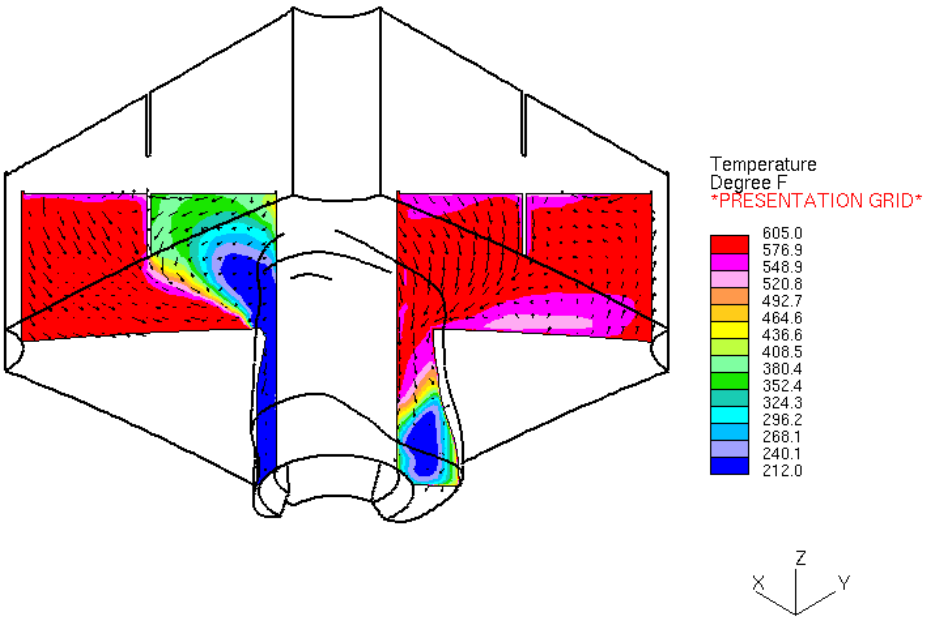

Figure C.72 Case 4: Temperature contour plot through a section of final wastage fluid volume. Viewpoint is looking from below the RPV head at the opposite side of the crack.

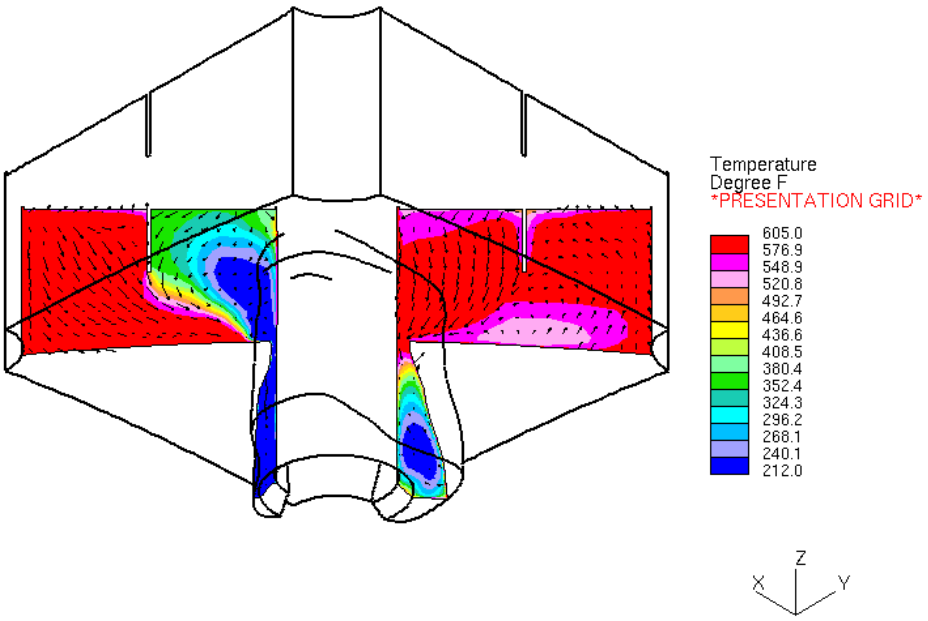

Figure C.73 Case 4: Temperature contour plot through a section of final wastage fluid volume. Viewpoint is looking from below the RPV head at the opposite side of the crack.

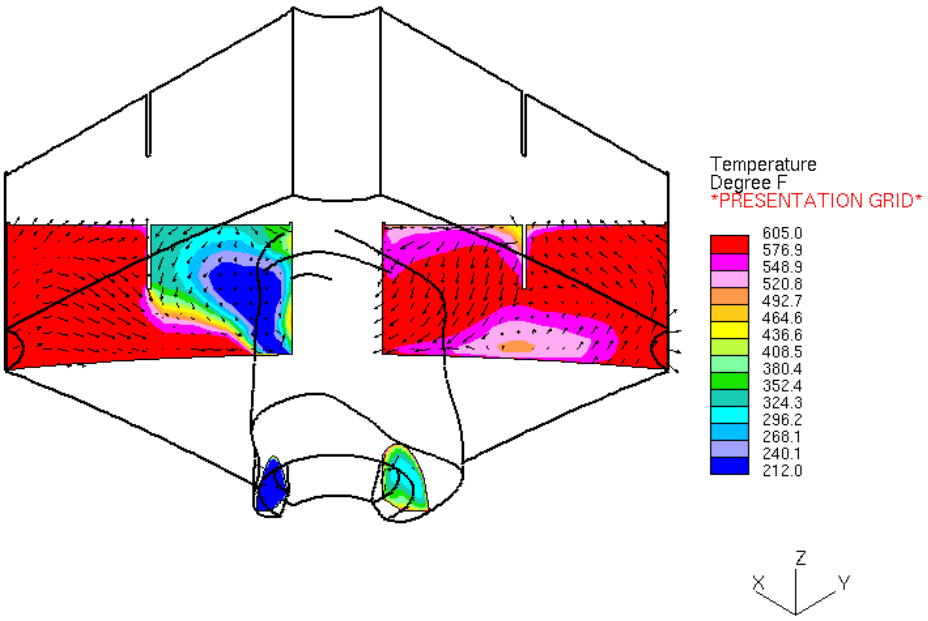

Figure C.74 Case 4: Temperature contour plot through a section of final wastage fluid volume. Viewpoint is looking from below the RPV head at the opposite side of the crack.

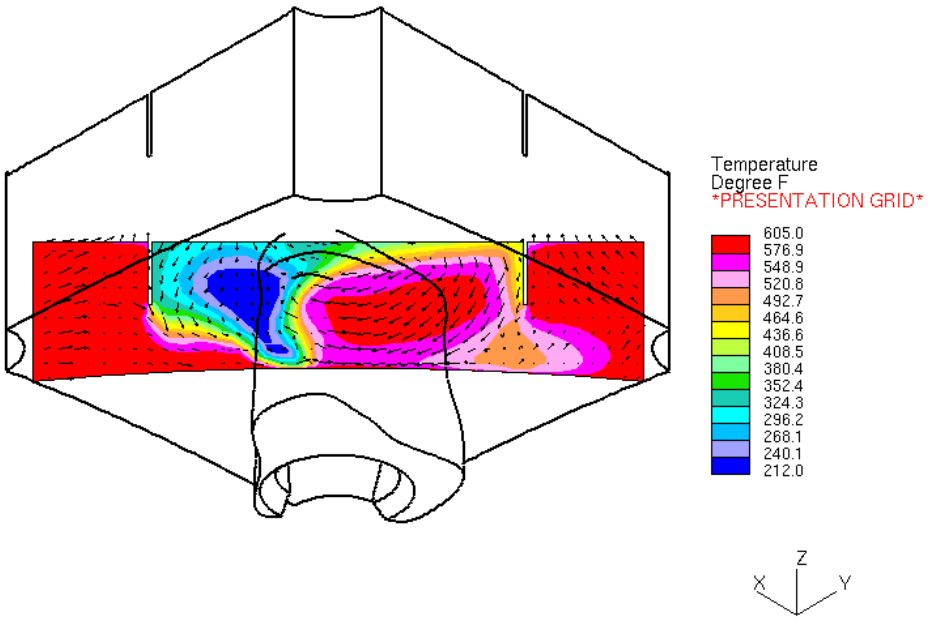

Figure C.75 Case 4: Temperature contour plot through a section of final wastage fluid volume. Viewpoint is looking from below the RPV head at the opposite side of the crack.

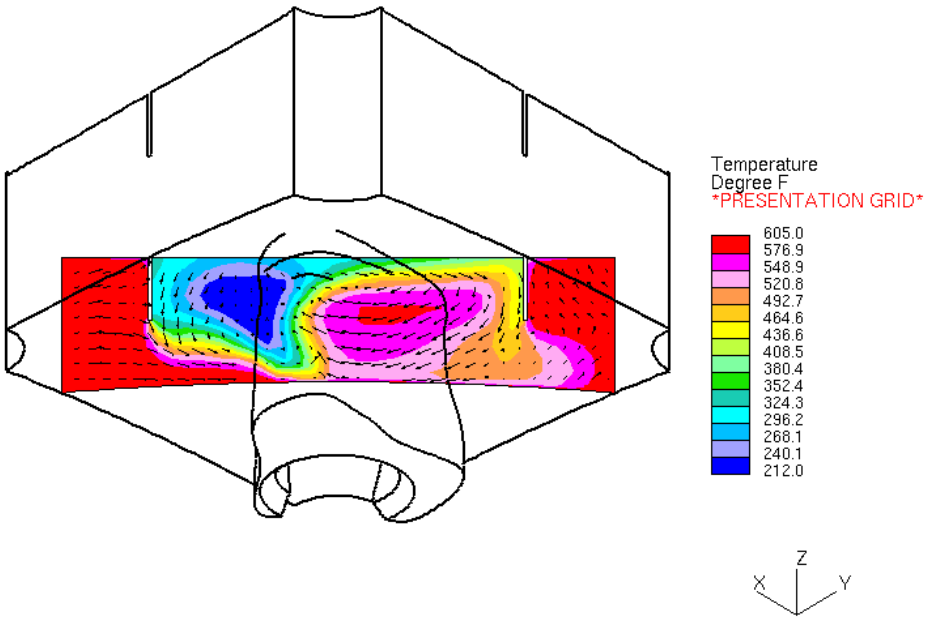

Figure C.76 Case 4: Temperature contour plot through a section of final wastage fluid volume. Viewpoint is looking from below the RPV head at the opposite side of the crack.

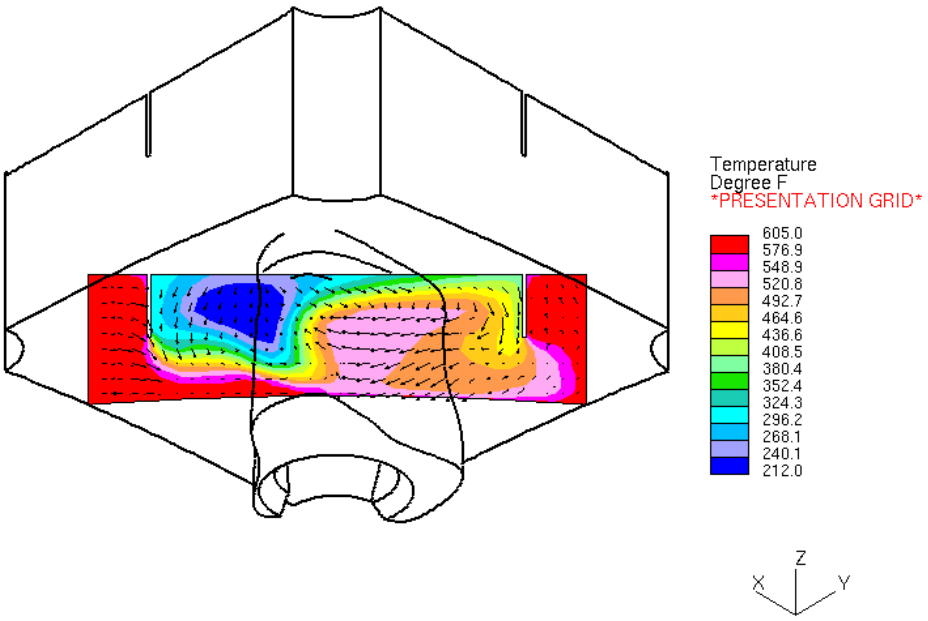

Figure C.77 Case 4: Temperature contour plot through a section of final wastage fluid volume. Viewpoint is looking from below the RPV head at the opposite side of the crack.

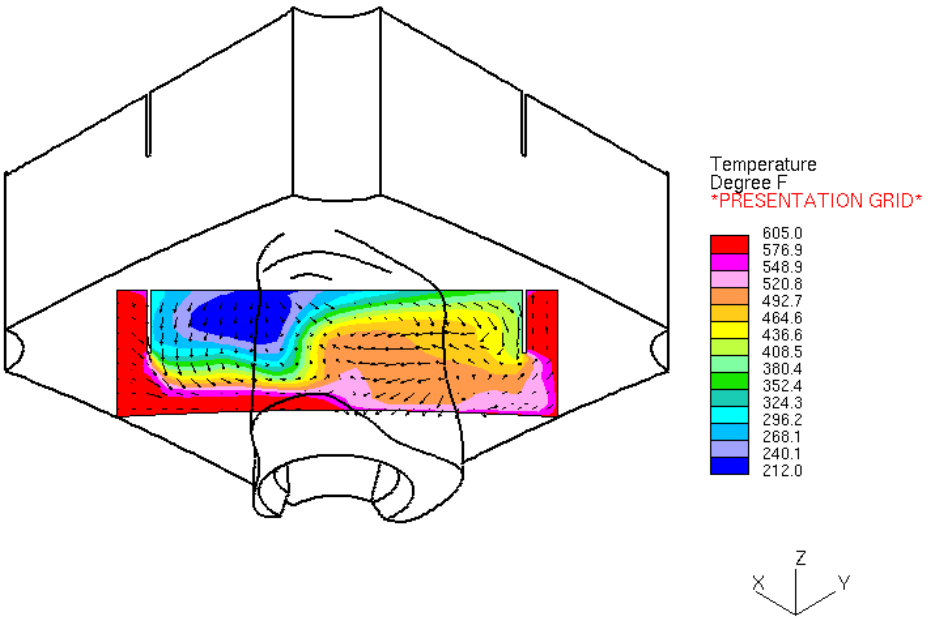

Figure C.78 Case 4: Temperature contour plot through a section of final wastage fluid volume. Viewpoint is looking from below the RPV head at the opposite side of the crack.

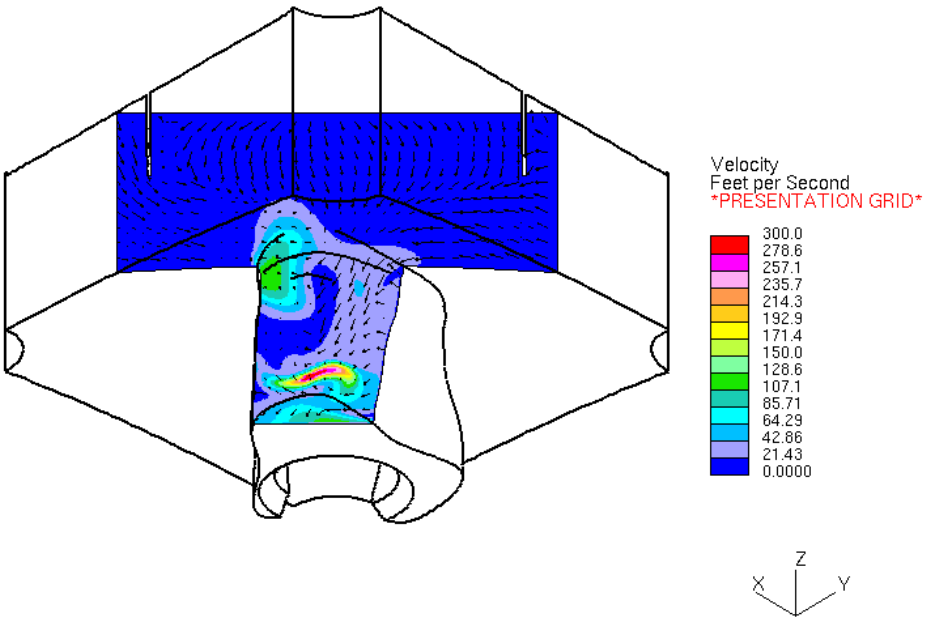

Figure C.79 Case 4: Velocity magnitude contour/vector plot through a section of final wastage fluid volume. Viewpoint is looking from below the RPV head at the opposite side of the crack.

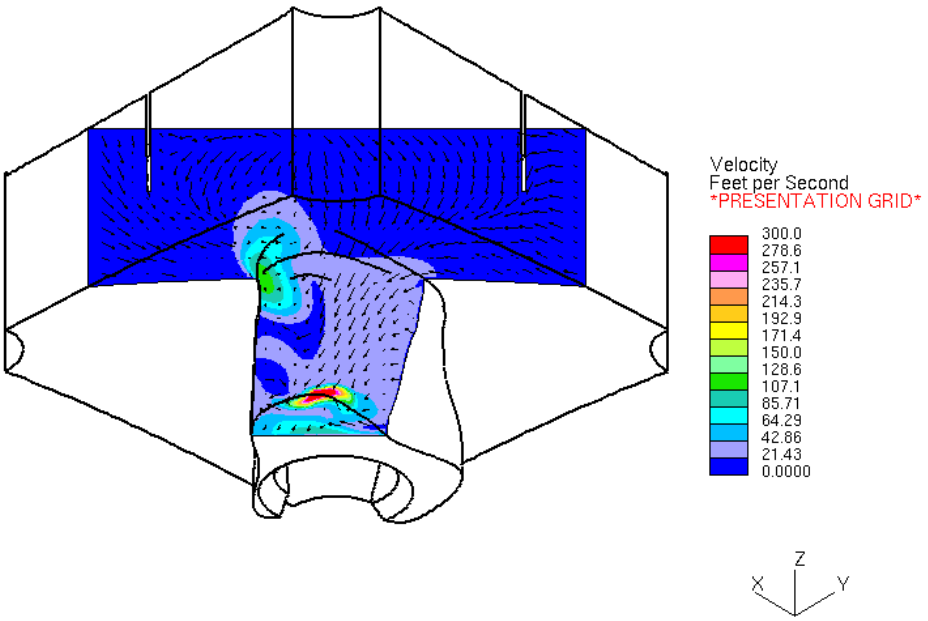

Figure C.80 Case 4: Velocity magnitude contour/vector plot through a section of final wastage fluid volume. Viewpoint is looking from below the RPV head at the opposite side of the crack.

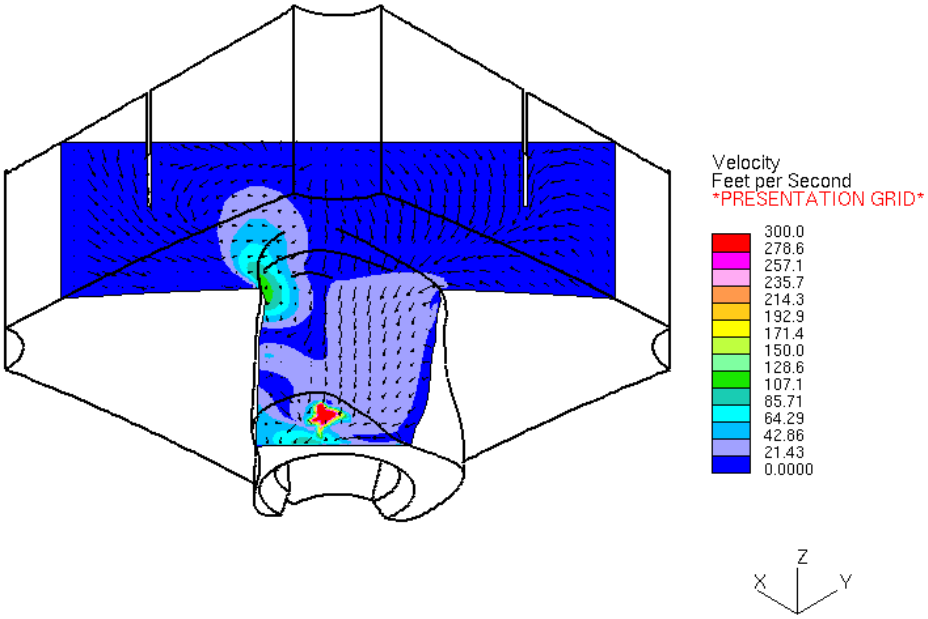

Figure C.81 Case 4: Velocity magnitude contour/vector plot through a section of final wastage fluid volume. Viewpoint is looking from below the RPV head at the opposite side of the crack.

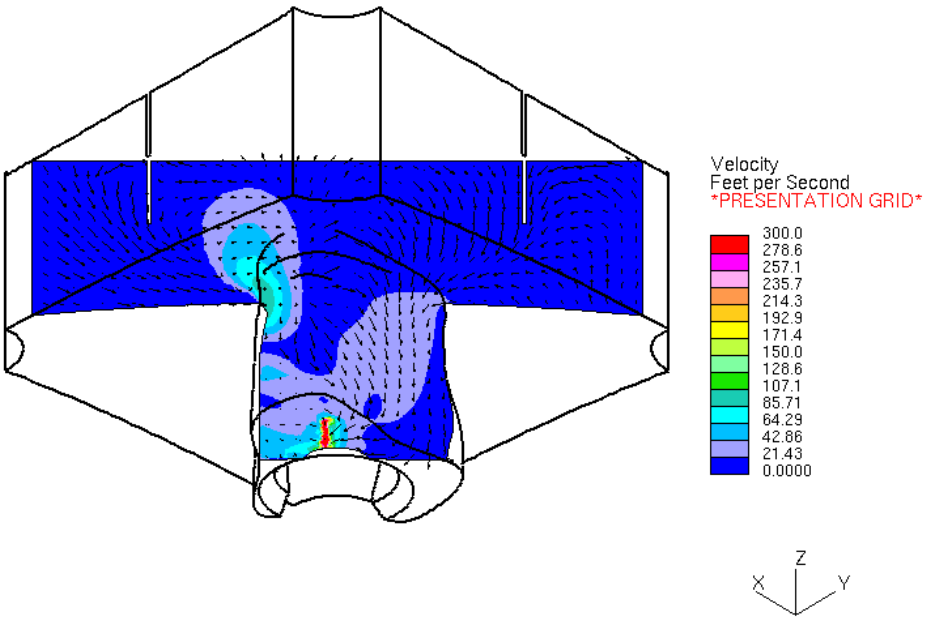

Figure C.82 Case 4: Velocity magnitude contour/vector plot through a section of final wastage fluid volume. Viewpoint is looking from below the RPV head at the opposite side of the crack.

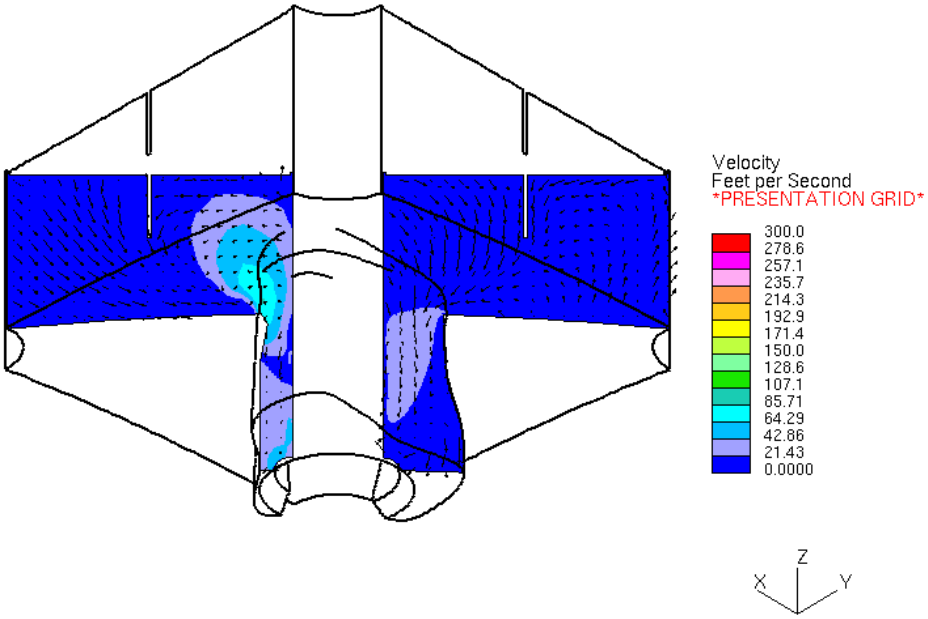

Figure C.83 Case 4: Velocity magnitude contour/vector plot through a section of final wastage fluid volume. Viewpoint is looking from below the RPV head at the opposite side of the crack.

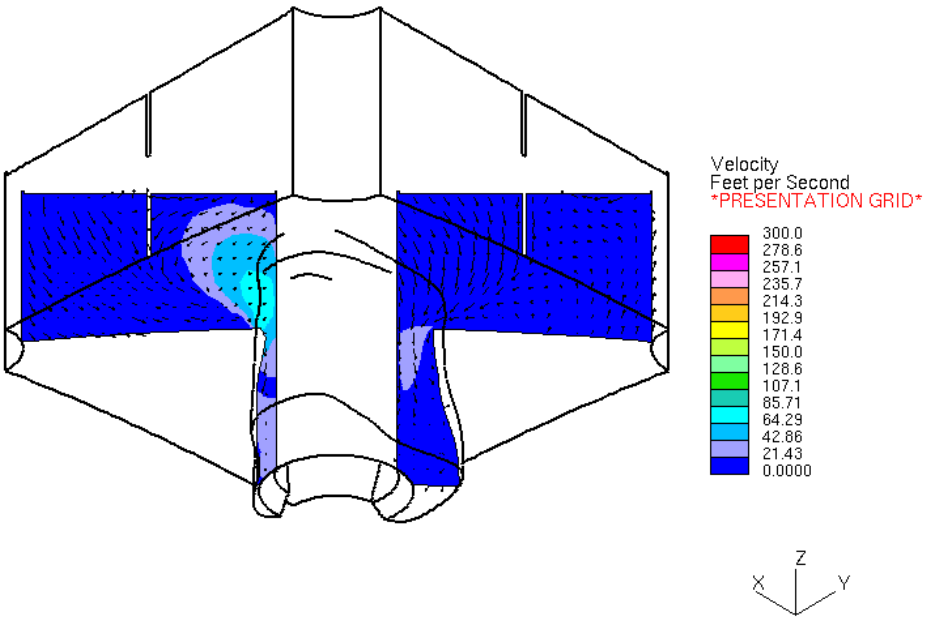

Figure C.84 Case 4: Velocity magnitude contour/vector plot through a section of final wastage fluid volume. Viewpoint is looking from below the RPV head at the opposite side of the crack.

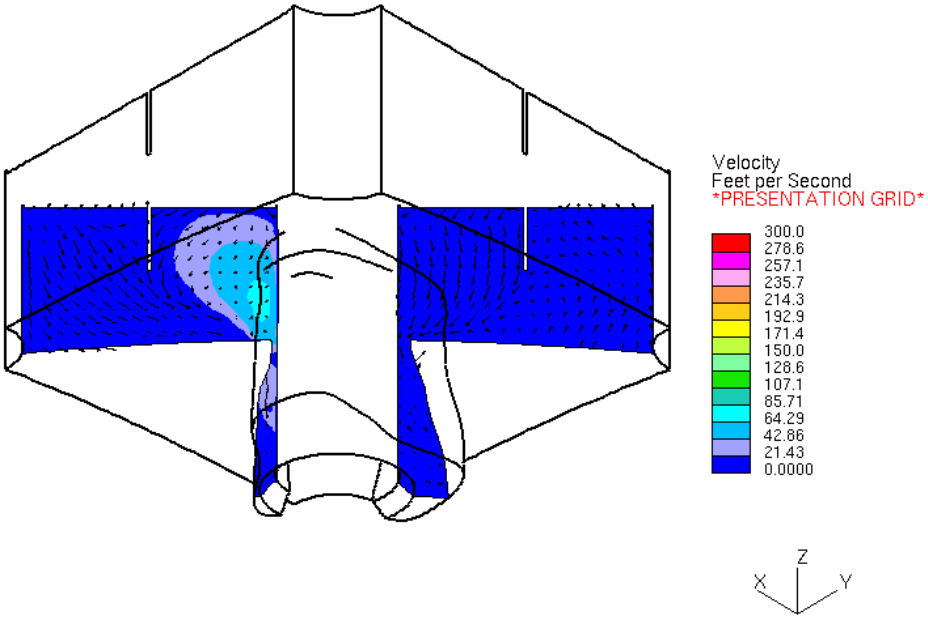

Figure C.85 Case 4: Velocity magnitude contour/vector plot through a section of final wastage fluid volume. Viewpoint is looking from below the RPV head at the opposite side of the crack.

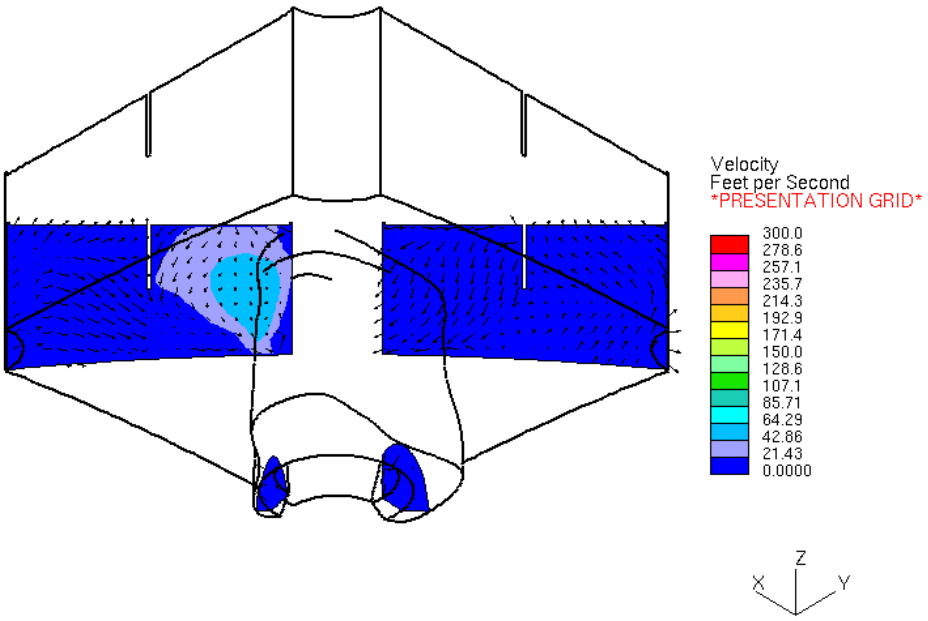

Figure C.86 Case 4: Velocity magnitude contour/vector plot through a section of final wastage fluid volume. Viewpoint is looking from below the RPV head at the opposite side of the crack.

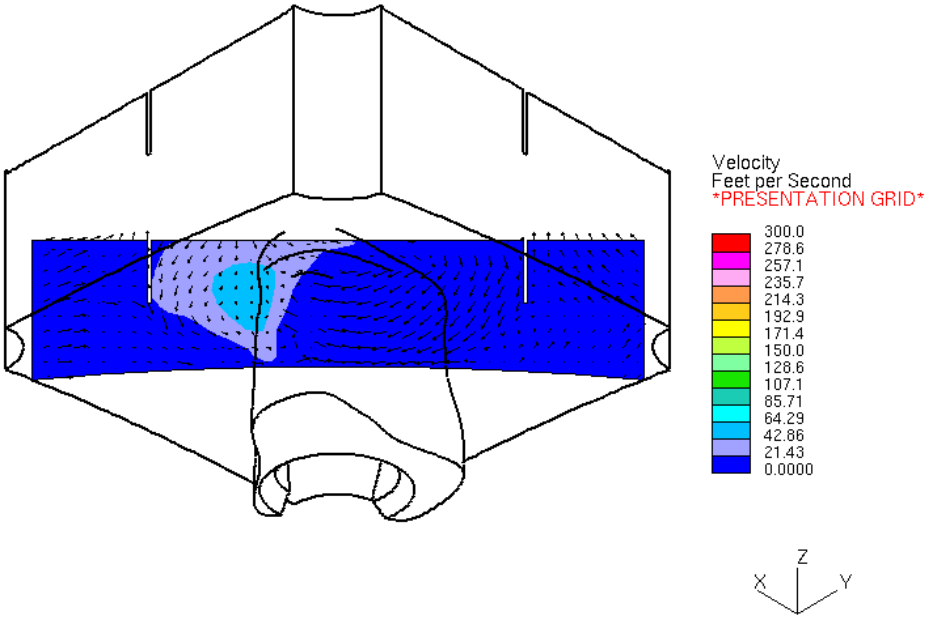

Figure C.87 Case 4: Velocity magnitude contour/ vector plot through a section of final wastage fluid volume. Viewpoint is looking from below the RPV head at the opposite side of the crack.

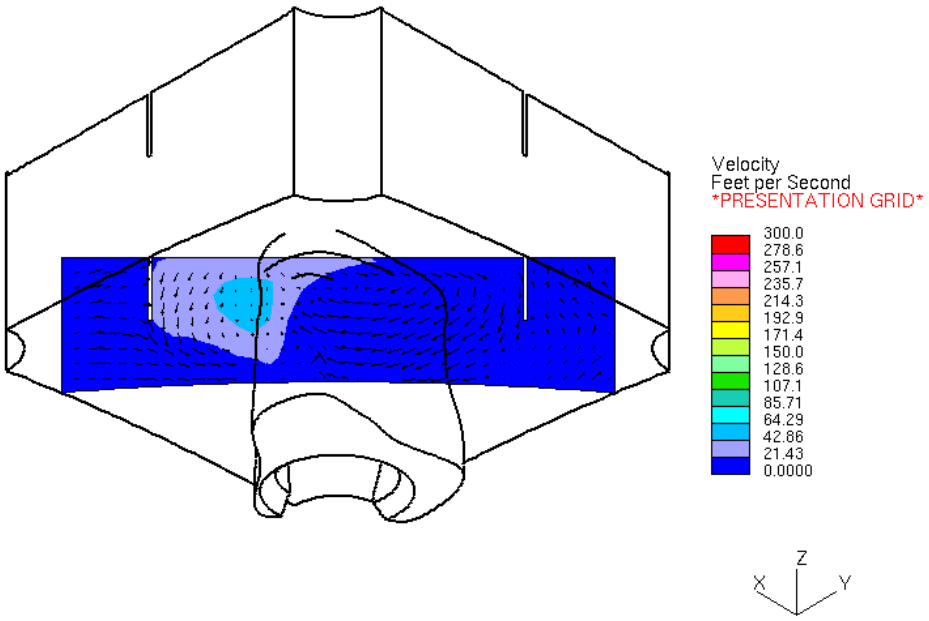

Figure C.88 Case 4: Velocity magnitude contour/ vector plot through a section of final wastage fluid volume. Viewpoint is looking from below the RPV head at the opposite side of the crack.

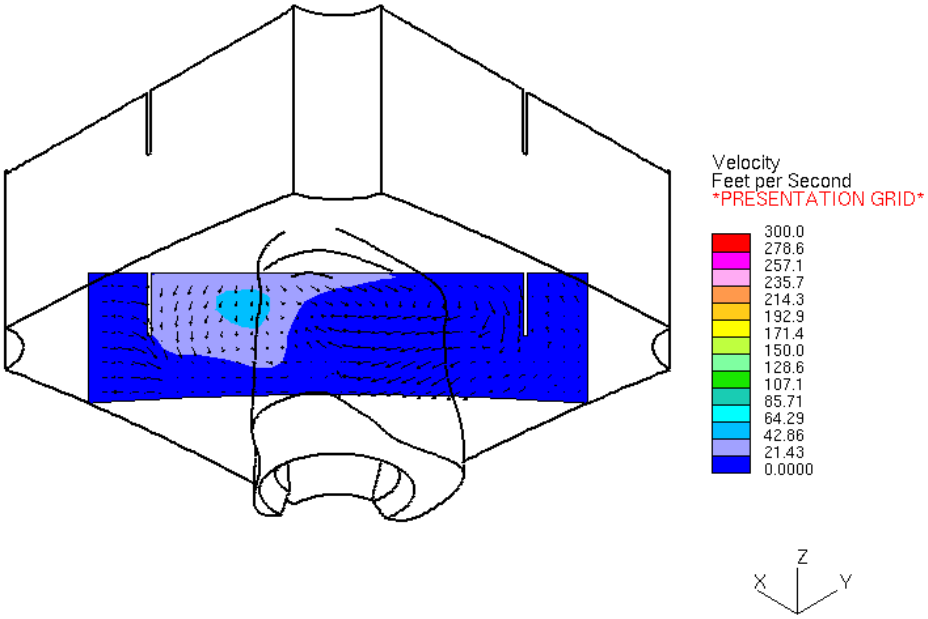

Figure C.89 Case 4: Velocity magnitude contour/ vector plot through a section of final wastage fluid volume. Viewpoint is looking from below the RPV head at the opposite side of the crack.

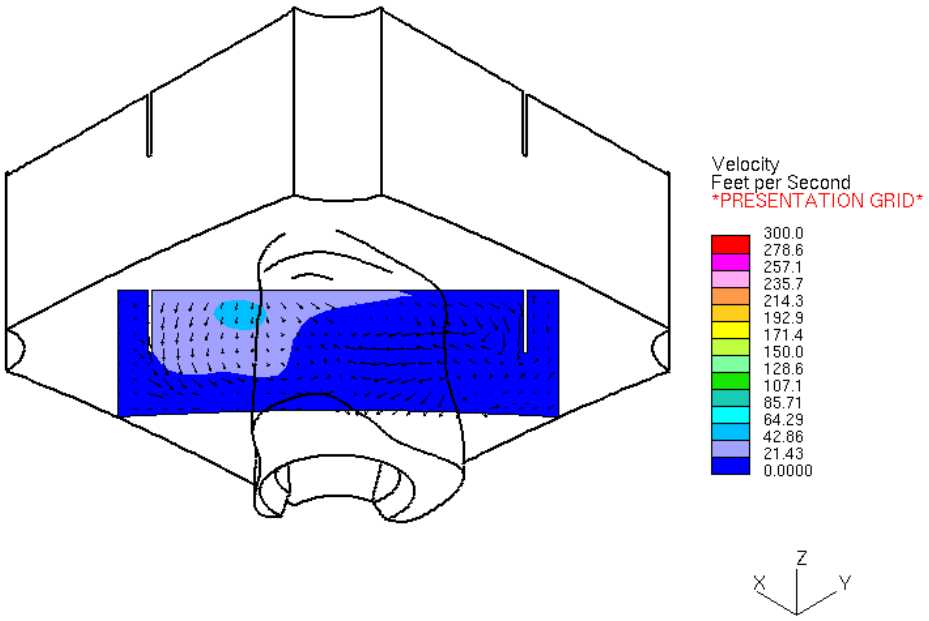

Figure C.90 Case 4: Velocity magnitude contour/vector plot through a section of final wastage fluid volume. Viewpoint is looking from below the RPV head at the opposite side of the crack.

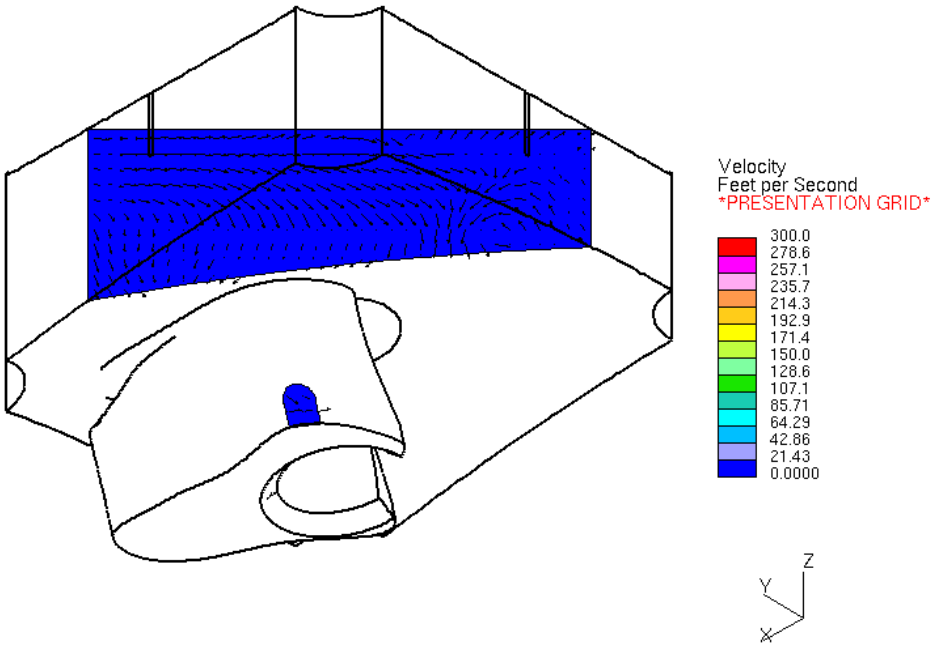

Figure C.91 Case 4: Velocity magnitude contour/vector plot through a section of final wastage fluid volume. Viewpoint is looking from below the RPV head at the opposite side of the crack.

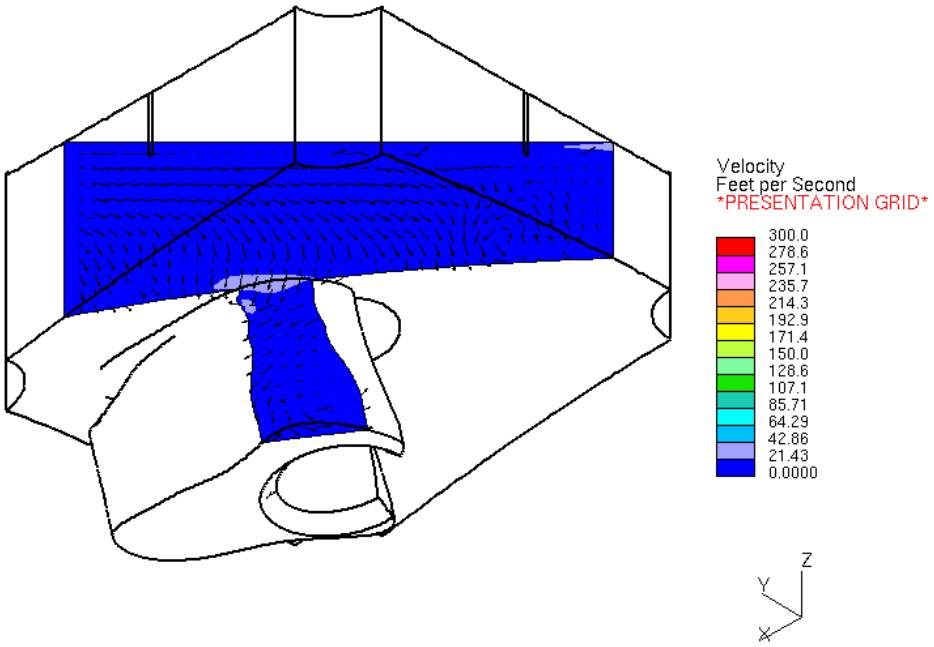

Figure C.92 Case 4: Velocity magnitude contour/vector plot through a section of final wastage fluid volume. Viewpoint is looking from below the RPV head at the opposite side of the crack.

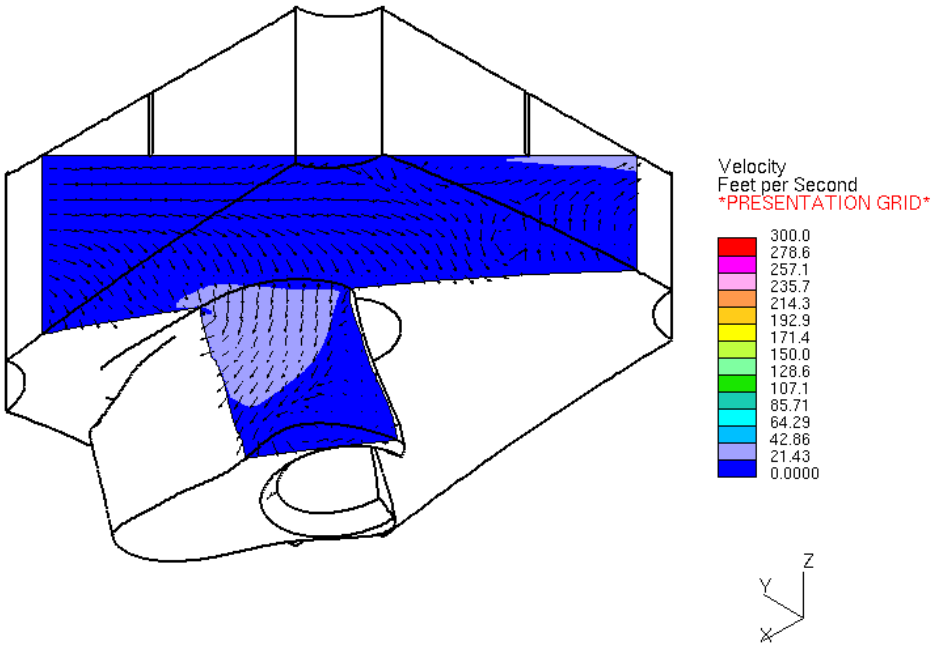

Figure C.93 Case 4: Velocity magnitude contour/vector plot through a section of final wastage fluid volume. Viewpoint is looking from below the RPV head at the opposite side of the crack.

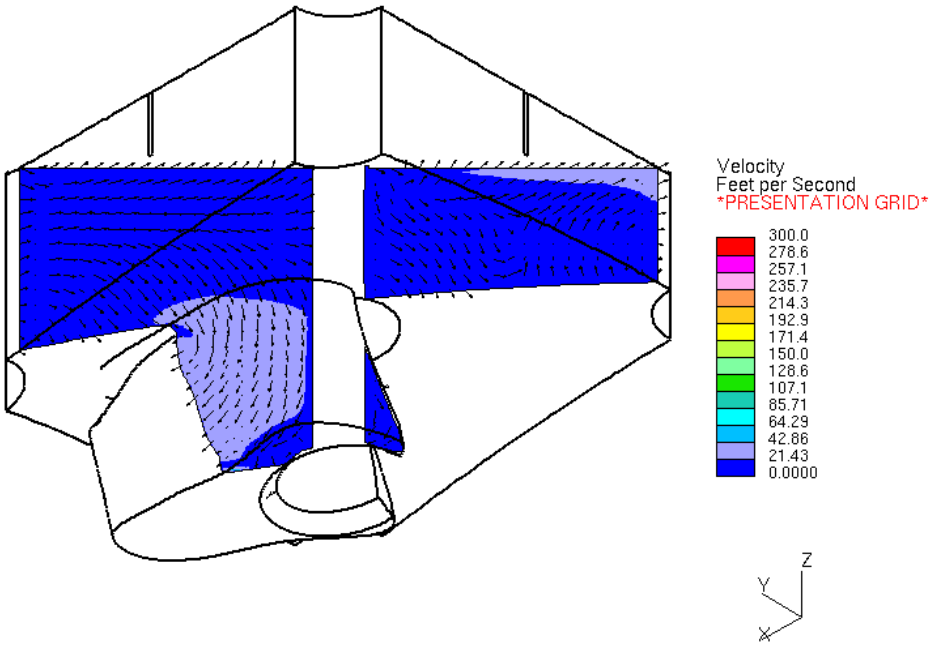

Figure C.94 Case 4: Velocity magnitude contour/vector plot through a section of final wastage fluid volume. Viewpoint is looking from below the RPV head at the opposite side of the crack.

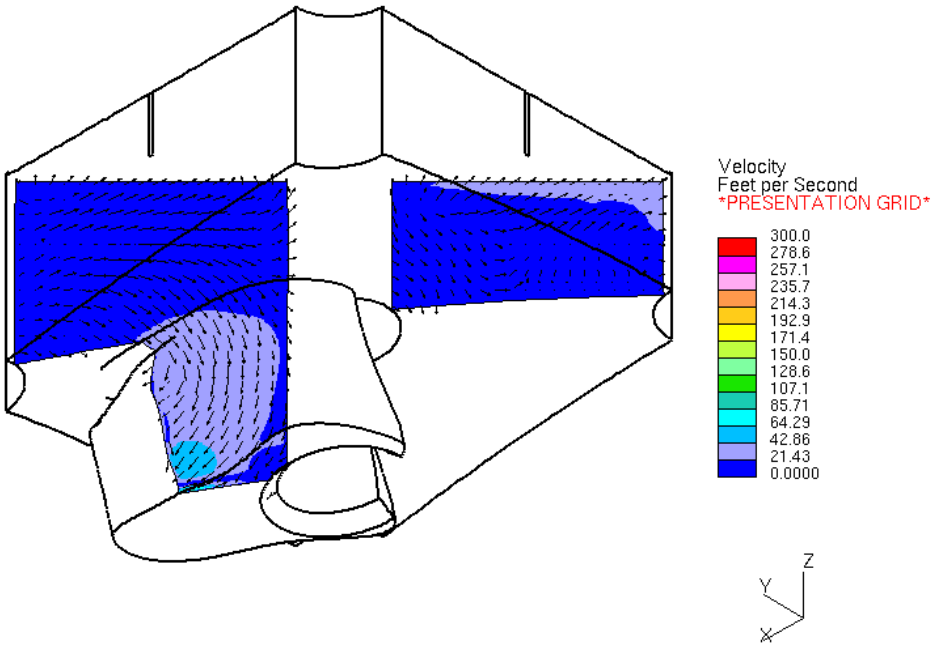

Figure C.95 Case 4: Velocity magnitude contour/vector plot through a section of final wastage fluid volume. Viewpoint is looking from below the RPV head at the opposite side of the crack.

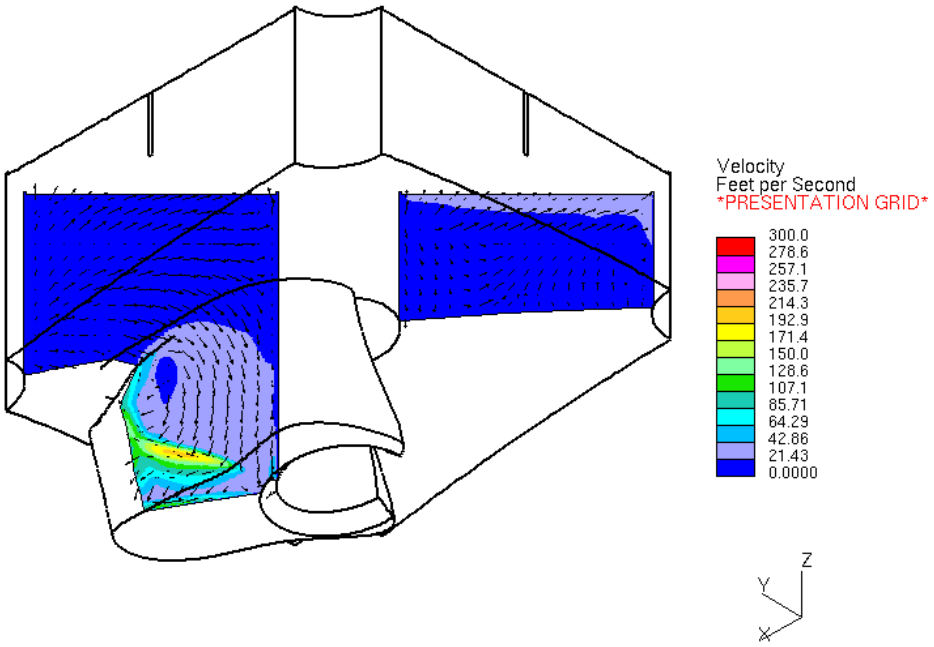

Figure C.96 Case 4: Velocity magnitude contour/vector plot through a section of final wastage fluid volume. Viewpoint is looking from below the RPV head at the opposite side of the crack.

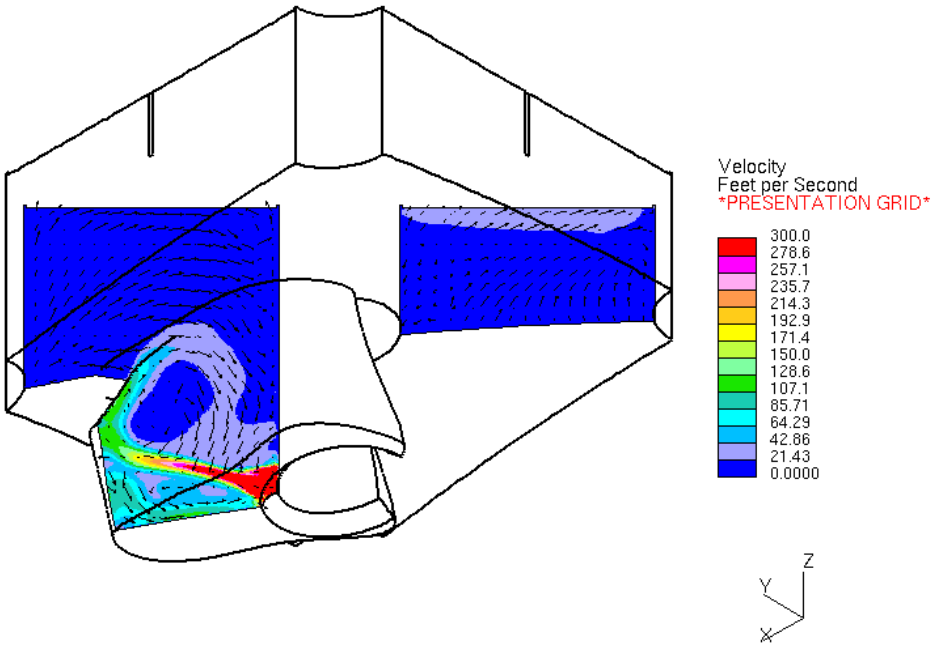

Figure C.97 Case 4: Velocity magnitude contour/vector plot through a section of final wastage fluid volume. Viewpoint is looking from below the RPV head at the opposite side of the crack.

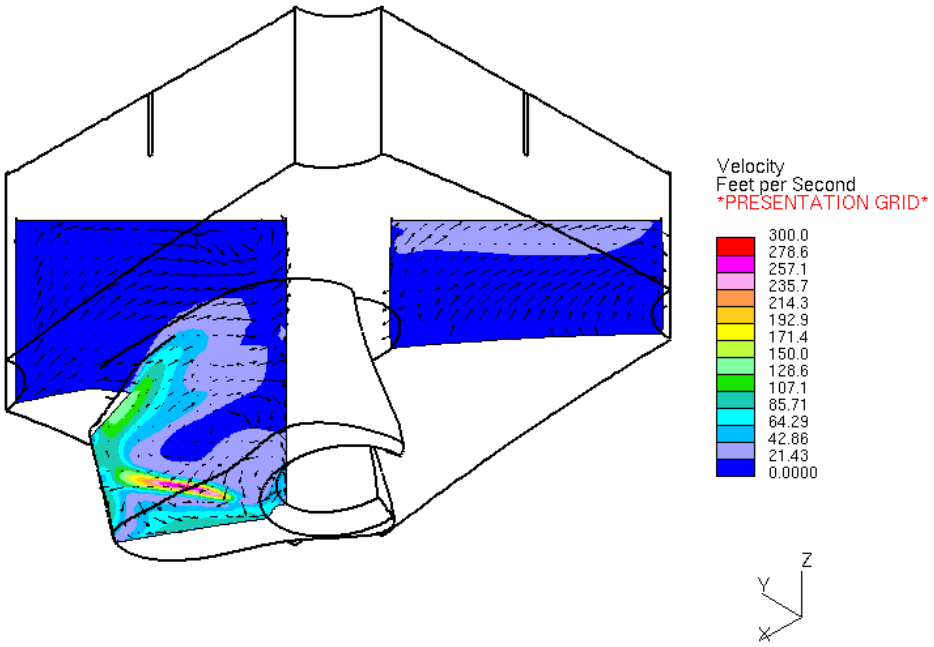

Figure C.98 Case 4: Velocity magnitude contour/vector plot through a section of final wastage fluid volume. Viewpoint is looking from below the RPV head at the opposite side of the crack.

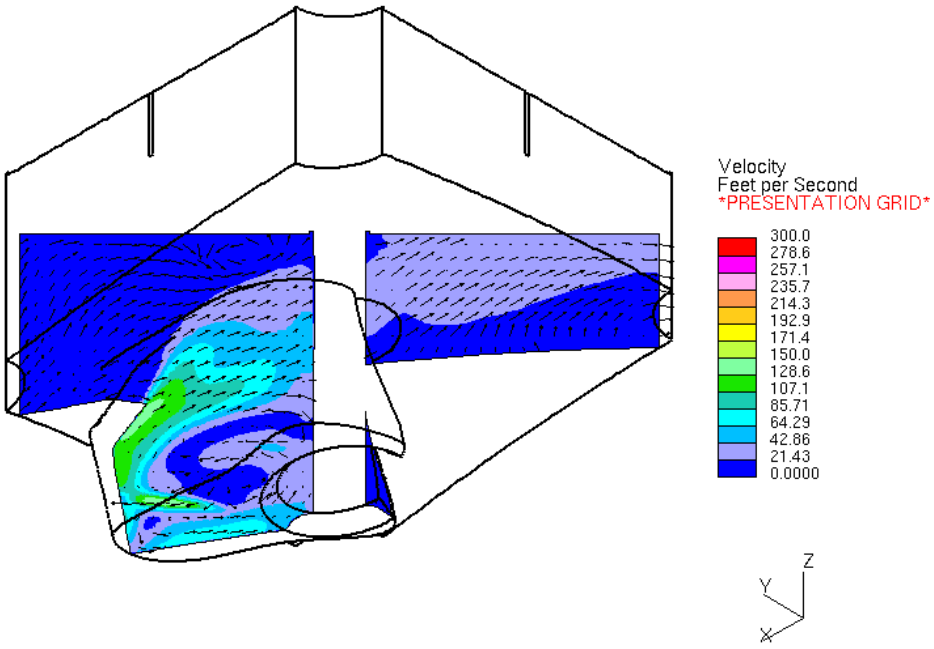

Figure C.99 Case 4: Velocity magnitude contour/vector plot through a section of final wastage fluid volume. Viewpoint is looking from below the RPV head at the opposite side of the crack.

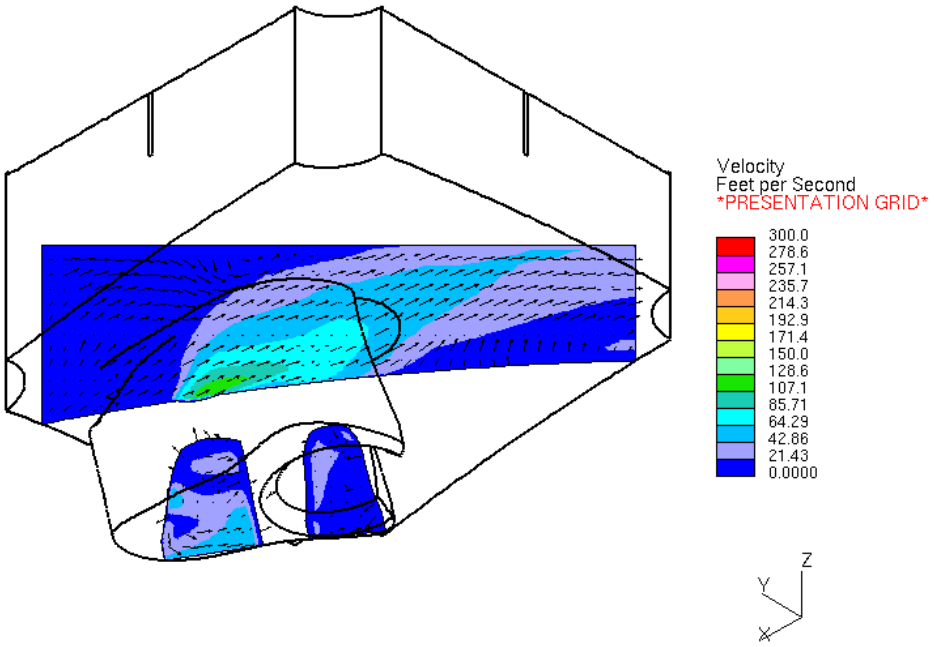

Figure C.100 Case 4: Velocity magnitude contour/vector plot through a section of final wastage fluid volume. Viewpoint is looking from below the RPV head at the opposite side of the crack.

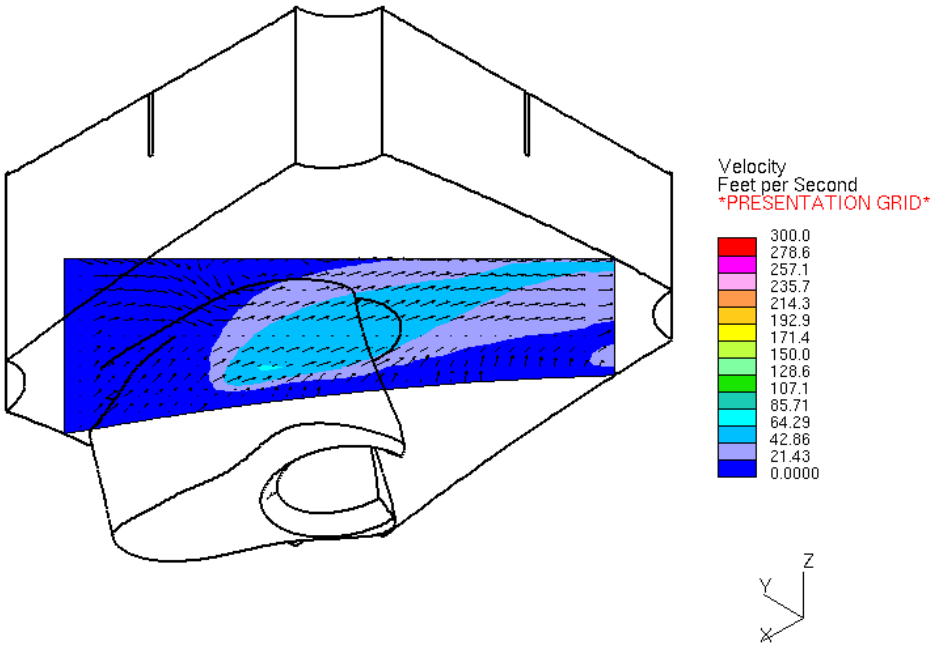

Figure C.101 Case 4: Velocity magnitude contour/vector plot through a section of final wastage fluid volume. Viewpoint is looking from below the RPV head at the opposite side of the crack.

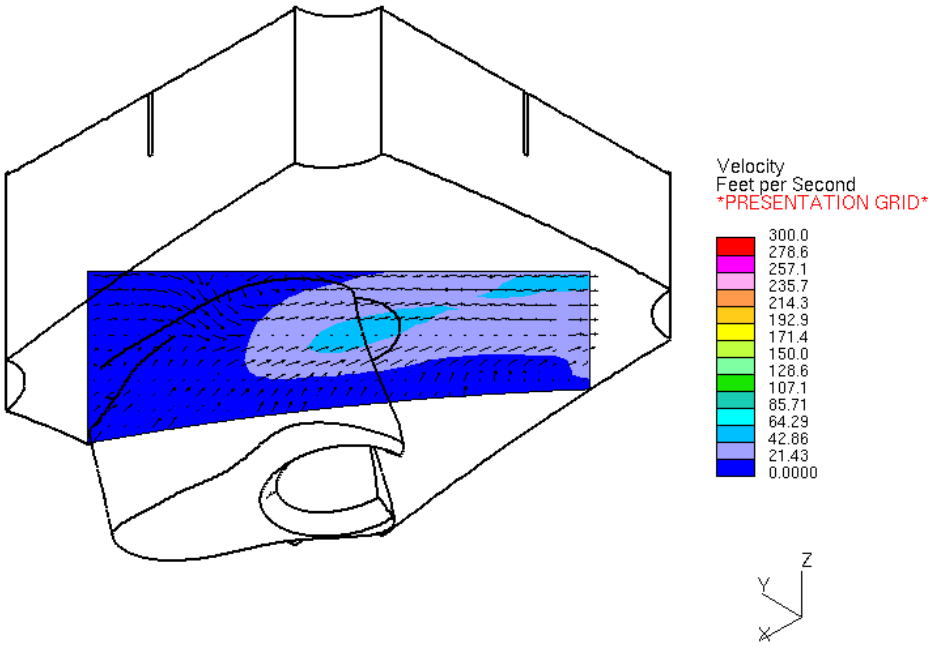

Figure C.102 Case 4: Velocity magnitude contour/vector plot through a section of final wastage fluid volume. Viewpoint is looking from below the RPV head at the opposite side of the crack.

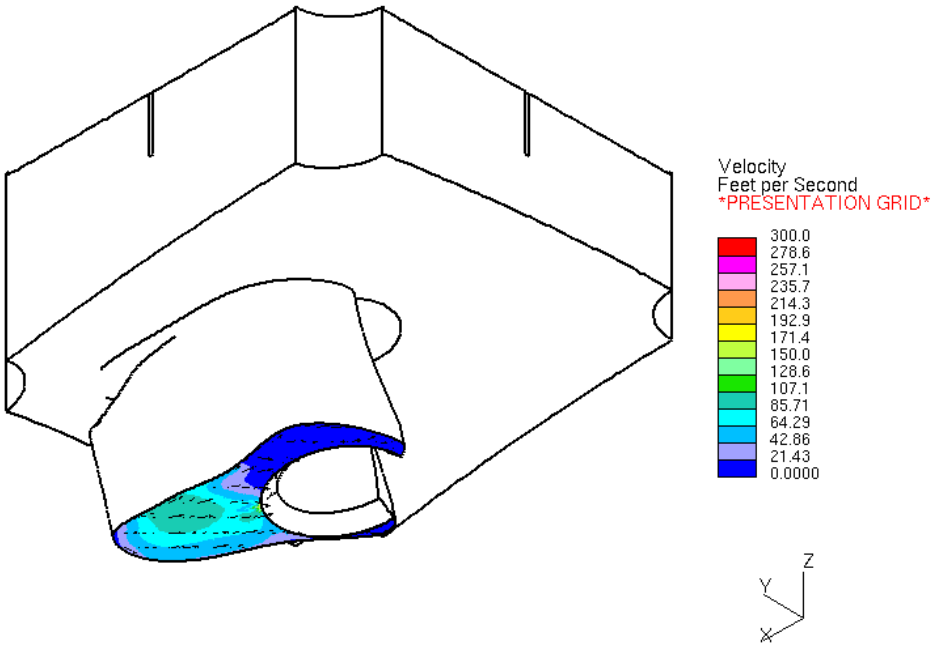

Figure C.103 Case 4: Velocity magnitude contour/vector plot through a section of final wastage fluid volume. Viewpoint is looking from below the RPV head at the opposite side of the crack.

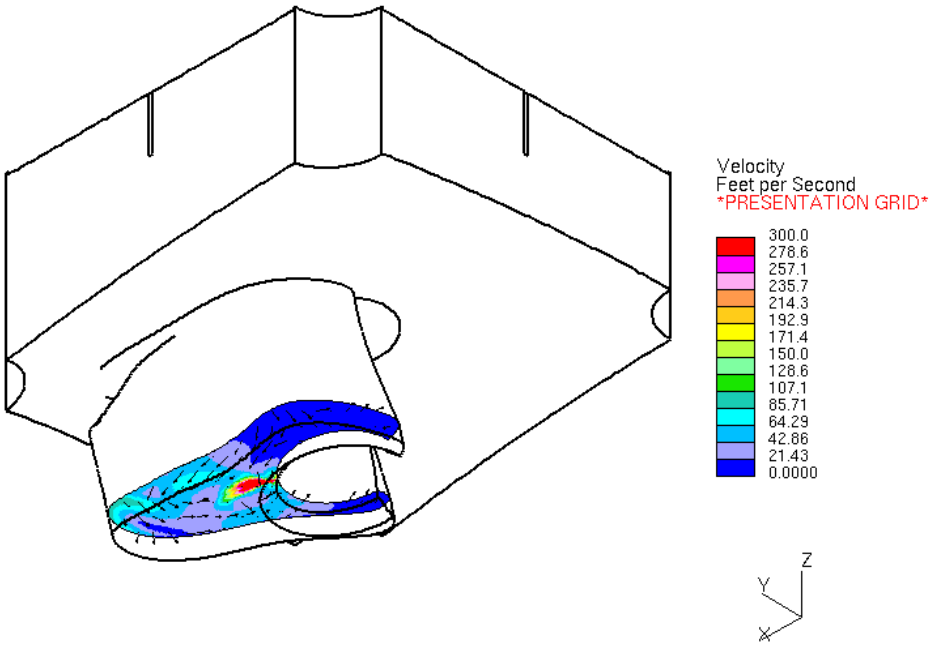

Figure C.104 Case 4: Velocity magnitude contour/vector plot through a section of final wastage fluid volume. Viewpoint is looking from below the RPV head at the opposite side of the crack.

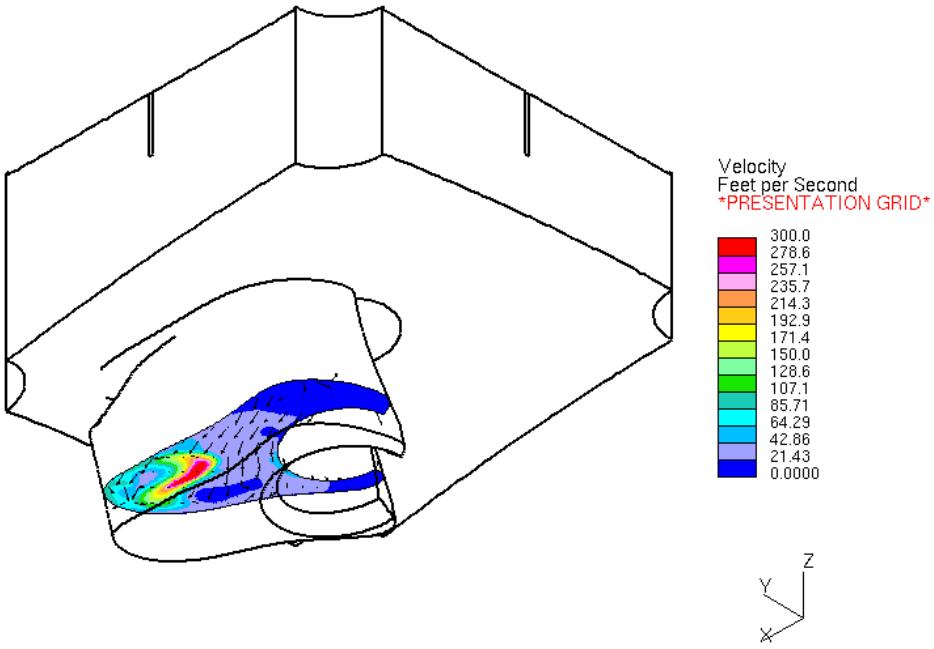

Figure C.105 Case 4: Velocity magnitude contour/vector plot through a section of final wastage fluid volume. Viewpoint is looking from below the RPV head at the opposite side of the crack.

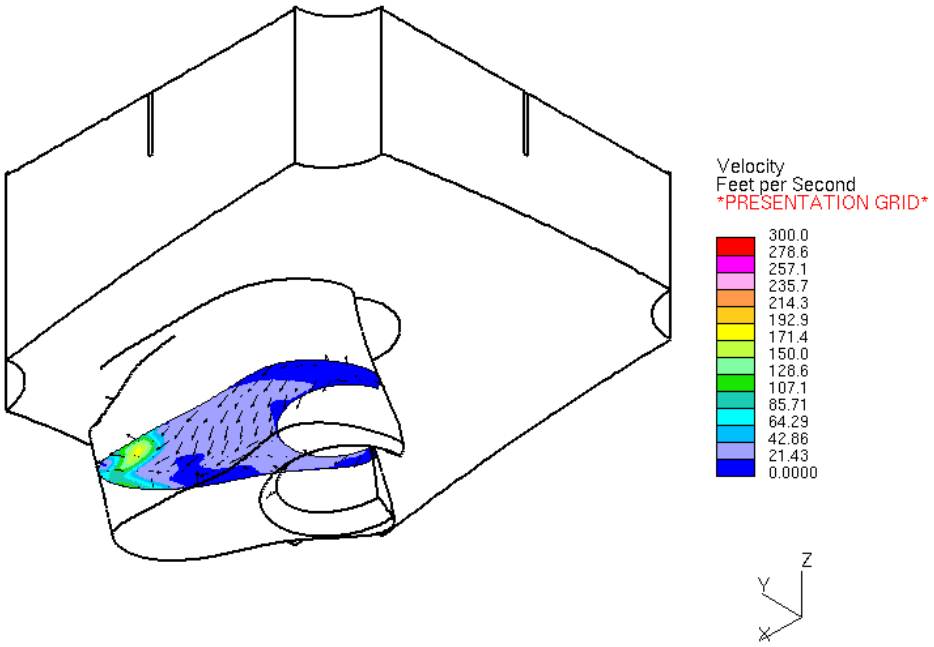

Figure C.106 Case 4: Velocity magnitude contour/vector plot through a section of final wastage fluid volume. Viewpoint is looking from below the RPV head at the opposite side of the crack.

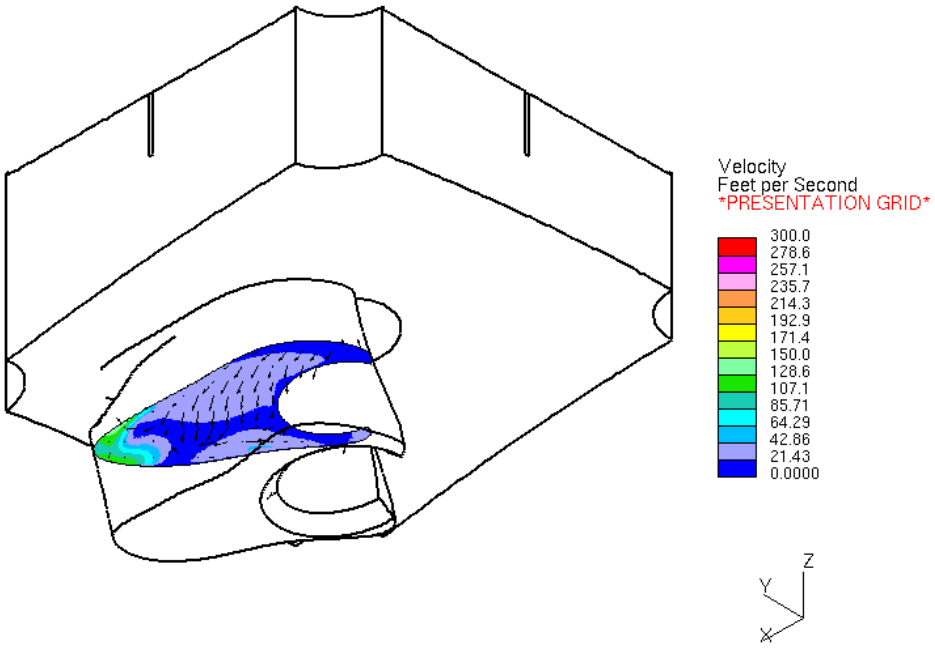

Figure C.107 Case 4: Velocity magnitude contour/vector plot through a section of final wastage fluid volume. Viewpoint is looking from below the RPV head at the opposite side of the crack.

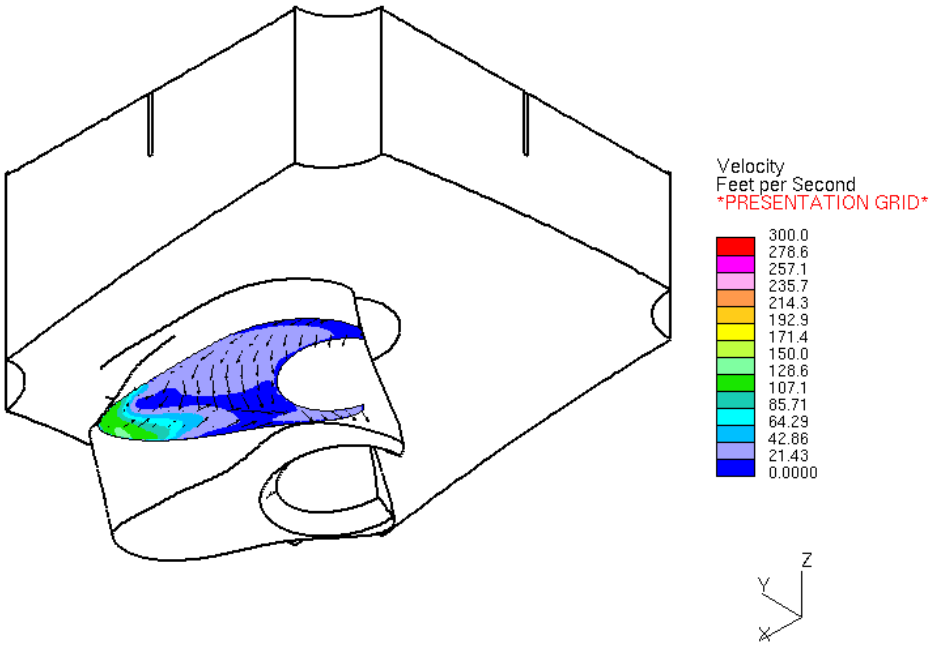

Figure C.108 Case 4: Velocity magnitude contour/vector plot through a section of final wastage fluid volume. Viewpoint is looking from below the RPV head at the opposite side of the crack.

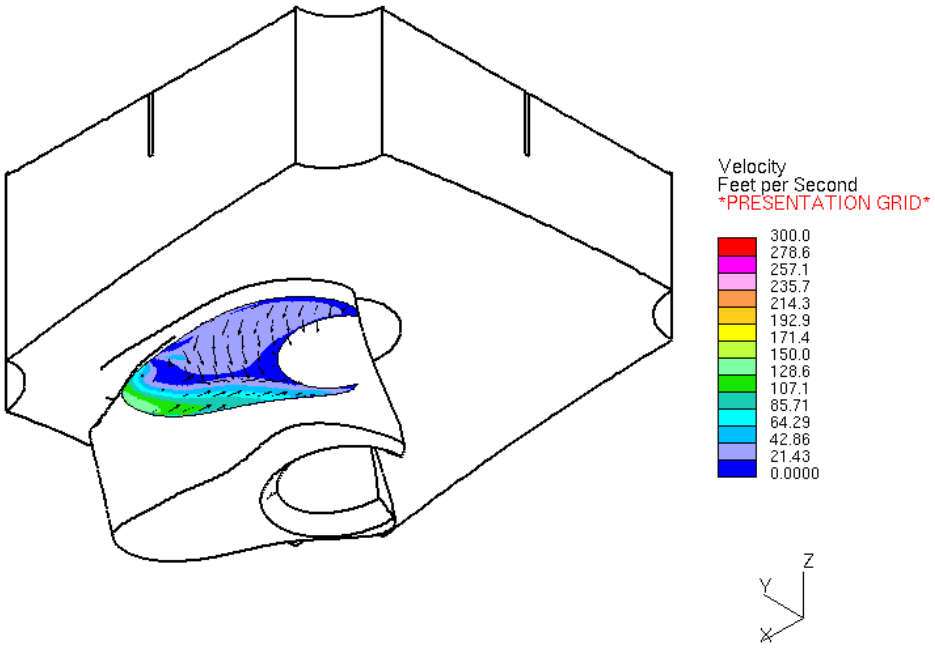

Figure C.109 Case 4: Velocity magnitude contour/vector plot through a section of final wastage fluid volume. Viewpoint is looking from below the RPV head at the opposite side of the crack.

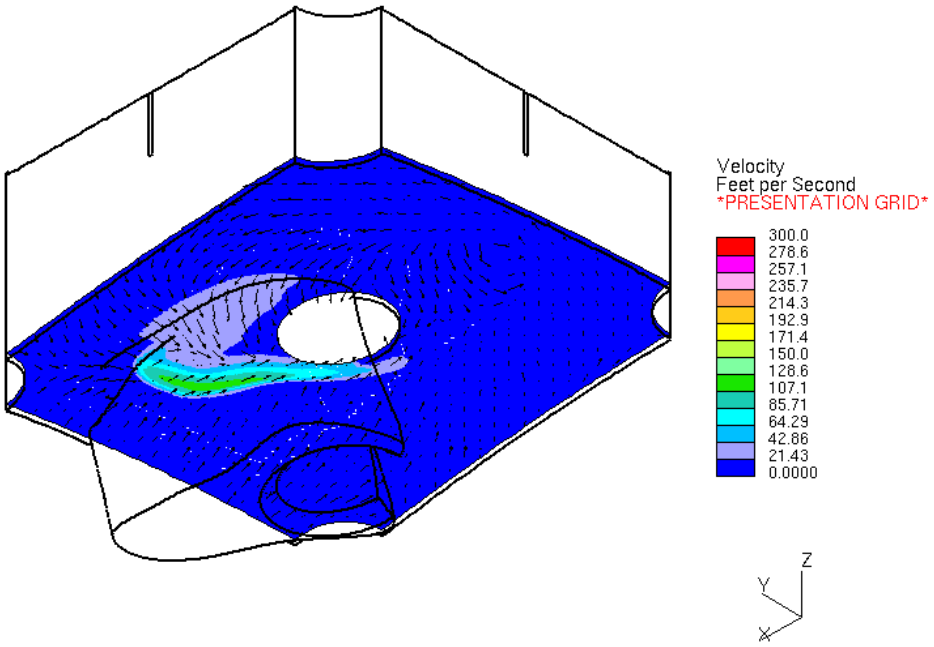

Figure C.110 Case 4: Velocity magnitude contour/vector plot through a section above final wastage fluid volume. Viewpoint is looking from below the RPV head at the opposite side of the crack.

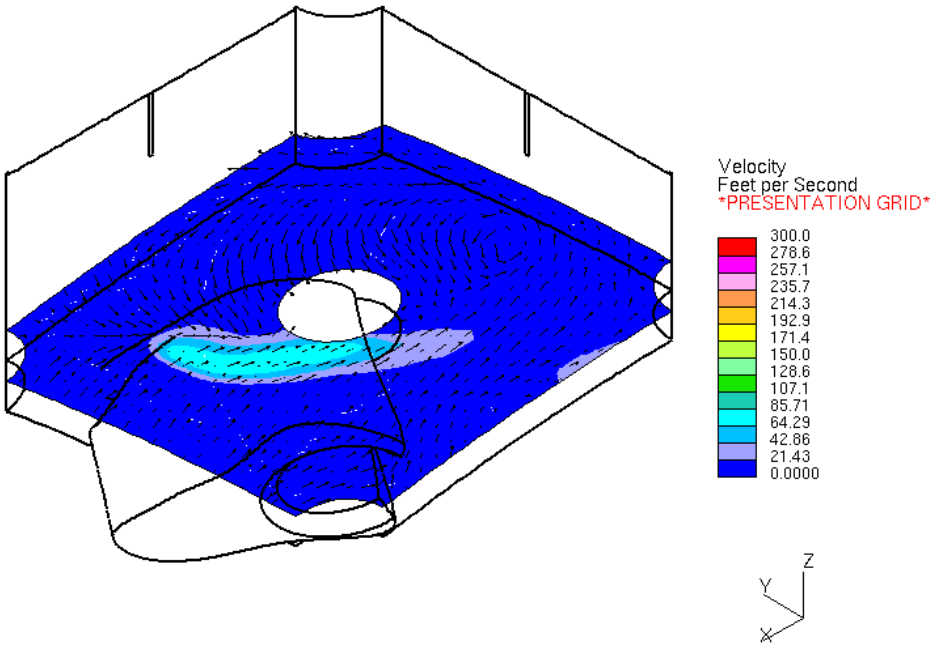

Figure C.111 Case 4: Velocity magnitude contour/vector plot through a section above final wastage fluid volume. Viewpoint is looking from below the RPV head at the opposite side of the crack.

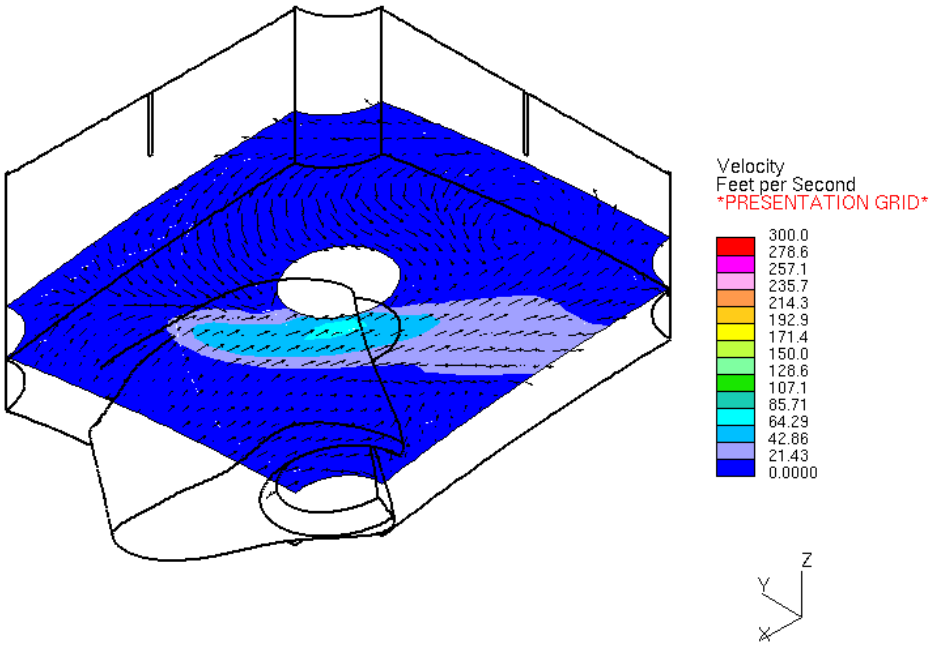

Figure C.112 Case 4: Velocity magnitude contour/vector plot through a section above final wastage fluid volume. Viewpoint is looking from below the RPV head at the opposite side of the crack.

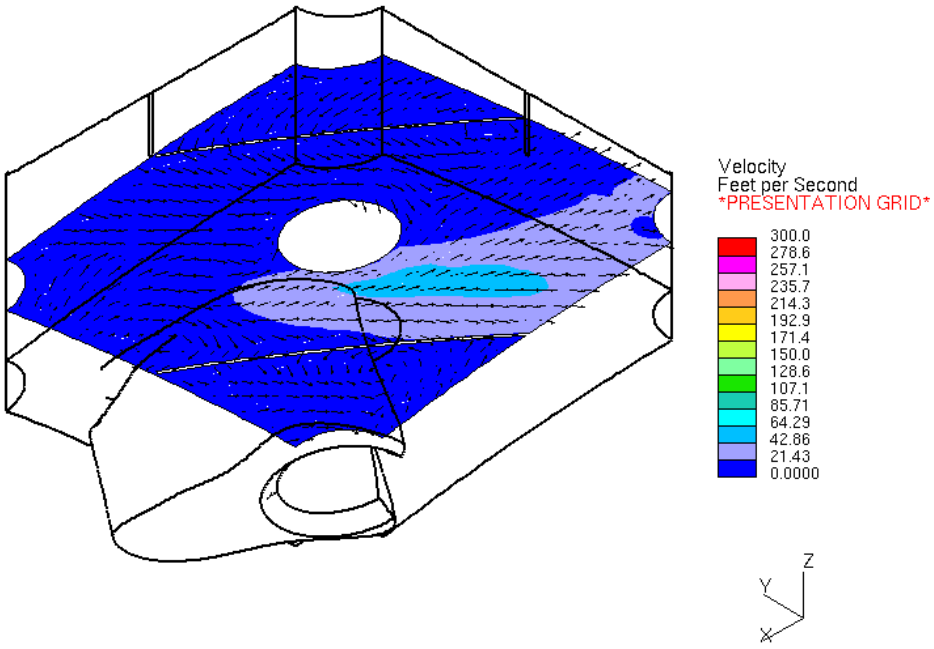

Figure C.113 Case 4: Velocity magnitude contour/vector plot through a section above final wastage fluid volume. Viewpoint is looking from below the RPV head at the opposite side of the crack.

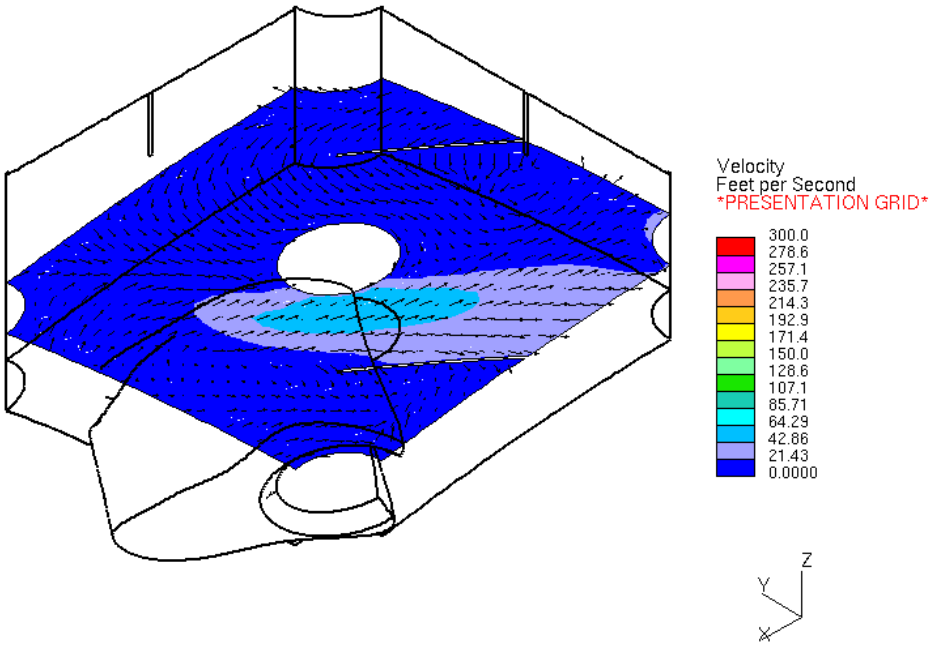

Figure C.114 Case 4: Velocity magnitude contour/vector plot through a section above final wastage fluid volume. Viewpoint is looking from below the RPV head at the opposite side of the crack.

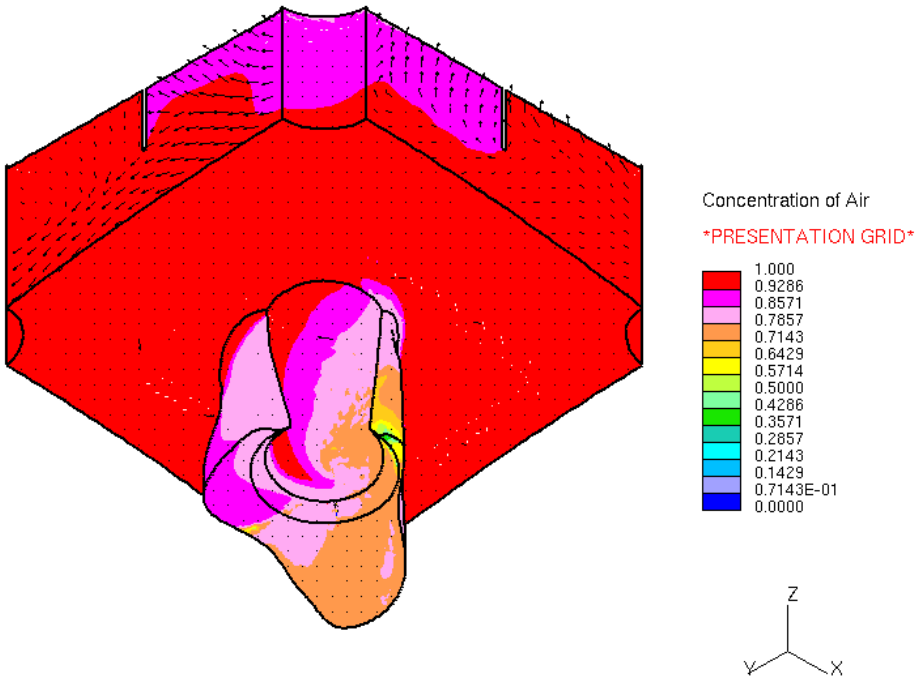

Figure C.115 Case 4: Mass fraction of air near boundary surfaces of final wastage fluid volume. Viewpoint is looking from below the RPV head at the crack.

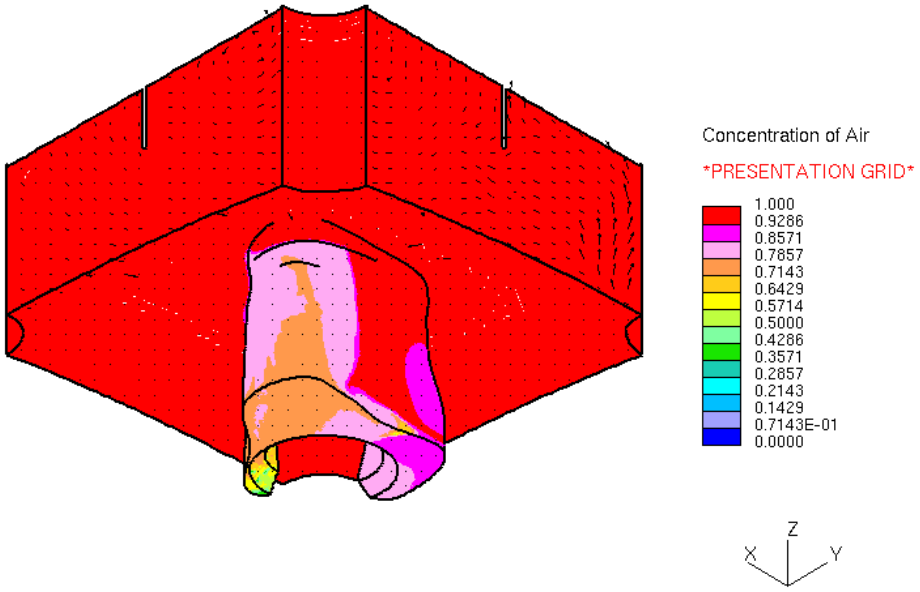

Figure C.116 Case 4: Mass fraction of air near boundary surfaces of final wastage fluid volume. Viewpoint is looking from below the RPV head at the opposite side of the crack.

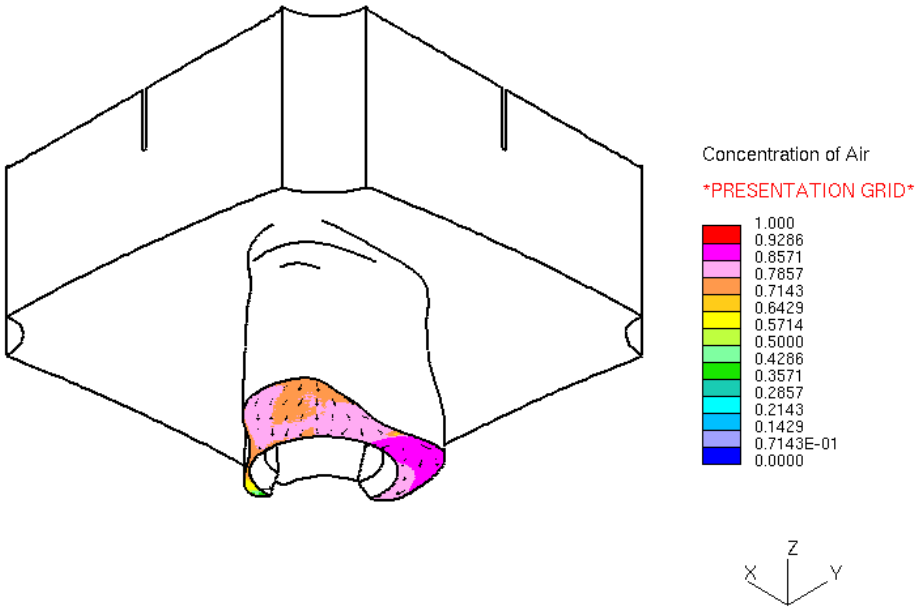

Figure C.117 Case 4: Mass fraction of air through a section of final wastage fluid volume. Viewpoint is looking from below the RPV head at the opposite side of the crack.

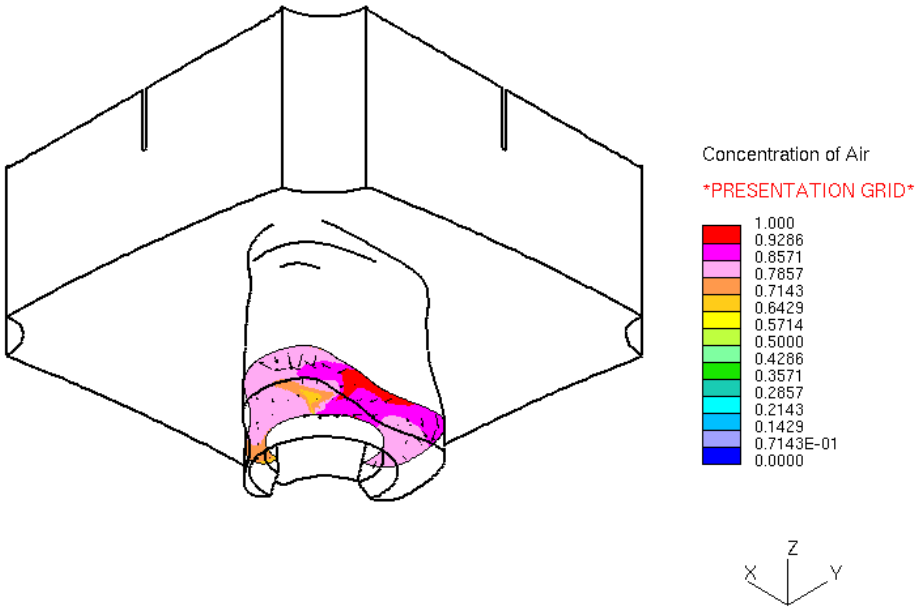

Figure C.118 Case 4: Mass fraction of air through a section of final wastage fluid volume. Viewpoint is looking from below the RPV head at the opposite side of the crack.

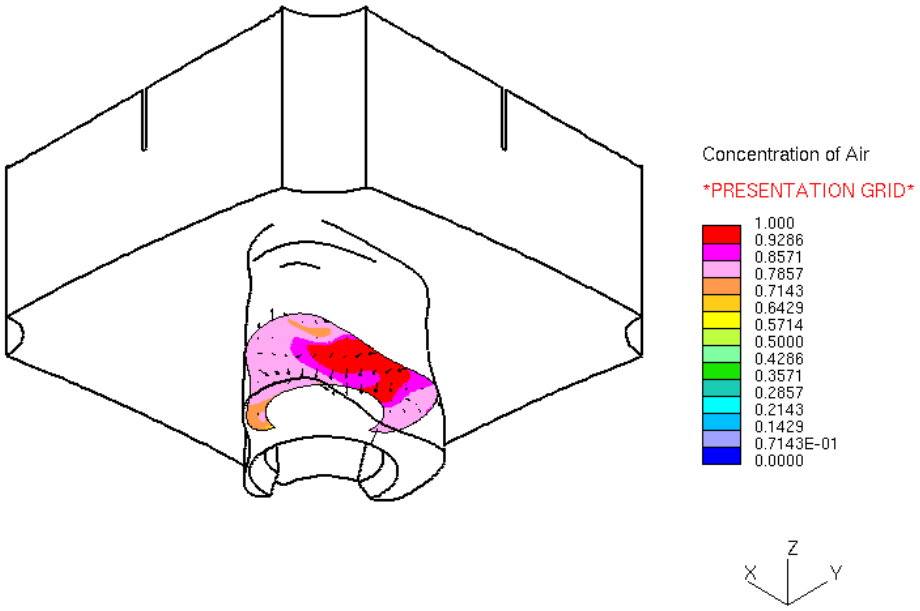

Figure C.119 Case 4: Mass fraction of air through a section of final wastage fluid volume. Viewpoint is looking from below the RPV head at the opposite side of the crack.

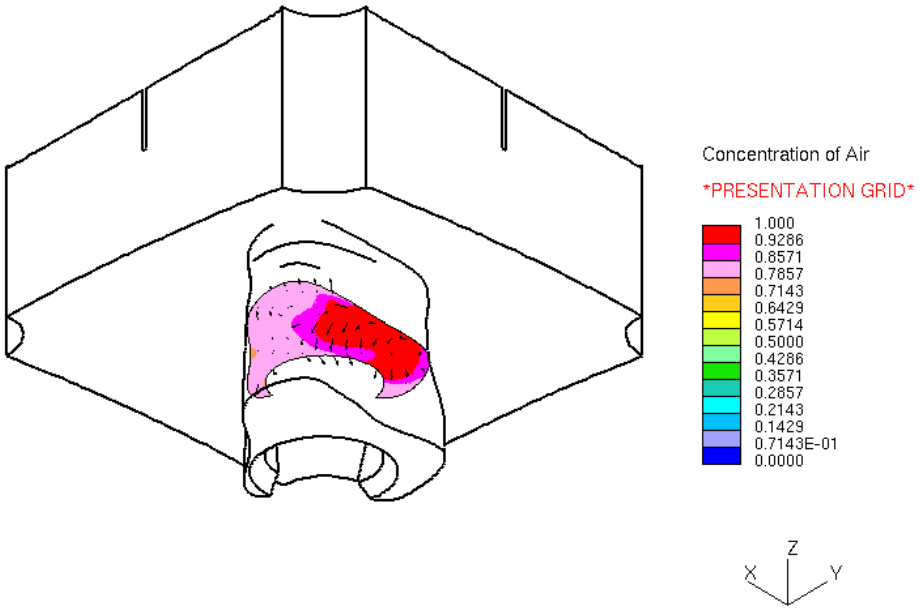

Figure C.120 Case 4: Mass fraction of air through a section of final wastage fluid volume. Viewpoint is looking from below the RPV head at the opposite side of the crack.

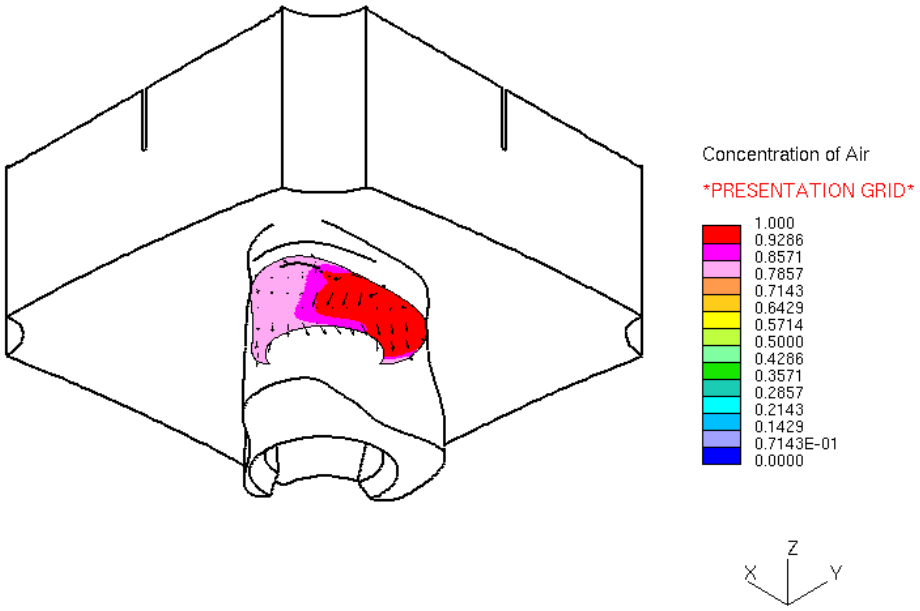

Figure C.121 Case 4: Mass fraction of air through a section of final wastage fluid volume. Viewpoint is looking from below the RPV head at the opposite side of the crack.

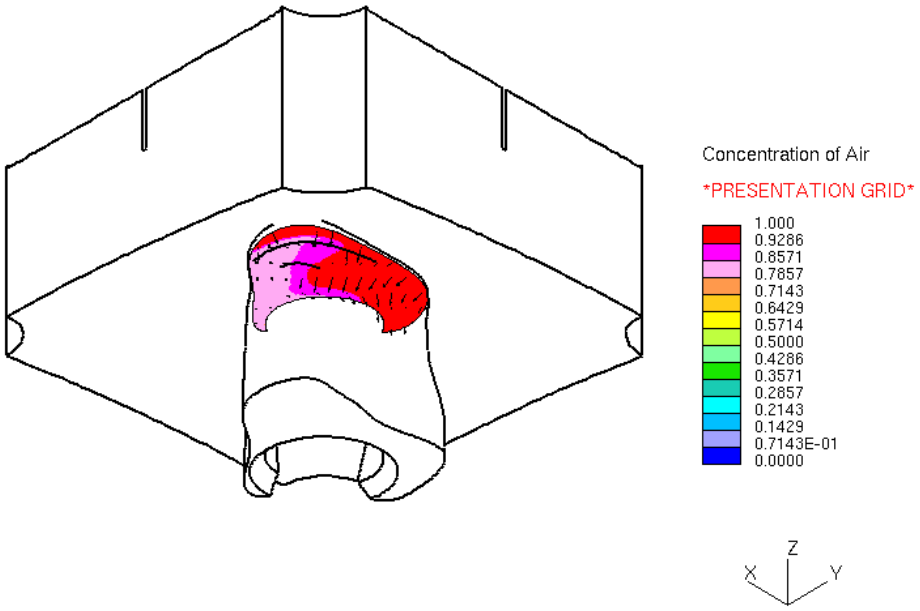

Figure C.122 Case 4: Mass fraction of air through a section of final wastage fluid volume. Viewpoint is looking from below the RPV head at the opposite side of the crack.

(a) Top View Time – 0.001 seconds Perspective View

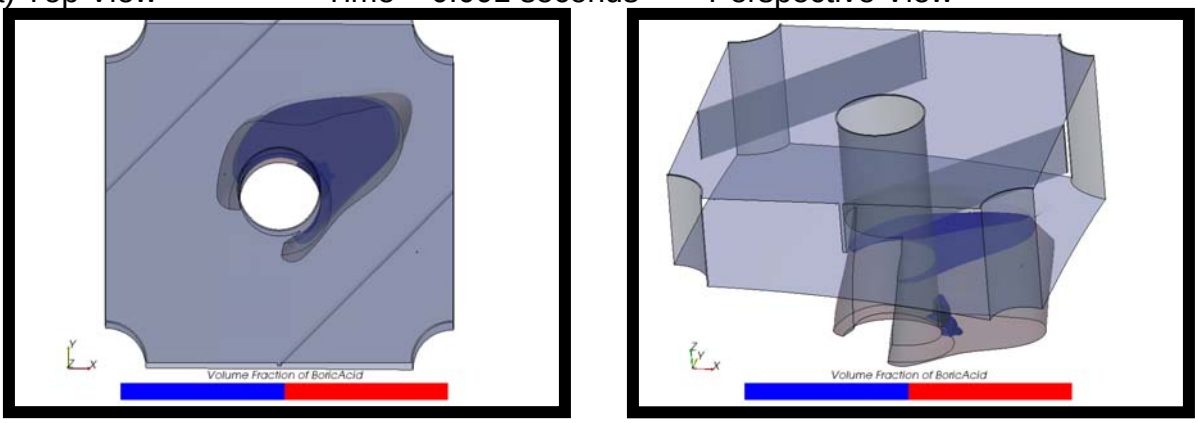

(b) Top View Time – 0.005 seconds Perspective View

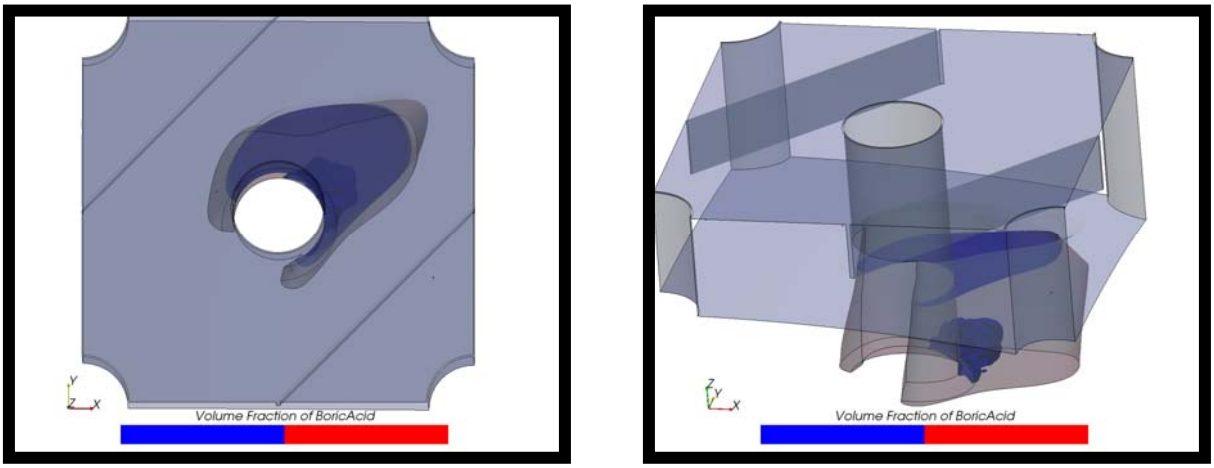

(c) Top View Time – 0.02 seconds Perspective View

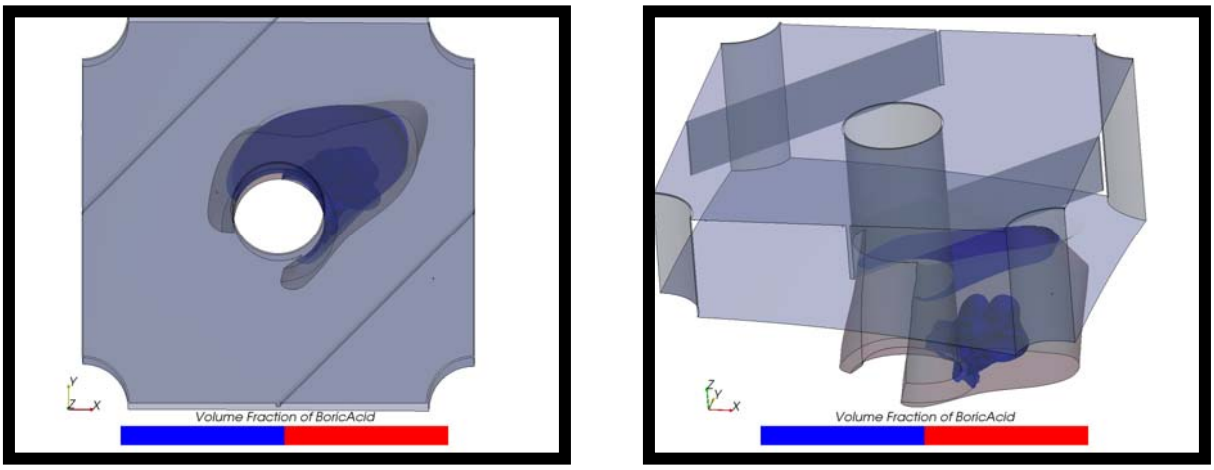

Figure C.123 Case 5: Transient analysis results for final wastage cavity filled with boric acid solution for time steps from 0.001 seconds to 0.02 seconds.

(a) Top View Time – 0.05 seconds Perspective View

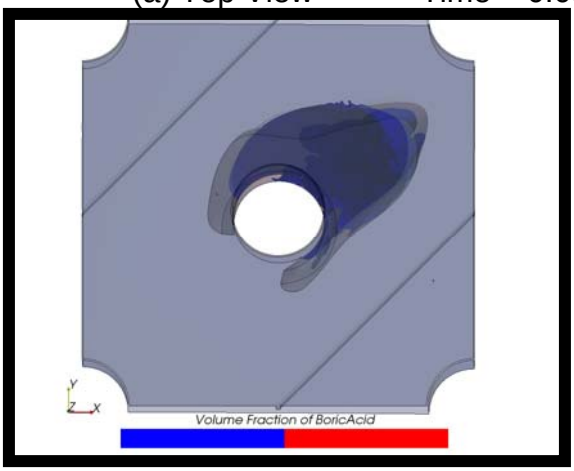

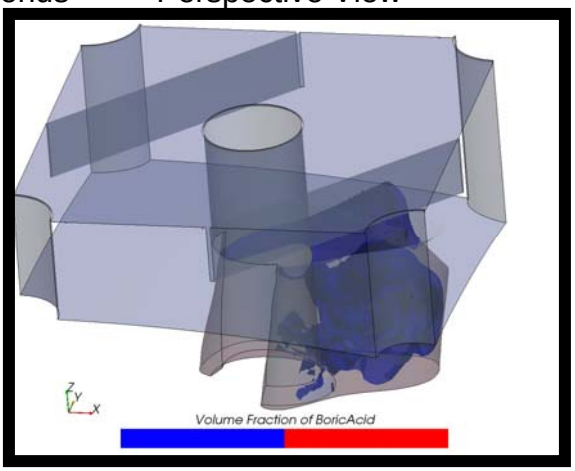

(b) Top View Time – 0.07 seconds Perspective View

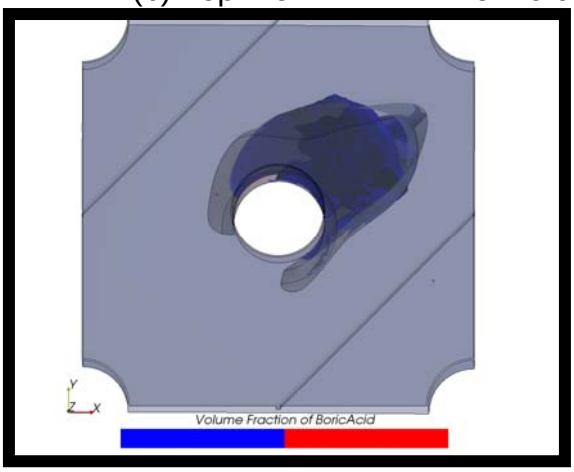

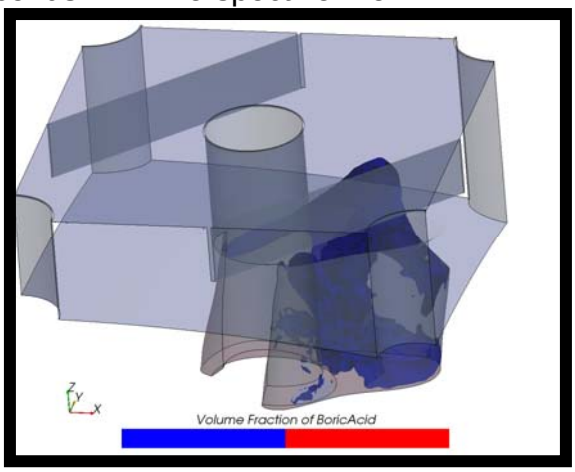

(c) Top View Time – 0.10 seconds Perspective View

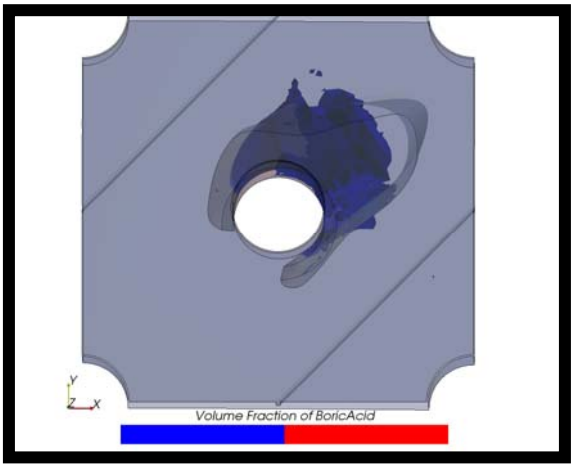

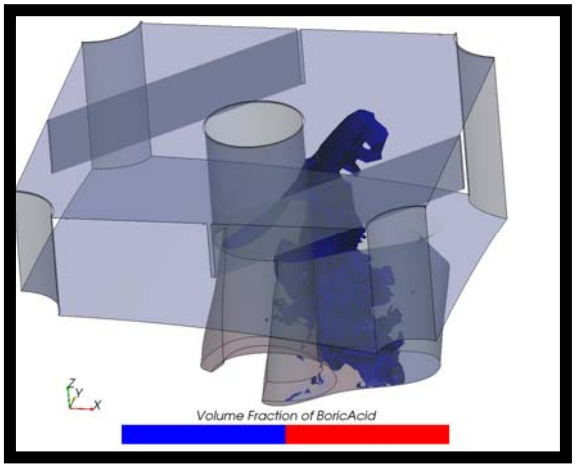

Figure C.124 Case 5: Transient analysis results for final wastage cavity filled with boric acid solution for time steps from 0.05 seconds to 0.10 seconds.

(a) Top View Time – 0.12 seconds Perspective View

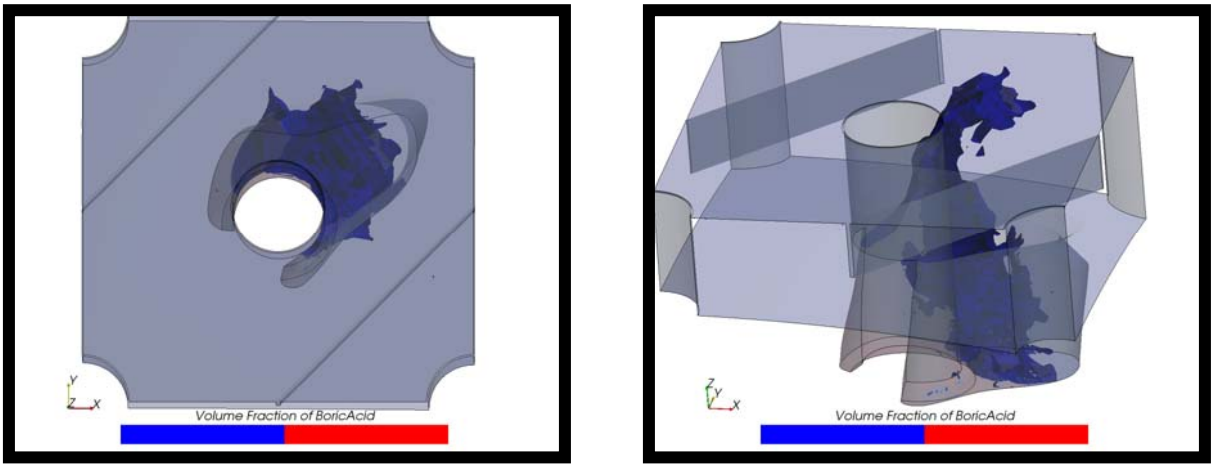

(b) Top View Time – 0.15 seconds Perspective View

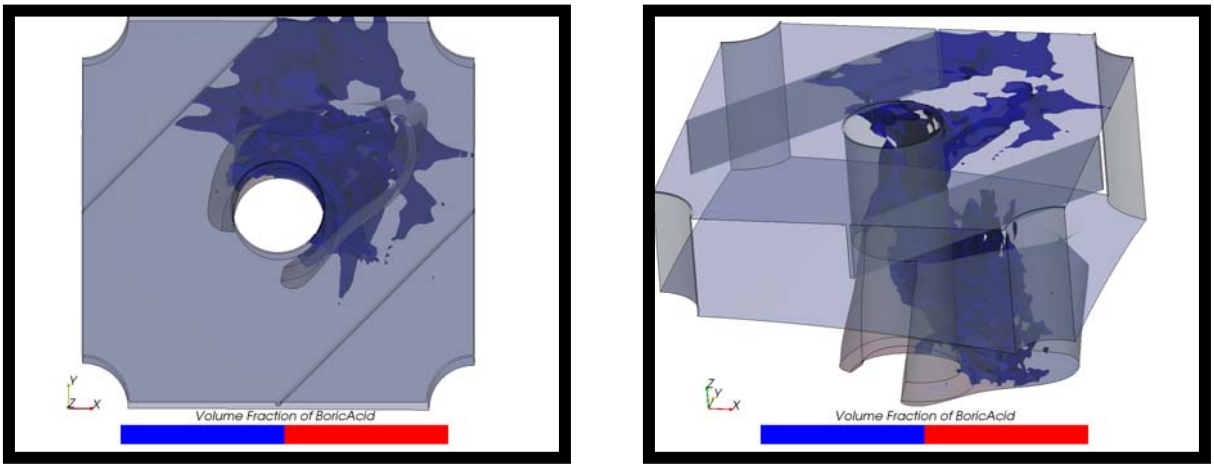

(c) Top View Time – 0.20 seconds Perspective View

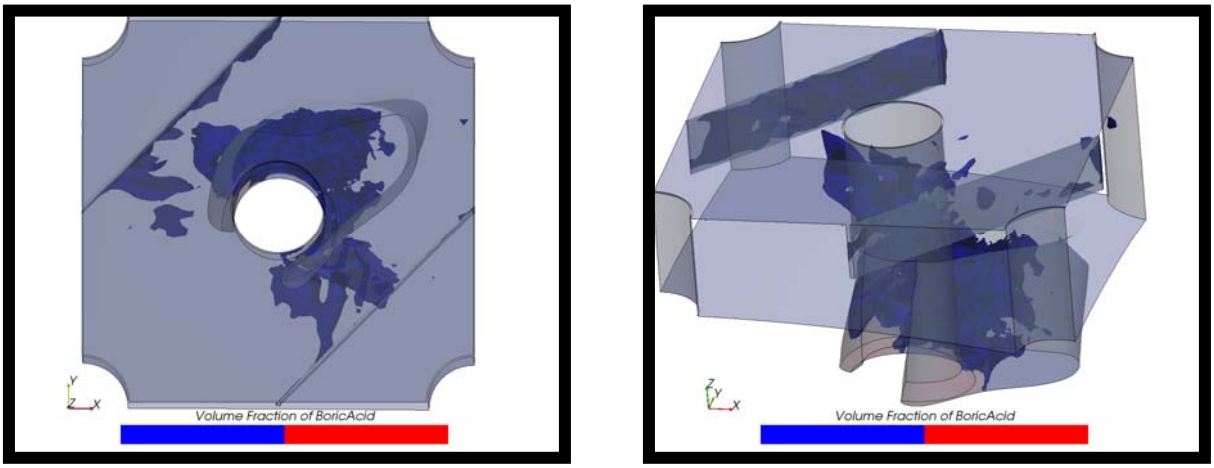

Figure C.125 Case 5: Transient analysis results for final wastage cavity filled with boric acid solution for time steps from 0.12 seconds to 0.20 seconds.

(a) Top View Time – 0.25 seconds Perspective View

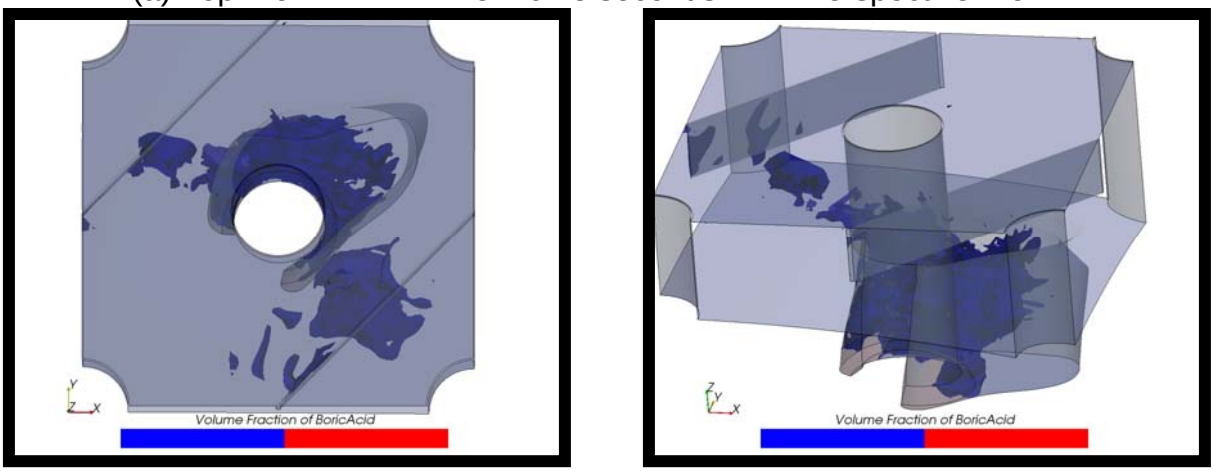

(b) Top View Time – 0.32 seconds Perspective View

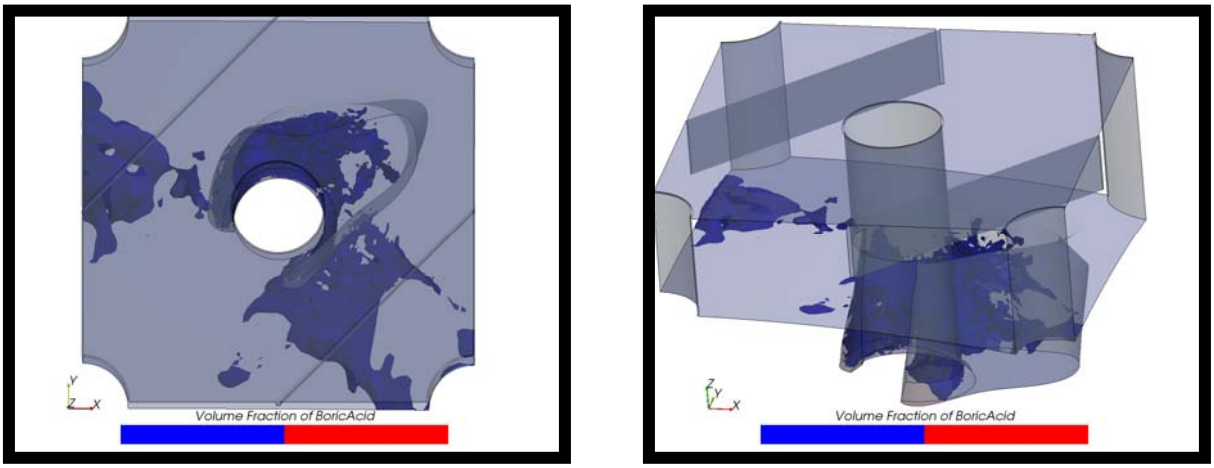

(c) Top View Time – 0.40 seconds Perspective View

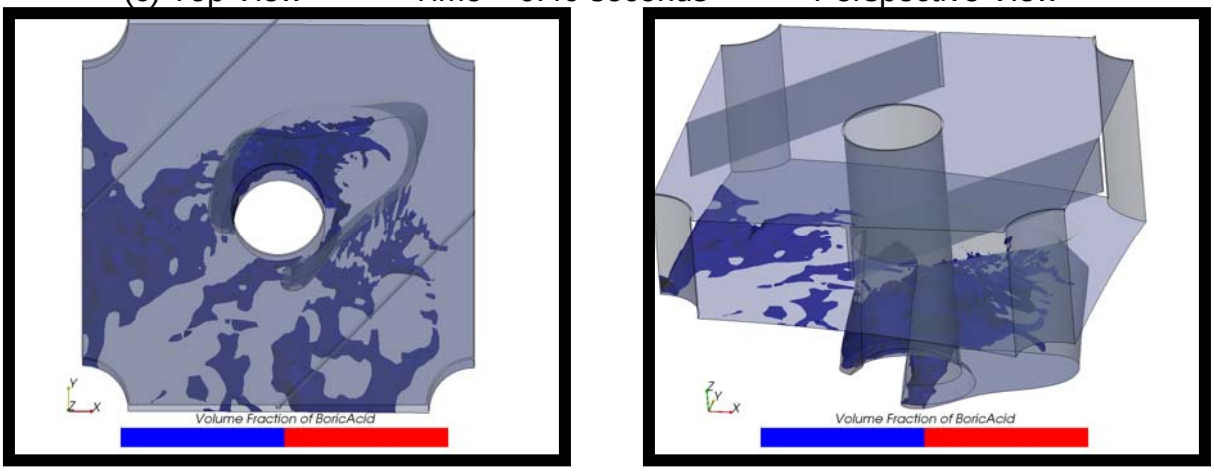

Figure C.126 Case 5: Transient analysis results for final wastage cavity filled with boric acid solution for time steps from 0.25 seconds to 0.40 seconds.

References

1. Aamir, M. A. and Watkins, A. P., “Numerical Analysis of Depressurisation of Highly Pressurised Liquid Propane”, International Journal of Heat and Fluid Flow, Vol. 21, pp. 420-431, 2000.

2. STAR-CD Version 3.27 Methodology Manual.

3. STAR-CCM+ 2.0206 User Documentation, 2006.

4. H. John, J. Reimann, F. Westphal, L. Friedel, “Critical Two-Phase Flow Through Rough Slits” Int. J. Multiphase Flow Vol. 14, No. 2, pp 155-174, 1988.

5. Dominion Engineering Inc., “Davis Besse CRDM Leak Rates Using ANSYS Crack Opening Area (non-safety related) C-5509-00-6, Rev. 0 Report.

6. Nicholls, J.A. 1972. ‘Stream and droplet breakup by shock waves’, *in* NASA SP–194 (Eds. D.T. Harrje and F.H. Reardon), pp. 126–128.

7. Bai, C., and Gosman, A.D. 1995. ‘Development of methodology for spray impingement simulation’, SAE Technical Paper Series 950283.